POLITECNICO DI MILANO
DIPARTIMENTO DI ELETTRONICA, INFORMAZIONE E BIOINGEGNERIA
(DEIB)
DOCTORAL PROGRAMME IN INFORMATION TECHNOLOGY

INNOVATIVE SOLUTIONS FOR HIGH-BIT RATE BACKPLANE-BASED DATACOM INTERCONNECTION

Doctoral Dissertation of:
Anna Boletti

Supervisor:
Prof. Pierpaolo Boffi

Tutor:
Prof. Mario Martinelli

The Chair of the Doctoral Program:
Prof. Carlo Fiorini

2013 – XXV

”An unexamined life is not worth living for human being.”
Socrates

”When something happens and you know why, you say it is a scientific fact, if not you say it is a magic.”
Rubens P.

Acknowledgements

I would like to thank everyone in these four last years have supported and helped me, always giving me strength to face the most difficult moments, especially my love Johnny, my little knight Alessandro, my whole family and all my friends who always have understood and encouraged me.
I thank Professor Martinelli and Professor Boffi for giving me the opportunity to do a PhD. Thanks to Maddalena who helped me and advised in the darkest moments and for sharing ideas and projects together. I want to thank the boys of Policom, in particular the two 'Marcos' for the daily sympathy and support. Thanks to Alberto, my room mate because he has always believed in me, motivated and encouraged.
Thanks a lot to Daniela and Giorgio from Alcatel for their valuable teachings, for their smiles and their support. Thanks again to Chiara, Raffaela and all the people involved in the project Backop who have constructively worked with me, always so friendly and nicely.
A special thanks to Dr. Bert Offrein for welcoming me in his group at IBM with high competence and kindness, thanks for supporting, giving me precious advices and appreciating me. Thanks to Antonio and Thomas so much for the kind cooperation, for helping and supporting me all the time.

Abstract

The present doctoral dissertation aims at finding innovative solutions for the realization of an optical backplane characterized by high capacity interconnections and low energy consumption.

Electrical copper based backplanes have been the solution adopted so far, but with growing bit rates, beyond 10 Gbit/s, they can hardly fulfill the above mentioned requirements. The proposed idea is to move towards an optical backplane, where interconnections between electrical cards or servers (connected to the backplane) are realized with optical links, through a mesh of optical fibers. A preliminary comparison between standard electrical backplanes and a fiber-based optical one has been carried out in order to estimate the advantages in terms of power consumption and capacity at increasing bit-rate. A practical solution for a fiber-based optical backplane has then been designed. In order to realize a cost-effective full mesh interconnection, different topologies of fiber layout have been taken into consideration and cost-effective, energy efficient solution for the optical transmitter and receiver sides has been selected. In particular, a first prototype of the optical backplane will be based on directly modulated Vertical Cavity Surface Emitting Laser (VCSEL) and multimode optical links at 850 nm. Optical data links should also guarantee a complete transmission transparency in the interconnection with the external network, i.e. a traveling signal should be allowed to pass through the backplane network on a determined internal link without any need of opto-electrical (OE), electro-optical (EO) conversion and processing. Under this hypothesis, very high

bit rate optical signals also with complex modulation formats and multiplexing (for example in wavelength or in polarization) should be able to be transferred throughout the fiber-based optical backplane. In this configuration, input/output signals will presumably travel in a single-mode fiber (SMF) coming from or going towards the external network. The employment of center-launching technique has thus been considered to guarantee single mode propagation through the multimode fiber-based optical backplane. Center-launching robustness to mechanical perturbations up to 1kHz, have been experimentally investigated in a multimode fiber link with VCSEL sources, proving error-free transmission.

In order to increase the capacity and improving the power efficiency of the whole system, we addressed the most up-to-date technologies, like VCSEL and Silicon Photonics, for the EO transceivers and their evolution for backplane-based interconnections. We will focus the attention on modulation formats as a way of increasing the link total capacity, maintaining the same number of optical interconnections. For both technologies, a performance simulative analysis of standard On-Off-Keying (OOK) and M-Pulse Amplitude Modulation (M-PAM) is reported. Furthermore, a power consumption comparison between 4-PAM and Non-Return-to-Zero (NRZ) OOK has been discussed in order to highlight the different performances and limitations for VCSEL-based and Silicon Photonics-based links.

Riassunto

Questa tesi di dottorato riguarda lo studio di possibili soluzioni innovative per la realizzazione di un backplane ottico che possa gestire interconnessioni ad alta capacita' garantendo contemporaneamente basso consumo di energia.

Fino ad ora sono stati impiegati backplanes basati su piste elettriche in rame. Con la continua richiesta di aumento della capacita' trasmissiva, oltre i 10 Gb/s, difficilmente questi possono soddisfare i requisiti sopra citati. L' idea che viene sviluppata e proposta in questo lavoro di tesi e' quella di passare all'utilizzo di un backplane ottico, dove le interconnessioni tra le schede o servers (connessi al backplane) sono realizzate con fibre ottiche. Per valutare i vantaggi all'aumentare della capacita' trasmissiva (aumento del bit rate) e in termini di consumo di potenza, e' stato effettuato un confronto preliminare tra un backplane elettrico standard e un backplane basato su fibre ottiche. Successivamente e' stato progettato, analizzando tutte le fasi necessarie per la realizzazione reale fisica, un backplane con fibre ottiche. Per poter realizzare una connessione punto-punto tra tutte le schede connesse al backplane, diverse configurazioni su come distribuire le fibre ottiche sul backplane sono state prese in considerazione. Per la parte di trasmissione e ricezione sono state selezionati componenti a basso consumo di energia e costo. In particolare, per il primo prototipo di backplane ottico sono stati utilizzati sorgenti Vertical Cavity Surface Emitting Laser (VCSEL) modulate direttamente e collegamenti ottici multimodo a 850nm.

I collegamenti ottici devono anche garantire una completa trasparenza dei dati trasmessi, per esempio un segnale proveniente da una rete esterna deve poter passare attraverso un determinato collegamento interno sul backplane senza la necessita' di effettuare una conversione elettro/ottica (EO) o ottico/elettrica (OE). Sotto questa ipotesi, segnali ad altissimo bit rate e anche con formati di modulazione complessi e multiplazione (per esempio, in lunghezza d' onda o in polarizzazione) devono essere in grado di essere trasportati attraverso il backplane costituito con fibre ottiche senza problemi. In questo contesto i segnali di ingresso/uscita viaggiano presumibilmente in una fibra singolo modo proveniente da o diretta verso una rete esterna. Pertanto e' stata presa in considerazione la tecnica di "center-launching" per garantire la propagazione singolo modo nel backplane costituito da fibre ottiche multimodo. Inoltre, la stabilita' della tecnica di "center-launching" a vibrazioni meccaniche fino a 1KHz, e' stata sperimentalmente testata, ottenendo una trasmissione senza errori.

Nell' ambito di applicazioni che impiegano il backplane, per poter aumentare la capacita' trasmissiva e migliorare il consumo di potenza dell'intero sistema, abbiamo puntato la nostra attenzione sui transceivers e una loro possibile evoluzione, analizzando due tecnologie molto attuali come il VCSEL e la Silicon Photonics. In particolare ci siamo concentrati sullo studio dei formati di modulazione come un modo per poter aumentare la capacita' totale del singolo collegamento, mantenendo lo stesso numero di interconnessioni ottiche. Per entrambe le technologie, simulazioni relative alle prestazioni trasmissive di On-Off-Keying (OOK) and M-Pulse Amplitude Modulation (M-PAM) sono state effettuate. Inoltre, un confronto in termini di consumo di potenza tra 4-PAM e Non-Return-to-Zero (NRZ) OOK e' stato discusso con lo scopo di identificare limiti e prestazioni di collegamenti che usano tecnologia VCSEL e Silicon Photonics.

Contents

Introduction

In the next years telecom operators plan to expand the range of innovative services to guarantee the telecom market growth: the HD television, the teleworking, the digital health care system, the digital public administration, the digital learning, the Internet gaming are only some of the considered high quality telecom services. Hence, in the next future the telecom network will be characterized by an always increasing demand of bandwidth and transmission rate, which increase the need to have transmission equipments with always increasing information transmission capacity. The state of the art in the field of the transmission equipment consists of electro-optical boards with external optical interfaces, interconnected by means of high-speed electrical backplanes in the same subrack. The solutions currently used are based on copper interconnections via backplane, driven by a suitable transceivers subsystem. Looking at high-end telecommunication equipment transceivers are directly integrated on the same silicon chip used for the switching function or Input/Output (I/O) function. The transmitting and receiving interfaces, the connectors, and the Printed Board (PB) technology evolved and allowed us to increase the single interface bandwidth. In parallel the amplitudes of the transmitted signals has been reduced, to limit power consumption and increase the integration.

In general we can observe the progressive capacity to enhance the power density in a single device and while the consumption measured in mW per Gb/s has had an exponential decrease, the consumption of the interface including Serdes, clock data recovery (CDR), pre-emphasis and equalization is growing. Furthermore, complexity and density increase is supported by

evolving silicon technology able to manage more W/mm^2. The realization of the transmission lines in PB even if based on the most sophisticated materials available on the market, shows very significant losses at very high operation frequency. Also connectors, even if now very optimized, contribute to increase loss and crosstalk. The electrical backplane is close to reach its limit and for that reason we need to explore alternative solutions.

Due to the fact that optical technologies are able to provide higher capacity over longer distances than electrical transmission systems, a natural answer to the limitations shown by the copper-based interconnection is to exploit optical solutions.

For optical interfaces the bandwidth density scaling necessary to face the future Ethernet requirements may be achieved through the reduction of the pitch size (presently to about 50μm,) and applying 2D arrays of Vertical Cavity Surface Emitting Lasers (VCSELs) and PINs. Optical fibers constitute a good trade off in terms of bending losses, coupling efficiency with VCSEL sources, costs and attenuation. Multimode multicore fiber and/or 2D polymer waveguides are being prototyped to match the demand. The reduction of the distance at increased bit data rates for the existing multimode fibers is an important trend and continuous development is offered. Last but not least novel approaches to increase bandwidth density and transmission length are being investigated, for example based on multi-level coding like Pulse Amplitude Modulation (PAM) and compact wavelength-division multiplexing systems realized in silicon photonics or InP-based photonic integrated circuit approaches. Furthermore, many studies are carrying out to better achieve the integration using silica or polymeric waveguides, instead of copper striplines.

The aim of this doctoral dissertation is to understand and quantify the real benefits of an optical backplane from a point of view of cost and complexity of implementation, transmission performance and power consumption. In particular, it has been tried to identify solutions that ensure simplicity of implementation, and which exploit nowadays on- the-shelf technology. The objective is to understand the real applicability of the proposed optical solutions and their potential for evolution to next capacity upgrade in data center applications.
Thesis contents can be summarized as follows.

In Chapter 1 an overview of different levels and types (electrical or/and optical) interconnections used in network applications is presented. Limitations of the electrical and optical approaches are discussed, considering their capabilities to support more than 20-Gb/s transmission and the possi-

bility to evolve towards higher bit-rates. Some possible alternative optical solution to integrated the source into the transmitter module on the boards, interconnected via backplane are presented. Based on optical interconnection the exploitation of low cost, power efficiency source as Vertical Cavity Surface Emitting Laser (VCSEL) is also described.

Chapter 2 focuses on a comparison between an electrical and optical backplane. Based on the nowadays technology and through simulations, it has been possible to design the best achievable electrical backplane. Then, a comparison with respect a possible optical fiber-based backplane, using VCSEL as sources, in terms of power consumption and capacity have been presented. A detailed analysis on different specifications (as scalability, low cost, low complexity and transparency) that a real optical backplane has to satisfy have been discussed. Some of relevant aspects, like material, choice of optical fibers, type of connectors, design and layout have been taken into account to allow a physical realization of a real fiber-based optical backplane.

Focusing on one of the backplane requirements, the transparency, in Chapter 3 further studies and experimental analysis have been made. Optical data links should guarantee a complete transmission transparency in the interconnection also with the external network, i.e. a travelling signal must be allowed to pass through the backplane network on a determined internal link without any need of opto-electronic and electro-optic conversion and processing. A center-launching technique between single mode optical fibers and multimode fibers has been exploited to satisfy that requirement. Experimental and simulative analyses have been carried out in order to test the achievable performances and robustness of this technique, making it suitable for fiber-based backplane connections. To reproduce different operating conditions in backplane applications, two experimental configurations have been taken into account and bit error rate curve have been obtained.

Chapter 4 focuses on how to increase the optical backplane transmission capacity, maintaining the same number of optical connections and, in the meantime, satisfying stringent requirements like low cost, low complexity and low power consumption. Multi-level modulation format have been considered, in particular close attention is paid on Pulse Amplitude Modulation (PAM) and On-Off-Keying (OOK) modulation format. Beyond a common VCSEL-based technology, a possible alternative technology as

Silicon Photonics have been analyzed, comparing them in terms of power consumption and performances through simulations results.

In the Conclusions of this work, after a quick summary of presented results, we provide some considerations related to the best technology suitable for short and medium reach applications in the near future, taking into account power efficiency, cost, complexity and integration aspects.

CHAPTER 1

Electrical and optical interconnects

In this Chapter an overview of different levels and types (electrical or/and optical) interconnections used in network applications is given. Limitations of the electrical and optical approaches are discussed, considering their capabilities to support more than 20-Gb/s transmission and the possibility to evolve towards higher bit-rates. Some possible alternative optical solutions to integrated the source into the transmitter module on the boards, interconnected via backplane are presented. Based on optical interconnection the exploitation of low cost, power efficiency source as Vertical Cavity Surface Emitting Laser (VCSEL) is also described.

1.1 Different levels of interconnections

The distance of a data transmission line has a strong impact on the quality of the transmitted signal and determines the absolute values of important physical quantities, e.g.electrical resistance, optical absorption, optical dispersion, overall losses etc. Therefore it appears clear the need to classify the data transmission lines in respect to their length. The longest communication lines span distances of many thousand kilometers, for example the intercontinental fiber-based links between North America and Europe,

Asia and Australia etc. The shortest interconnects could be only several micrometers or even shorter in length, for example within a microprocessor chip in a personal computer. Since computers, both personal computers and high performance computers (HPC), are nowadays the main tools for the information processing, it makes also sense to distinguish between data transmission lines outside the computer and inside the computer. Depending on the transmission distance it's possible to distinguish between the global area network (GAN), wide area network (WAN), metropolitan area network (MAN) and local area network (LAN). Historically, it's use to refer to longer distances, as in the case of the GAN, WAN and MAN, with the term "telecommunication" (Telecom), while to shorter distances, like within a LAN or shorter, with the term "data communication" (Datacom). To bring the signal to a computer is only one important part of the information transfer process. Equally important part is to provide technologies for the data exchange between different components within a computer. For this task it's possible to distinguish between different levels of interconnects, depending on the transmission distance, as shown in Fig.1.1 [1], [2]. The distances of interconnects could vary from several hundred meters for

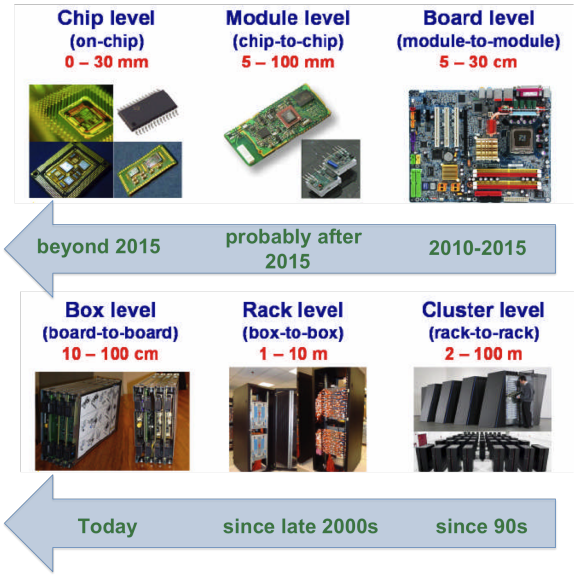

Figure 1.1: *Different levels of interconnects inside the computer and approximate date of the entering of the optics into the corresponding market segment.*

the rack-to-rack connections in a supercomputer down to only several millimeters or even several micrometers for the on-chip interconnects. Nowadays optics is common at the cluster level for the rack-to-rack interconnects

and on the rack level for the box-to-box interconnects. Currently optical technologies are coming to the box level for the board-to-board interconnects with data transmission distances of several tens of centimeters. The penetration of optics into ever shorter interconnects will continue in the near future. Just in the next few years it is expected that optical interconnects will expand to the board level for the module-to-module data transfer. After approximately 2015 optics will come also to the module level for the chip-to-chip and to the chip level for the on-chip data transmission. As can be seen from the overview of the optics in the Telecom and Datacom applications, optical interconnects are ubiquitous for data transfer outside the computer on the LAN, MAN, WAN and GAN levels. They penetrate unstoppable to ever shorter distances and will reach in five to ten years the chip level. The major role is played by VCSEL [3], as inexpensive, low power and reliable laser light sources on all levels of optical interconnects starting from LAN down to the cluster, rack and box levels.

1.2 Electrical backplane towards optical backplane

In the next years the telecom operators plan to expand the range of innovative services to guarantee the telecom market growth: the High Definition television, the teleworking, the digital health care system, the digital public administration, the digital learning, the Internet gaming are only some of the considered high quality interactive telecom services. In the next future, then, the telecom network will be characterized by an on going increasing demand of bandwidth and transmission rate, which translates into transmission equipment with always increasing information transmission capacity [4]. The current state of the art in the field of the transmission equipment consists of electro-optical boards with external optical interfaces, interconnected by means of high speed electrical backplanes in the same subrack. Physically, these lines are optical cables inserted into the front of communications chassis. Even though the back of these chassis - the backplane in particular - is the conduit through which data move from one line interface to another. A typical modular chassis consists of communicating circuit cards connected by a backplane. It consists of a board in a composite material with embedded interconnections, so that different subsystems, connected to the backplane, mutually interact. The backplane is passive (without active components along the datapath) to facilitate circuit card upgrade. The backplane in essence is a large printed circuit board (PCB) with a network of copper traces among backplane connectors into which circuit cards are inserted. Electrical transceivers are the predomi-

nant active circuits at both ends of a backplane link. If the communication system is arranged in a shelf, the subsystems are cards hosted in parallel slots and plugged onto the backplane, see Fig.1.2. In particular, Fig.1.3 defines a canonical backplane model [5]. Each of the two circuit cards, labeled "Card 1" and "Card 2" contains a Backplane Interface Chip (BIC). The two BICs communicate with each other over a passive backplane. The BIC models an electronic logic device with either integrated electrical or optical transceivers. Buffers may be optionally inserted between a BIC and backplane connectors. For instance, a BIC having only short-reach electrical transceivers incapable of operating over long backplane links requires electrical buffers between it and the backplane connectors. Of course, in this case, the buffers must have backplane transceivers. Specifically, three kinds of links are modeled in Fig.1.3:

- S1 link: Intra-card link between the BIC and the buffer if one exists, or between the BIC and the backplane connector if the buffer is absent
- S2 link: Intra-card link between the buffer (if one exists) and the backplane connector
- S3 link: Inter-card link between the two connectors on the backplane

Between two BICs, an S1 link and an S3 link are mandatory, whereas an S2 link is present if and only if a buffer is present. A backplane connector is either between an S2 link and an S3 link if a buffer is present, or between an S1 link and an S3 link otherwise. The backplane connectors in the canonical backplane model are passive.
Following the trend, the transmission equipment of the next future should use electrical backplanes with traces supporting the propagation of electrical signals at bit rates of tents of Gbps. However, electrical interconnects become much more difficult to successfully design as data rates begin to exceed 10 Gbps, due to frequency dependent losses, crosstalk, and frequency resonance effects [6]. Figure 1.4 shows a typical electrical backplane consisting of a set of cards plugged into a backplane. Copper traces suffer from increasingly large losses at higher frequencies due to skin effect (and dielectric losses to some degree). This can be mitigated by using fatter wiring, but this only exacerbates wiring density and routing problems. At each packaging or connector juncture, the line impedance must be well matched or signals will be partially reflected causing signal degradation. Via stubs, a consequence of typical drill and fill printed circuit board (PCB) technology also cause reflections, and although these can be eliminated with back drilling or stubless manufacturing methods, these generally

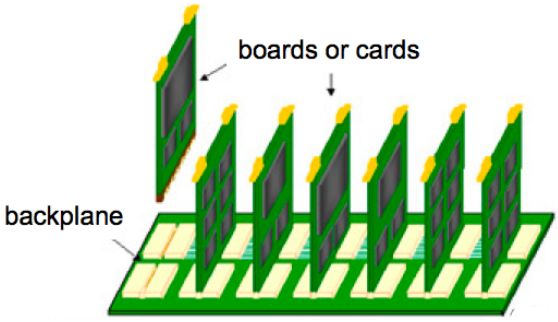

Figure 1.2: *An example of a backplane structure.*

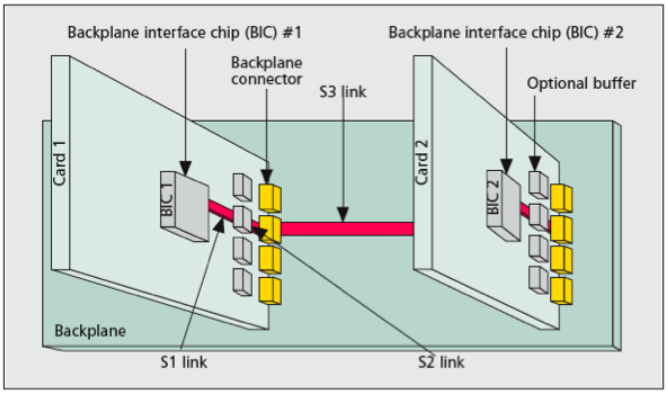

Figure 1.3: *Canonical backplane model.*

increase the costs of the PCB boards. To increase bit rate beyond 10G with electrical backplane it will be a great challange for future engineers. The transmission rate of the digital signals depends on the technology of the integrated circuits (ICs) that generate them. For instance, greater speed means integrated transistors with smaller dimensions. In fact the reduced channel length of the integrated transistors and the corresponding reduced switching time lead to a higher integration (more logical functions in less physical space) and to an increased data rate of the transmitted signals (reduced timing budget for the interconnection links). Moreover in the submicron semiconductor world the power consumption is a critical factor, because the static power dissipation increases significantly with the integration. To solve this problem a lower power supply is used. In any case note that, at lower semiconductor dimensions, physical effects such as the dielectric breakdown , the hot current injection, the electrostatic discharge and the electromigration limit the power supply on board. The reduced

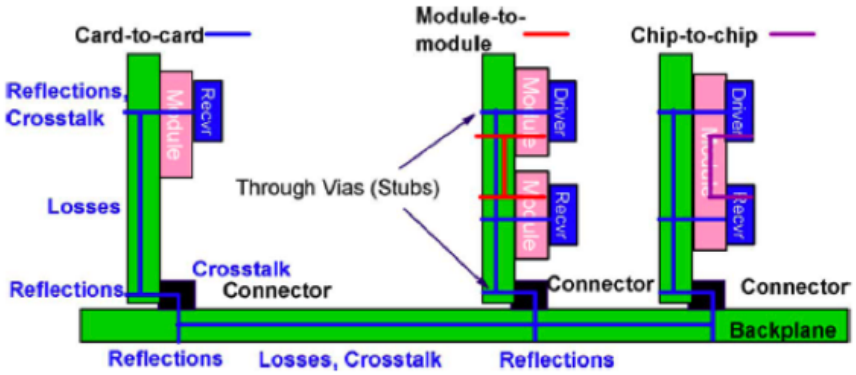

Figure 1.4: *Electrical links suffering from multiple signal integrity degradations as channel rates increase, including high losses, crosstalk, and reflections*

on board power supply and the increased signal data rate - consequently the reduced signal swing, the reduced noise margin and the increased simultaneous switching noise (SSN) - have a negative impact on the high speed electrical interconnections intra rack [7]. The need of equalization and pre-emphasis to compensate the high speed electrical losses on the interconnections, the increased electromagnetic problems and the increased cost for transmitted bit force to move to a totally optical transmission layer, where totally optical boards in the same subrack have to be interconnected by means of optical interconnections.

The optical interconnection among different boards in the same rack can guarantee the bandwidth needed to the future telecommunication services, reducing the power dissipation, increasing the electromagnetic immunity and transmitting at data rates of tens of Gbps without signal integrity problems. In this case the signal transmission could be eco-compatible - light rather than electrical signals - and could reduce the cost of each transmitted bit of information.

Recently, ”computercom” is getting importance as a distinct market segment, alongside the traditional datacom and telecom markets [8]. The very high aggregate BW demands of these systems have opened up opportunities for optics to compete with electrical interconnects at shorter and shorter distances. What distinguishes the computercom market is not only the need for very short, less than 10 m interconnect lengths, but also an enormous pressure for reduced cost, power, and reliability to meet the demands of future systems. Power considerations require placement of optics very close to the signal source, which in turn is driving the need for very high density interconnects and highly integrated packaging as well. As shown in

Fig. 1.5, over the last two decades, High Performance Computing (HPC) has maintained a performance improvement trend of 85-90 % compound annual growth rate, almost doubling performance every year. Historically, growth in transistor speed and improved CPU design (taking advantage of ever cheaper and smaller devices) provided a large part of this growth. As chip speeds have leveled off more recently, multicore architectures have helped fill the gap. Moving forward, new innovations will be required, such as the increased use of specialized computing elements or accelerators (e.g., graphics processing units), as well as a further increase in the reliance on continued growth in large scale system parallelism to make up the difference. Thus, interconnect BW requirements continue to scale at all physical levels of the system. Typical server interconnects include a core-to-core bus on a single chip, chip to chip (for CPU-to-cache- or CPU-to-CPU communications), chip-to-memory on card, CPU-to-CPU cluster fabric between cards and racks, CPU node to storage (typically rack to rack), and LAN/WAN links which go beyond the immediate computing or data center building [9]. Typically, CPU-to-memory links and symmetric multiprocessor links, a cache-coherent architecture, are the most latency sensitive, though much of that latency is due to the memory controller, with a smaller dependence on time of flight delays (about 5 ns/m for optical fiber). Historically, storage links were the first to utilize optical inter-

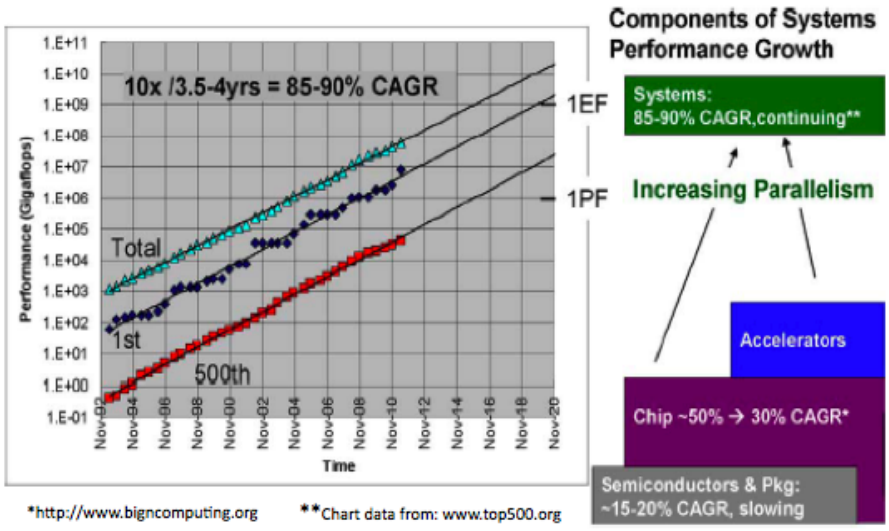

Figure 1.5: *HPC performance trends. (Left side) Historical and future trend based on Top500 data. (Right side) Additive components needed to make up the overall growth at the system level*

connects (e.g., IBM's ESCON technology since 1990 [10]), in large part based on the longer distances from compute to storage racks and the relativelymodest, and therefore low total cost, BW required (the need is limited by disk access speed). In 2005, IBM introduced the ASCI Purple system, which was one of the first systems to utilize optics for rack-to-rack cluster links. Initially, the system deployed all electrical links for rack-to-rack cluster interconnects; however, as the price of optics continued to drop during this period, the longer links were replaced with optics. This change relieved significant cable congestion in these systems, and is shown in Fig.1.6. More recently, the IBM Power 775 has made use of a fiber cable optical backplane within the rack as well as for the rack-to-rack cluster fabric. In order to reap the further benefits of an all optical backplane, the optics modules are located on the same first level package as the router chip, in this case on a glass-ceramic multichip module (MCM). In general the optical intercon-

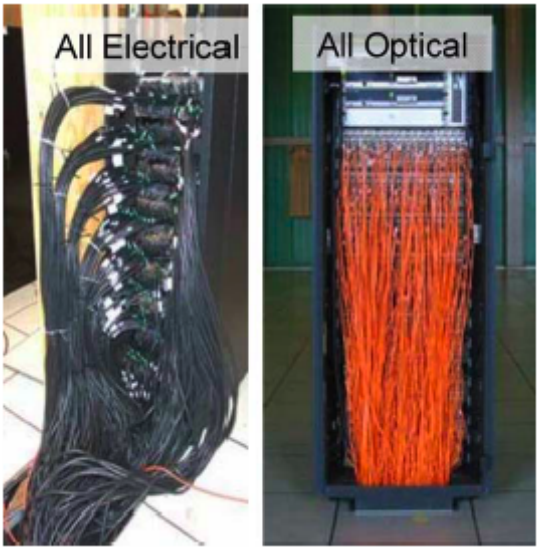

Figure 1.6: *IBM Federation switch rack for ASCI Purple. (Left side) Preproduction system with all electrical cabling. (Right side) Rack with all optical cabling.*

nect on short distance as in board to board link, offers many advantages: besides scalability to higher bit rate without strong signal degradation as along copper connections, the optical solution offers reduced cable bulk, smaller connector size, and reduced electromagnetic interference. Due to the benefits of optical interconnects, there has been a steadily increasing use of optics in these large systems, so much, the number of optical channels in

a single supercomputing system today can be the same as in the worldwide volume in parallel optical interconnects just a few years ago. The considerations will be the cost of optical interconnects versus copper interconnects and the resultant performance tradeoffs, i.e., the ability to create topologies coupled with algorithms which maintain performance despite thinner networks and longer latencies to more distant nodes.

1.3 Optical technology

The evolution of networks to support higher data rates is driven by market demand, standardization activities, and the availability of next generation optical transceiver technology [11]. Standardizing a new data rate requires standards for optical transmission and framing, as well as the details of an optical transceiver implementation. For the 100Gb/s data rate, for example, the IEEE defined the 100 GbE client interface, while the International Telecommunication Union - Telecommunication Sector (ITU-T) provided the optical transport unit 4 (OTU4) framing. The Optical Internetworking Forum (OIF) developed implementation agreements for both the transmitter and receiver that define the functionality, interfaces, and mechanical requirements. The optical communications community has now started to search for the next milestone for client port speed, transport channel rate, and channel spectral efficiency. The speed of the next generation Ethernet physical layer is still being debated, with both 400 GbE and 1 TbE under consideration. To respond to the severe requirements of future systems, optical interconnects will need to continue to make improvements in four major areas: power, cost, density, and reliability. To achieve cost goals, careful rethinking of optical interconnects for low-cost high-volume manufacturing will be required. Furthermore, to achieve the lowest power links, optics modules will need to be situated close to the signal source, requiring very dense modules, of order 1 Tbps/cm . Achieving these goals will require careful balancing of tradeoffs, as shown in Fig.1.7. For example, trimming power will narrow link margins, lowering yields, and, therefore, increasing costs. By locating optics closer to the signal source, electrical link power can be reduced, but optimization of optics packaging close to the signal source will require much denser and more integrated optical modules which will require greater cooperation between systems providers and optical interconnect suppliers. Inside this frame, VCSEL optical sources, at the transmitter side, are the optical technology mainly exploited for board to board and datacom link, since they offer a low cost, high integration

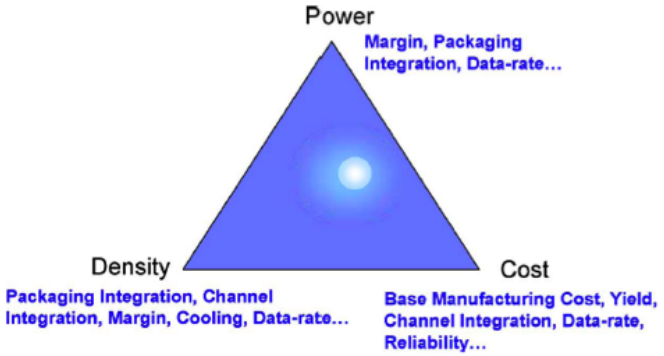

Figure 1.7: *Optimized solutions will require detailed analysis of tradeoffs.*

and low power consumption solution. The following paragrafths will give a brief description of these novel optical sources (compared to Distributed Feedback laser -DFB) and their different way of integration inside the transmitter modules.

1.3.1 VCSEL optical sources

A VCSEL, shown in Fig.1.8, is a semiconductor laser diode which emits light perpendicular from its top surface. These surface emitting lasers offers several manufacturing advantages over conventional edge-emitting lasers, including wafer-scale testing ability and dense 2D array production. Vertical-cavity surface-emitting lasers (VCSELs) are well established as cost and power efficient optical sources in transmitters for short-reach, high-capacity optical interconnects. Much effort has consequently been spent on improving the high-speed performance of VCSELs and, due to intensified research, much progress has also been made.

VCSEL Theory

As shown in Fig.1.9, once a threshold current I_{th} is reached and stimulated emission, or lasing, occurs, the optical power emitted by the VCSEL is a linear function of the current flowing through the device. As the threshold current magnitude is a function of the active area current density, it is often reduced by confining the current with an oxide aperture. Typical threshold current densities for conventional quantum well 850nm VCSELs are below 1mA for devices with apertures less than 7-8μm. Once the VCSEL begins lasing, the optical output power is related to the input current by the slope efficiency η (typically 0.3-0.5mW/mA) and a high contrast ratio between a logic ”one” signal and a logic ”zero” signal can be achieved by placing the

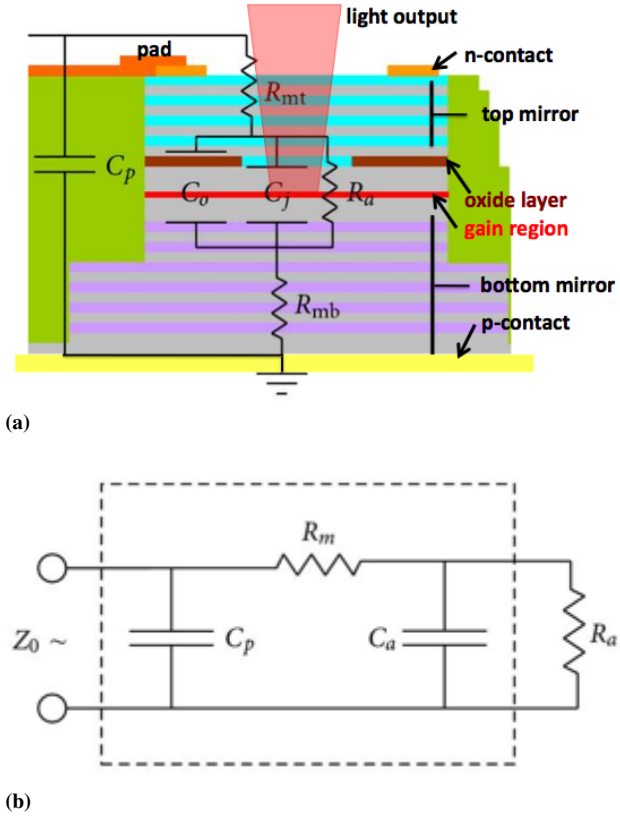

Figure 1.8: *Electrical parasitic capacitances and resistances in VCSEL cross section (a) and the corresponding equivalent circuit with two parallel capacitances C_n and C_j combined together to C_a and resistances of the both mirrors R_{mt} and R_{mb} joined to R_m (b).*

"zero" current value near threshold. While a low "zero" level current allows for high contrast, a speed limitation does exist due to the VCSEL bandwidth being a function of the device current level. VCSEL bandwidth is limited by a combination of electrical parasitics and the electron-photon interaction described by a set of second-order rate equations. A two stage model is generally used to simulate the total frequency response, with an equivalent electrical parasitic model shown in Fig.1.8b, and the junction resistance current from this electrical model is then converted into optical power via stimulated emission governed by the rate equations. The VCSEL's dominant electrical time constant comes from the bias-dependent junction RC, with the dominant junction capacitor value typically between 45 $\div$150fF for 5μm-diameter 850nm VCSELs rated at 25Gb/s [12]. In addition to the

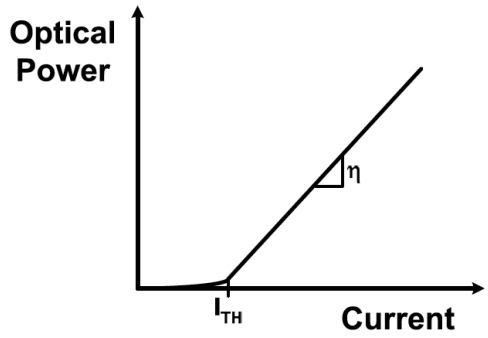

Figure 1.9: *VCSEL output power vs. current (L-I) curve.*

bias-dependent junction resistance, there is also significant series resistance due to the large number of distributed Bragg reflector (DBR) mirrors used for high reflectivity, with a total device series resistance typically between 30 to 120Ω. VCSEL optical bandwidth is regulated by two coupled differential equations which describe the electron density N and the photon density Np interaction [12]. The rate of the electron density change is set by the amount of carriers injected into the laser cavity volume V via the device current I and the amount of carriers lost via desired stimulated and non-desired spontaneous and non-radiative recombination

$$\frac{dN}{dt} = \frac{I}{qV} - \frac{N}{\tau_{sp}} - GNN_p \tag{1.1}$$

where τ_{sp} is the non-radiative and spontaneous emission lifetime and G is the stimulated emission coefficient. Photon density change is governed by the amount of photons generated by stimulated and spontaneous emission and the amount of photons lost due to optical absorption and scattering:

$$\frac{dN_p}{dt} = GNN_p + \beta_{sp}\frac{N}{\tau_{sp}} - \frac{N_p}{\tau_p} \tag{1.2}$$

where β_{sp} is the spontaneous emission coefficient and τ_p is the photon lifetime. Combining the two rate equations and performing the Laplace transform yields the following second-order low-pass transfer function of optical power P_{opt} for a given input current

$$\frac{P_{opt}(s)}{I(s)} = \frac{h\nu\nu_g\alpha_m}{q}\frac{GN_p}{s^2 + s(GN_p + \frac{1}{\tau_{sp}}) + \frac{GN_p}{\tau_p}} \tag{1.3}$$

where v_g is the light group velocity and α_m is the VCSEL mirror loss coefficient. The VCSEL relaxation oscillation frequency ω_R, which is related

to the effective bandwidth, is equal to

$$\omega_R = \sqrt{\frac{GN_p}{\tau_p}} \propto \sqrt{I - I_{th}} \tag{1.4}$$

Thus, due to the photon density being directly proportional to the amount of injected current above threshold, the VCSEL bandwidth scales with the square-root of this current. From equation 1.4, it is evident that in order to increase VCSEL bandwidth, the operating current must be scaled in a quadratic manner. Unfortunately, output power saturation due to self-heating [13] and also device lifetime concerns [14] restrict excessive increase of VCSEL average current levels to achieve higher bandwidth [15].

VCSELs are built using different technology, in particular for short - wavelength range they are based on GaAs technology, allowing today to achieve very reliable optical sources, operating at very high speed, high power and characterized by record performance in power dissipation with respect to InP technology used for longer wavelength (1260nm ÷1680nm). Moreover, as shown in the Fig.1.10, the GaAs technology appears today also more convenient in terms of cost and temperature performances. InPGaAs

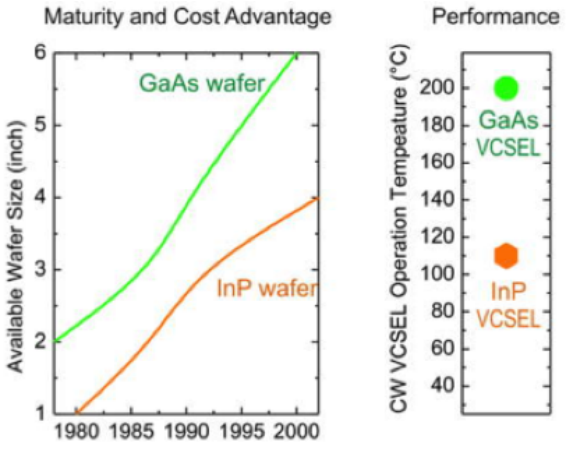

Figure 1.10: *Advantages of GaAs technology in VCSEL development with respect to InP technology.*

VCSELs grown on InP substrates suffer from several critical problems, resulting in an increased threshold current, poor temperature characteristics and low output power. The thermal issues are a consequence of the small conduction band offset between InGaAsP and InP, enabling electrons with enough thermal energy to escape from the quantum well. This

limited carrier confinement together with significant Auger non-radiative recombination at high injection densities which tremendously limits high-power lasers. GaInNAs(Sb)/GaAs VCSELs offer several advantages over InGaAsP/InP lasers. Since GaAs is an effective thermal conductor, VCSELs grown on GaAs substrates can operate without special cooling requirements. Also, DBRs grown using GaAs/AlAs achieve high reflectivity with a decreased number of pairs, due to the large refractive index contrast between GaAs and AlAs. The growth time and mirror thickness are decreased, thus lowering the electrical resistance as well as optical losses due to sidewall scattering and diffraction. Finally, the conduction band offset is much deeper than for the InGaAsP/InP system, leading to better electron confinement. This also provides a better matching of the valence and conduction band densities, yielding higher temperature characteristics, higher operating temperature, efficiency and output power [16]. Figure 1.11 summarizes the speed vs. temperature performance for GaAs based VCSEL reported in the literature [17]. While VCSELs at 850 nm (the wavelength

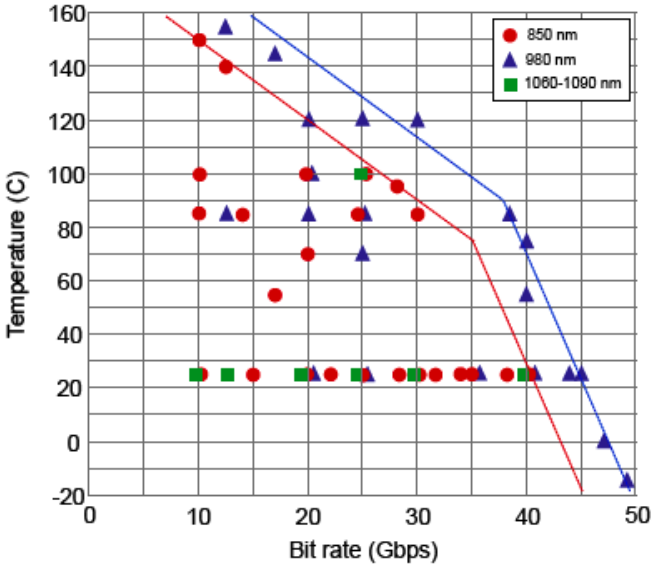

Figure 1.11: *A compilation of data rates and operating (ambient) temperatures for GaAs-based VCSELs at different wavelengths from the literature. The lines indicate state-of-the-art for VCSELs at 850 (red) and 980 nm (blue).*

in existing datacom standards) operate up to 40 Gbps at 25°C and up to 30 Gbps at 85°C, VCSELs at 980 nm operate at an even higher data rate at a given temperature. This suggests that the use of deeper and more strained

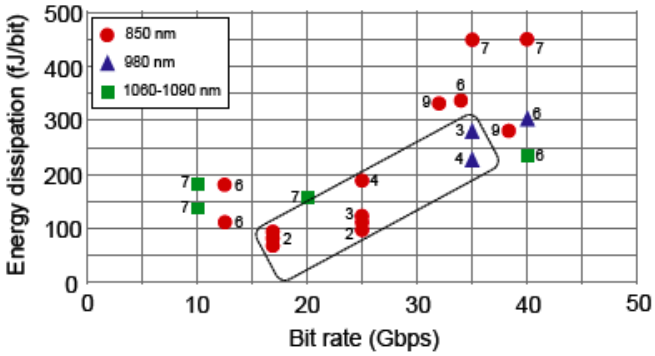

Figure 1.12: *Energy dissipation per bit for GaAs-based VCSELs at different wavelengths compiled from the literature. The numbers next to the symbols show the diameter in μmÕs of the current/optical aperture. VCSELs within the box are single or quasi-single mode while the others are multimode. The ambient temperature is 25°C.*

InGaAs quantum wells (QWs) and the more extensive use of binary compounds favors speed.

850-nm VCSEL performances

Figure 1.12 presents a summary of reported values for 850nm VCSEL energy dissipation at different data rates. Clearly, small aperture VCSELs can be very energy efficient (<100 fJ/bit) while the dissipated energy increases with increasing data rate as the VCSEL has to be biased at a higher current for sufficient bandwidth. To date the maximum reported error-free bit rate (BR) of VCSELs operating at room temperature is 47Gb/s using multimode VCSELs with oxide aperture diameters of 7-11μm [18], obtained by optimizing the doping profiles of the DBRs to reduce resistance, using a short (0.5-λ) cavity to improve longitudinal optical confinament and optimizing the photon lifetime for optimal damping. It has been demonstrated that VCSEL with oxide aperture diameters of $\sim$4μm or less emitting in a single or quasi-single fundamental transverse mode are more energy efficient than VCSELs with larger oxide aperture diameters when operated at low bias above threshold [19]. The intrinsically larger D-factors are then beneficial. The D-factor is the rate at which the resonance frequency increases with bias current. Recently it has been demonstrated 850nm VCSELs operating error-free up to 40Gb/s with only $\sim$ 100fJ dissipated energy per bit [20]. By employing such small oxide aperture diameter VCSELs error free transmission has been achieved at 22Gb/s over 1.1km of OM4 fiber [21] and it has been simultaneously achieve long transmission distance [22] across multi-

mode fiber (500m of OM4 fiber) at high bit rate at record low dissipated energy per bit. Despite the small aperture diameters the current density (J) required for error-free operation is comparable to the J for VCSELs having larger aperture diameters [18], [23].

Longer wavelength VCSELs

Although the 850 nm wavelength for VCSEL links has been the standard for many years (i.e., 1GbE in 1998), the optimal wavelength has been debated for many years as well. Recently, there has been renewed interest in longer wavelengths in the 900-1100 nm range, based on AlGaAs and InGaAs alloys. This interest is spurred by a number of factors, including potential speed, efficiency and reliability improvements, ease in fabricating backside emitting VCSELs (the GaAs substrate is transparent at longer wavelengths, which allows new packaging options), and the potential for low-cost coarse wavelength division multiplexing (CWDM) transceivers [24]. In addition, longer wavelengths enjoy a slight photodetector responsivity advantage (producing more current per unit optical power), and more relaxed eye-safety power limits. There have been significant accomplishments for these longer wavelength VCSELs (e.g., [25] - [28]) demonstrating record power conversion efficiencies and good reliability.
With further increasing transmission distances, as required in warehouse-scale data centers (300m to 2000m), the small bandwidth-distance product of multimode fibers compromises the capacity of optical interconnects based on such short-wavelength VCSELs. Using single mode fibers instead of MMFs in combination with long-wavelength VCSELs strongly relieves this limitation. For instance, error-free transmission over 4.7 km of SMF at bit-rates of 25 Gbps was reported employing 1550 nm short-cavity (SC) VCSELs operating uncooled at room-temperature [29]. In back-to-back configuration even bit-rates of 35 Gb/s [30] and 40 Gbps [31] were demonstrated at 25∘C with corresponding bit-error rates below 10^{-12} and 10^{-5}, respectively. Moreover, comparably low energy-per-bit values of 230 fJ/bit [30], which are attributed to the typically half as large voltage drop at long-wavelength VCSELs, turn 1550 nm devices into an energy-efficient alternative to 850 nm VCSELs in short to medium range optical interconnect applications. Furthermore, these devices are interesting candidates for numerous Telecom applications on the level of access networks as standards like the IEEE 802.3 100 GBASE LR-4 standard confirm. Therefore, VCSELs emitting at 1550 nm exclusively feature the seamless usability in high capacity optical links with link lengths ranging from several micrometres to several kilometres. This comprises a major economic benefit from

1550 nm VCSELs compared to short wavelength competitors, as the Datacom and Telecom market may share development costs for these devices. In contrast, error-free VCSEL -links for the optical O-band (1260-1360nm) have only been reported for maximum bit rates up to 12.5Gb/s, over 20km SMF, and room temperature operation [32], and to elevated temperature up to 100°C, different concepts based on wafer fusion [33] and nitrite containing active regions [34] grown on GaAs-substrate have enabled error-free links of up to 10km at 10Gb/s. Corresponding small-signal modulation bandwidths do not exceed 10 GHz. Recently, the first 1.3 μm InP-based VCSELs has been reported, based on the short-cavity concept which in detail was introduced in [30] for 1.55 μm VCSELs. First 1.3 μm devices allowed small-signal modulation with bandwidths up to 12 GHz at 20°C [35]. The most recent work [36] has demonstrated the static and dynamic device performance of such 1.3 μm SC-VCSELs and reports on improved up-to-date results. To improve the modulation capability towards 25-40 Gbit/s both the inherent laser characteristics such as photon lifetime and the RC limitations have been optimized. By replacing the semiconductor output DBR with a large penetration depth for the optical field and consequently large photon lifetime with a high index difference dielectric DBR, the photon lifetime could be reduced by 40%. From measurements on such short cavity (SC) VCSELs at 1.3μm and 20°C a possible intrinsic bandwidth of 25.4 GHz has been obtained which would be sufficient for digital modulation at 40 Gbit/s. The actual bandwidth is still limited by parasitic capacitances including e.g. contact pads and depletion regions at the regrowth interface. Owing to the reduced damping, the SC-VCSELs have a maximum modulation of f_{3dB} = 15 GHz, which in the present devices is limited by the parasitic bandwidth of around 9 GHz. First large signal modulation results indicate the potential to achieve error-free data-transmission at 25 Gbps with these devices [37].

1.3.2 VCSEL and Silicon Photonics integration at board level

VCSEL-fiber technology

Historically, low-cost optical interconnects for datacom, and now computercom, have been based on multimode fibers and Vertical Cavity Surface Emitting Laser (VCSEL) technology [38] - [40]. Rack-to-rack cluster fabric in particular has made good use of parallel optical modules employing these technologies. In comparison to single-mode technology, more commonly used in telecom, multimode technology is more alignment tolerant as described in details in the Chapter 2. Multimode VCSELs provide a

cheaper and easier light source than edge-emitting single-mode lasers, and furthermore, are easy to make in compact arrays, and more power efficient as well. So, although multimode fiber has distance limitations due to path differences between the various modes (e.g., typically in the hundreds of meters range, getting worse with higher data rates), it is still the right choice for these primarily short datacom and computercom links. This technology already enjoys a low-cost manufacturing infrastructure, but still has room for improvement. Higher data rate VCSELS, as seen in the previous subsection, are already in development, with many suppliers now focusing on 25 Gbps technology for 100 Gbps Ethernet (4x25 Gbps parallel) [41]. Mass manufacturing methods are being adopted to further lower cost and meet future high volume demands, as evidenced by the panel-based Avago MicroPOD manufacturing approach [42]. This technology will continue to improve, with higher, lower cost, lower power, and more compact modules. Figure 1.13 shows a highly compact optical prototype module employing flip chip attachment of the VCSELS and photodiode arrays to a CMOS chip with optical vias (holes in the Si substrate) to permit coupling to an optical fiber array [43]. This module provides up to 300 Gbps (24x12.5 Gbps in each direction) at 8.2 pJ/bit with a density of 1 Tbps/cm . To further reduce

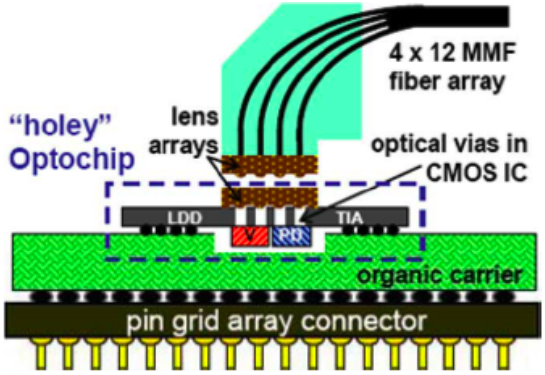

Figure 1.13: *Prototype high-density optical interconnect transceiver.*

overall costs of optical links, not only the cost of the transceivers should be reduced but also the cost of fiber connectors, cabling, and fiber management. Higher data rates will help reduce these costs to some degree, but further reduction may be required. One way to accomplish this is to use multiple multimode cores in a single fiber to achieve much higher data rates.

VCSEL-optical PCB technology

To make further gains in cost and level of packaging integration, and com-

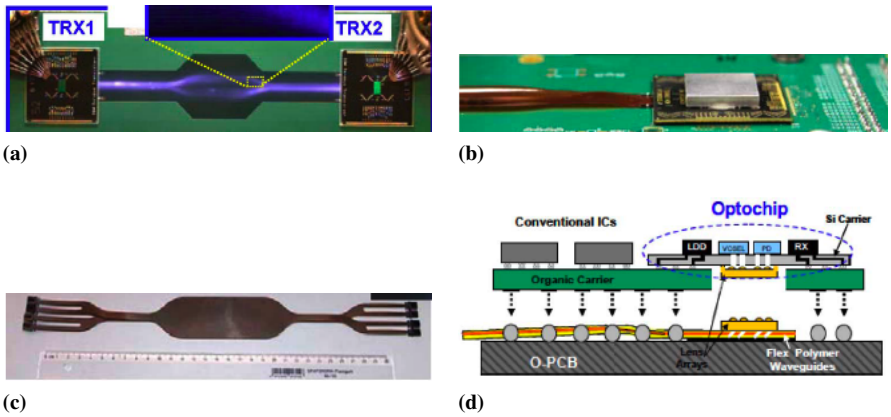

Figure 1.14: *(a) Polymer waveguides on the PCB substrate demonstrating 16 Tx and 16 Rx channels. (b) Polymer waveguides on a flexible substrate demonstrating 24 Tx + 24 Rx channels. (c) Passive shuffle cable. (d) Diagram of optical module construction and assembly.*

pete with copper at on-card distances, optical PCB technology based on polymer waveguide integration with VCSELs may provide the right combination of low-cost manufacturing, module density, and semicustomizable integration [44] - [48]. Fig.1.14 shows various elements of this technology, including examples of (a) waveguides fabricated directly on PCB, (b) waveguides on flex and (c) passive shuffle element. Fig.1.14(e) shows the construction of the optical module used in Fig.1.14(b). The Si driver and receiver IC along with the VCSEL and photodiode arrays are solder attached to a Si carrier. Holes in the Si carrier allow optical access. The optical path is completed through a two lens system to couple light into the waveguide mirrors. The two lens system allows a greater misalignment tolerance ($>$ 20μm for 1 dB loss) for the step of attaching the optical module to the PCB, although the single lens arrays must be attached to their respective sides of the assembly with better tolerance ($< \sim 5\mu$m). While thermal expansion mismatch is not a problem for attachment of the Si carrier to the underlying organic substrate, some curling of the flex can be observed due to some thermal mismatch between the underlying flex substrate and the polymer waveguide film. The prospective for this technology is to provide an optics technology with the characteristics of electrical PCB technology. PCBs are based on low-cost mass manufacturing methods, yet are customizable for a particular users needs. An optical PCB would mitigate fiber management problems within the card and provide high-density optical transceiver integration close to the processing chips. In order to facilitate a transi-

tion to this technology, early offerings would be in the form of an easily replaceable waveguide on flexible substrate assembly, mounted above the board, similar to a fiber ribbon. When, in the future, the technology is be more developed, the polymer waveguides would be incorporated on or within the PCB. While very promising, this technology still has some hurdles to overcome, including improvement in polymer and connector losses and achievement of an infrastructure to allow widespread use of the technology.

Silicon Photonics Technology

Finally, silicon photonics is a promising technology which has been studied since the mid 1980s [49], [50], as a platform for optical communications. The technology utilizes single-mode fiber in combination with unmodulated lasers and silicon-based modulators and detectors [51] . This technology may offer the ultimate in integration capability as well as low cost by utilizing mature CMOS fabrication to produce highly integrated assemblies with most elements fabricated directly in CMOS. In addition, by greatly reducing the costs of introducing wavelength division multiplexing (WDM) capability, which allows multiple wavelengths on the same fiber, the costs of fiber cabling and connectors can be amortized over much greater BW per fiber. Figure 1.15 shows some of the technology elements which are required [53] - [56]: Si waveguides, integrated Ge detector, modulator based on either a Mach-Zehnder interferometer or ring resonator and WDM multiplexing elements. The technology has matured significantly over the years with commercial products available today in an active cable form [51]. The technology requires use of single-mode fiber and longer wavelengths (typically $\sim$1300nm or $\sim$1550nm), to take advantage of already developed continuous wave (CW) telecommunications single-mode lasers which operate in a region where Si is transparent. Si-photonics-based transceivers are incompatible with the shorter wavelength and multimode technology based on VCSELs. Active cables offer a good initial entry into the market, since interoperability is not an issue. In addition, the lower signal distortion and losses experienced in single-mode fiber at these longer wavelengths allows longer lengths (e.g., 2 km) at high data rates which are of potential interest in very large installations, and not easily attainable with multimode links. The much lower parasitics of highly integrated electrical and optical devices will be of great help in improving power consumption at high data rates. In order to design modulators, Si photonics will, however, have to contend with the nature of Si as an indirect bandgap material which must be coaxed into performing optically. Modulator design is an exercise in balancing optical BW, temperature sensitivity and control, power con-

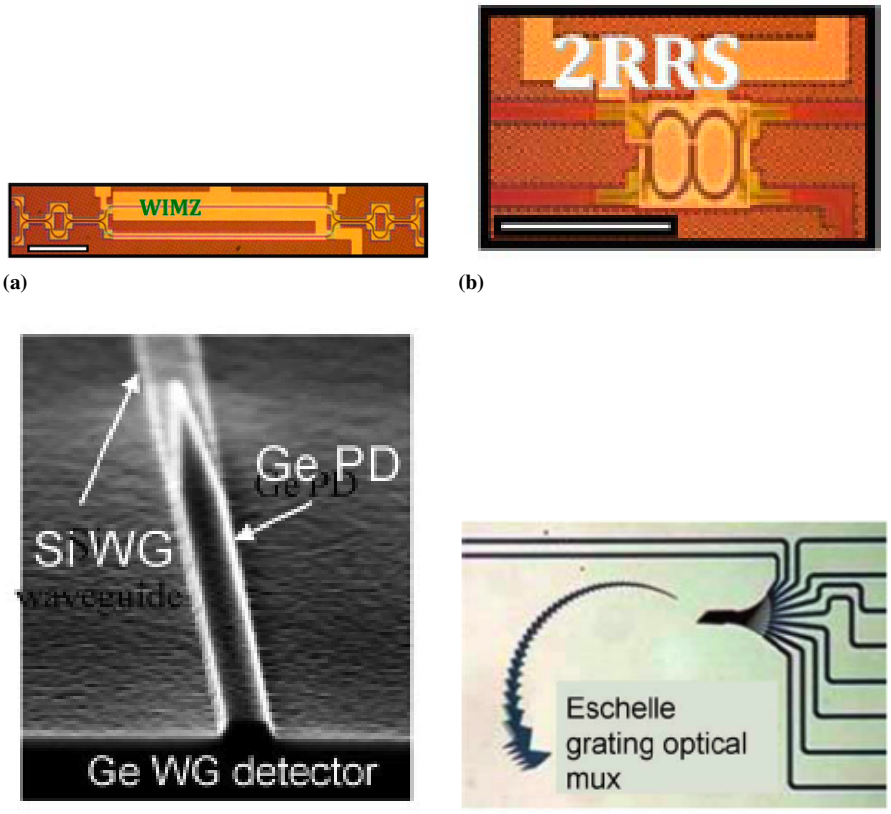

(a) (b)

(c) (d)

Figure 1.15: *(a) Wavelength insensitive Mach-Zehnder modulator. (b) Double-ring resonator modulator. (c) Integrated Ge photodetector and Si waveguide. (d) Optical multiplexing/demultiplexing based on an Eschelle grating.*

sumption, and optical losses. Laser light sources can be packaged onto the chip [49] or located at a convenient location off-chip and coupled to the chip via fiber. The on-chip location offers the convenience of more integrated and potentially lower cost packaging but will be exposed to a more challenging thermal environment. The off-chip location offers a separated environment for the laser, such that the temperature (and therefore wavelength) can be more accurately controlled. A lower temperature environment may help improve laser reliability as well. In addition, one might conceive of high-power off-chip lasers which could be split among many transceivers thereby amortizing the cost of the laser and the laser packaging and cooling across many more optical channels. Packaging is another area that is often overlooked in discussions on Si photonics. While the Si photonics chip itself may be of relatively low cost, the coupling of the chip to fiber and the addition of a CW laser can add substantial cost. Packaging which meets single-mode tolerances (typically < 1μm) can be considerably more expensive than packaging which meets multimode tolerances ($\sim 10\mu$m). In addition to the cost of the laser, an optical isolator may be required, as single-mode edge-emitting lasers are more sensitive to reflected light than multimode VCSELs, and the amount of optical feedback must generally be quite low ($\sim$-30 up to -40 dB). Finally, one must consider total power consumption for the Si photonics links. While there is significant potential for very low power optical links (e.g., modulator performance in the $\sim$100fJ/bit range [57]), designs with a practical balance of performance and temperature tolerance and a proper accounting for all power sources (including temperature control, CW laser, and any control or clocking logic) may find that this potential advantage is significantly eroded. Ultimately, another big challenge for Si photonics may be to integrate these optical transceivers directly into a 3-D chip stack, and although, this will require significant development and maturation, will be difficult for any other technology to match.

In addition to the active transceiver technologies discussed previously, linking these transceivers across cards, boards, or racks will require passive connectors and cabling. In the case of fiber-based VCSEL links, these rely on well-developed parallel fiber ribbon and connectors, e.g., MPO (Multi-fiber Push On), which have been used formany years for these multimode links. Connector losses are typically no more than 0.5 dB, including misalignment tolerances. For polymer-waveguide-based links, longer connections (e.g., 1 m between boards) will require improved losses if polymer waveguides are to be used; however, the use of a waveguide to fiber connector also allows use of lower loss fiber for these links. These connectors

can have additional losses of about 0.5dB due to the geometric mismatch between the round fiber core and the square waveguide core (may be asymmetric depending on choice of dimensions). Si photonics technology will require single-mode fiber and connectors. These connectors can typically have 0.25 dB additional loss (over multimode) due to the tighter alignment tolerances required, although lower loss components are available at higher costs. In addition, greater care must be paid during assembly to prevent contamination from ambient particulates, which can more easily degrade these single-mode fiber connections than multimode connections as dust can more easily occlude the smaller single-mode core size (9μm versus 50μm for multimode).

1.4 Interest and relevance

In this chapter an overview of the different interconnection levels, from the WAN to intra-chip has been presented. In particular, the interest of this thesis focuses mainly on the board-to-board connections. As described, in this particular field, connections are made typically through electrical backplane, but, for the today required transmission capacity they started to present some limits in terms of transmitted bit rate and power consumption. In this frame, optical solutions arises interest and start to be taken into considerations, providing "transparent" interconnections matrices to the bit rate and modulation formats, characterized by a high scalability for future upgrading of the capacity and low levels of power consumption, also thanks to the use of transmission modules employing VCSEL array as sources. The aim of this thesis is to understand and quantify the real benefits from a point or view of complexity of implementation, transmission perfromance and power consumption of an optical solution. In particular, it has been tried to identify solutions that ensure simplicity of implementation, and which exploit nowaday off-the-shelf technology. The objective is to understand the real applicabiliy of the proposed optical solutions and their potential for evolution to next capacity upgrade. In the second chapter, a comparison between an electrical and optical backplane have been given. Through simulations, it has been possible to design the best electrical backplane obtained with the available technology on the market. Then, a comparison with respect a possible optical fiber-based backplane, using VCSEL as sources, in terms of power consumption and capacity have been presented. A real implementation of the fiber-based optical backplane have been carried out and the main steps and aspects have been discussed. As told before, optical data links should guarantee also a complete transmission transparency in the in-

terconnection also with the external network, i.e. a travelling signal must be allowed to pass through the backplane network on a determined internal link without any need of opto-electronic and electro-optic conversion and processing. A center-launching technique has been exploited to satisfy that requirement. Experimental and simulative analysis have been carried out in order to test the achievable performances and robustness of this technique, making it suitable for backplane-based connections. To increase the backplane transmission capacity, maintaining the same number of optical connections, multi-level modulation format have been considered, in particular we focused the attention on Pulse Amplitude Modulation (PAM) and On-Off-Keying modulation format. Beyond a common VCSEL-based technology, a possible alternative technology as Silicon Photonics have been analyzed, comparing them in terms of power consumption and performances through simulations results.

CHAPTER 2

Optical fiber-based backplanes

The present Chapter presents a comparison of the performance achievable with the best technologies available today for the electrical backplane with the ones provided by an optical backplane designed by means of fiber-based interconnections. A simulative analysis on different Cu-based electrical backplane architectures have been carried out to find the best Cu-based backplane configuration achievable nowadays to support 20Gb/s. Moreover, a fiber-based optical backplane realized exploiting VCSELs as optical sources is proposed. A comparative analysis in terms of capacity, power budget and consumption between the found best achievable electrical (Cu-based) backplane configuration and the proposed optical solution is finally presented. The last part of the chapter is dedicated to the description of the realization steps performed to achive a real fiber optic-based backplane solution.

2.1 Introduction

The exponential growing of the requested bandwidth capacity of backplane component is driven by information technology and telecommunication equipment [58]. The solutions currently used are based on copper

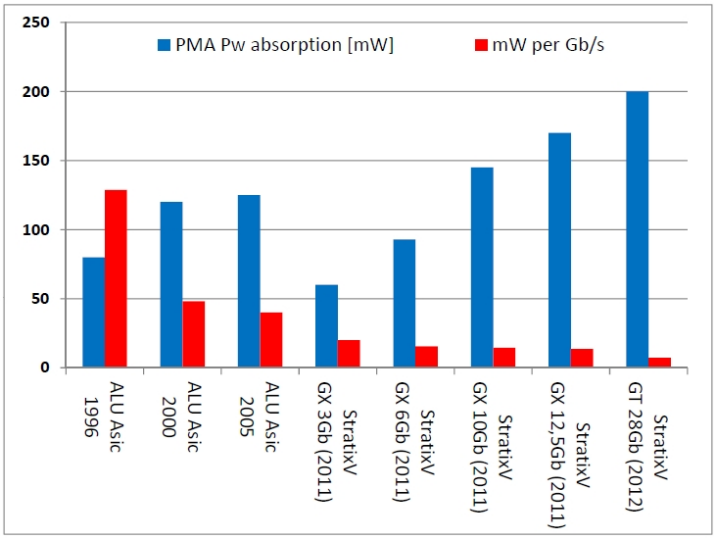

Figure 2.1: *Electrical transceivers evolution.*

interconnections via backplane, driven by a suitable transceivers subsystem. Looking at high-end telecommunication equipment transceivers are directly integrated on the same silicon chip used for the switching function or Input/Output (I/O) function. The transmitting and receiving interfaces, the connectors, and the Printed Board (PB) technology have evolved, allowing us to increase the single interface bandwidth. In parallel the amplitudes of the transmitted signals has been reduced, to limit power consumption and increase the integration. In Fig.2.1, as an example, the power consumption evolution of Optical Multi Service Network / Packet Transport Network (OMSN/PTN) product family exploited by Alcatel Lucent (ALU) is reported. The power figures take into account the complete chain from two blades attached to the backplane, including driver and receiver. According to the specific application, proprietary ASICs or standard commercial components are used (for ALTERA device Altera Stratix GT 28Gb device is considered where the Physical Media Attachment - PMA - includes serialization and de-serialization operations, pre-emphasis, Clock Data Recovery - CDR - and equalization). In general it's observed the progressive capacity to enhance the power density in a single device and while the consumption measured in mW per Gb/s has had an exponential decrease, the consumption of the interface including Serdes, CDR, pre-emphasis and equalization is growing. Furthermore, complexity and density increase is supported by the evolution and more maturity of silicon technology able to manage more

W/mm^2. The realization of the transmission lines in PB even if based on the most sophisticated materials available on the market, shows very significant losses at very high operation frequency. Also connectors, even if now very optimized, contribute to increase loss and crosstalk. The electrical backplane (as underlined explained in the first chapter) is close to reach its limit and for that reason we need to explore alternative solutions. Due to the fact that optical technologies [8] [59] are able to provide higher capacity over longer distances than electrical transmission systems, the natural answer to the limitations shown by the copper-based interconnection is to exploit optical solutions. For optical interfaces the bandwidth density scaling necessary to face the future Ethernet requirements is achieved through the reduction of the pitch size (presently to about 50μm,) and applying 2D arrays of Vertical Cavity Surface Emitting Lasers (VCSELs) and PINs [60]. Optical fibers constitute a good trade off in terms of bending losses, coupling efficiency with VCSEL sources, costs and attenuation [61]. Multimode multicore fiber and/or 2D polymer waveguides are being prototyped to match the demand [2]. However, the technological solutions to realize an optical backplane may be different and have recently been taken into account.

2.2 Simulative analysis of copper-based electrical link

In the present section the model of a complete connection from transmitter (TX) to receiver (RX) via copper-based backplane is presented. Then the model has been used to evaluate power consumption and transmission capacity of copper-based backplane, which will be presented in the next section.

Electrical backplane performances evolve year over year having the target to maximize both the line rate and the number of the connections. This evolution is driven by microelectronic technology and the material used for the backplane substrate. In the carried out simulations it has been considered a connection from a transmitter set on the I/O card to a receiver on the matrix card. The I/O card is connected to the matrix board through a Cu-based electrical backplane, as shown in Fig.2.2. In Fig.2.3 a block diagrams of the considered electrical system is shown. The target is to calculate the power consumption of this architecture together the transceiver data (for example from the ALTERA device) and the information about the attenuation of copper link, obtained through a simulative analysis. To simulate the attenuation of the Cu-based link the commercial simulation tool

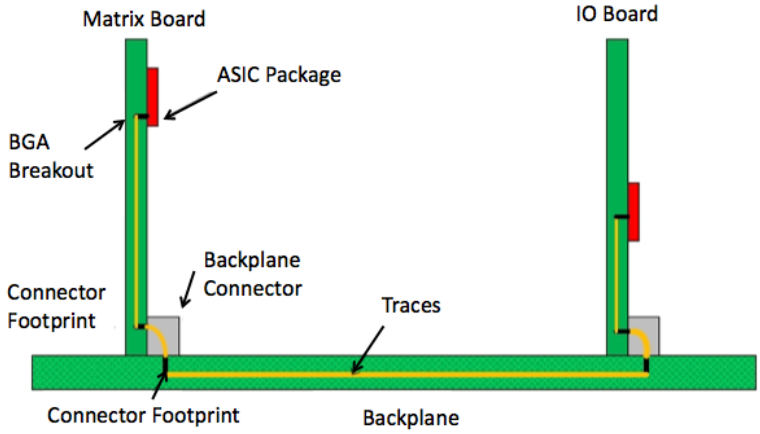

Figure 2.2: *Typical electrical interconnection via backplane*

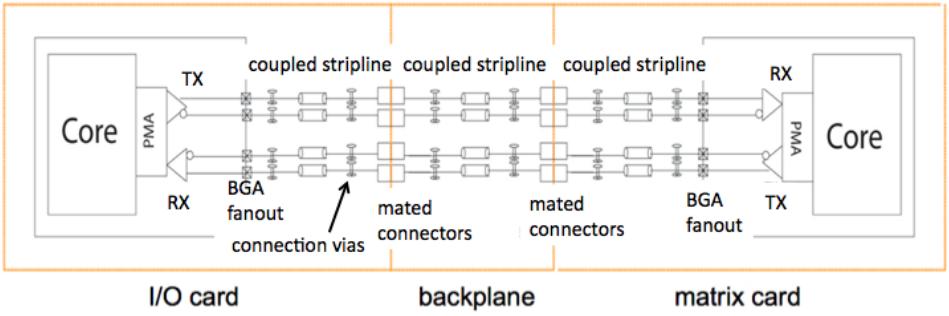

Figure 2.3: *Electrical solution scheme: copper-based interconnections.*

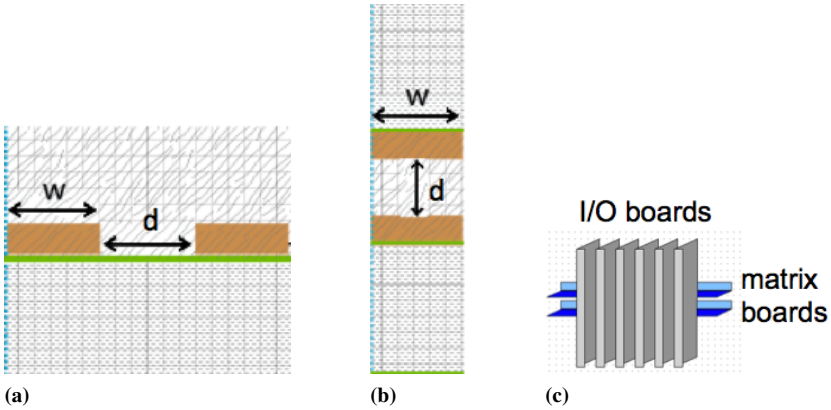

Figure 2.4: *The brown rectangles represent the striplines, w is the stripline width and d is the stripline distance. (a) the horizontal coupled backplane. (b) the vertical coupled backplane. (c) the so-called "midplane"*

HyperLynx has been used [62]. Three different possible backplane configurations have been analyzed: the horizontal coupled striplines in the backplane (Fig.2.4 (a)) , the vertical coupled striplines in the backplane (Fig.2.4 (b)) and the so-called midplane (Fig.2.4(c)). In the first geometry both the Cu coupled striplines are on the same plane. In the second one the coupled striplines are in two different plane of the backplane "stackup", separated by a dielectric layer. In the midplane configuration, I/O board and matrix board are orthogonally directly connected through ad-hoc connectors. A systematic series of simulations has allowed finding the best backplane configuration and I/O/matrix combination to optimize the performance of the copper-based link. To achieve this goal different dielectric materials available on the market and their related roughness have been considered (FR4, Megtron-6 and Rogers), the width of the copper striplines (copper thickness: 17μm -end processing 15μm) and the dielectric thickness have been changed with respect to the possible maximum thickness of the backplane. We simulated different lengths of the copper striplines (from 30 cm up to 60 cm), taking into account the presence of standards via or back drill via (the best case has been considered with a precision of $\pm$76μm). The back drill via model is shown in Fig.2.5. In Figures 2.6, 2.7, 2.8 are presented the screen shots of the backplane and board models used to calculate losses and the related "stackups". A "stackup" is a representation of the panel used to build a backplane or boards, and includes type of used material, number of layers, and the power supply and ground points. Impact Molex Connectors model has been used to simulate electrical connectors in all the

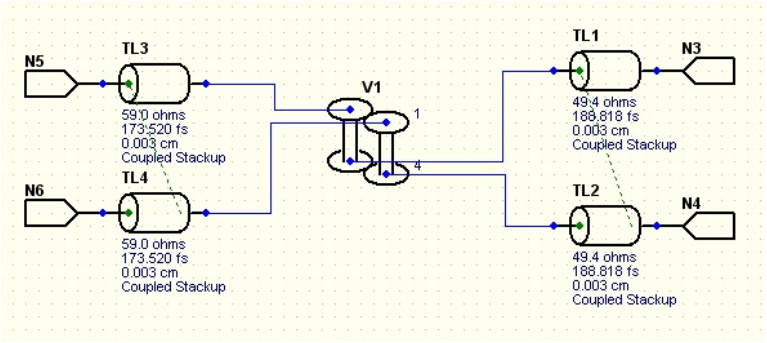

Figure 2.5: *Back drill via simulated model.*

Table 2.1: *Parameters used in simulations to achieve the best electrical configuration.*

	Unit	I/O PB	Matrix PB	Horizontal coupled backplane	Vertical coupled back-plane	Midplane
Material		Megtron-6	Megtron-6	Rogers	Rogers	Rogers
Thickness board	μm	2208	3207	7631	7631	3000
Number of dielectric layer		20	24	36	36	N/A
Stripline width w	μm	100	127	350	255	N/A
Stripline distance d	μm	150	178	340	344	N/A
Differential impedance	Ω	84	94	95	95	N/A
Core dielectric thickness ρ	μm	110	130	356	356	N/A
Line length	cm	10	20	30	30	0

boards/backplane models. Moreover, we have taken into account that in the same layer there are only co-directional signals. The simulations have been realized considering the board temperature at 55°C and 65°C, according to the real operating temperatures. Table 2.1 resumes the best I/O board, matrix board and the backplane characteristics used in the simulations to achieve the best condition for each configuration taken into account. The low impedance value of the I/O board is limited to the maximum thickness of the board. Figure 2.9 shows the attenuation of the three different Cu-based link configurations. In terms of attenuation the midplane seems to be the best solution, but this configuration is affected by cooling problems and for this reason it has not been considered in the following power analysis. Horizontal and vertical coupled configuration curves are similar up to 15 GHz, beyond this value the horizontal coupled backplane solution is more convenient. The ”holes” visible in the simulation curve are due to the residual stub in back drilled vias and connectors characteristics, which generate a discontinuity.

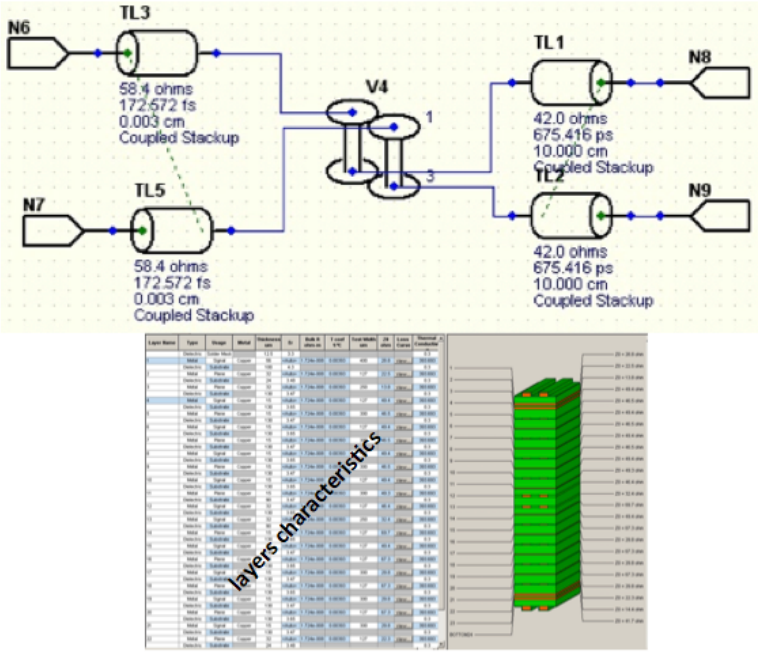

Figure 2.6: *IO card simulated model with standard vias (top) and related "stackup" with 20 dielectric layers (bottom).*

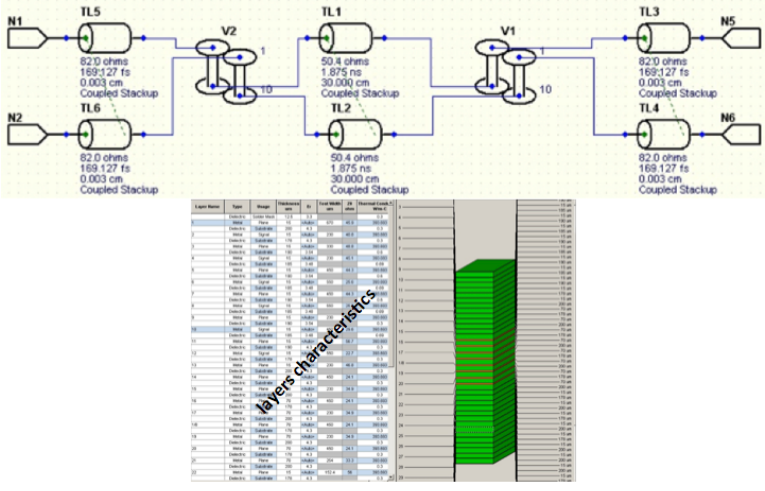

Figure 2.7: *Backplane simulated model with back drill vias (top) and related "stackup" with 36 dielectric layers (bottom).*

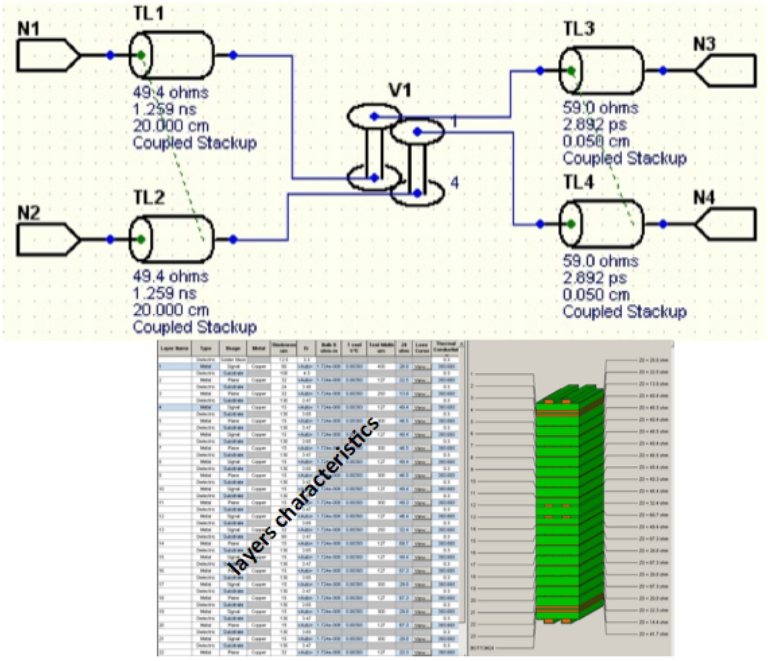

Figure 2.8: *Matrix card simulated model with back drill vias (top) and related "stackup" with 24 dielectric layers (bottom).*

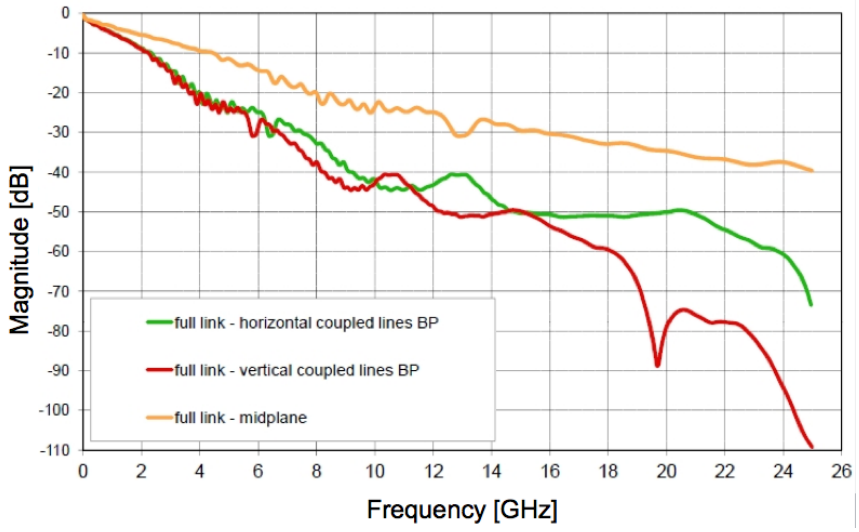

Figure 2.9: *Link attenuation vs frequency.*

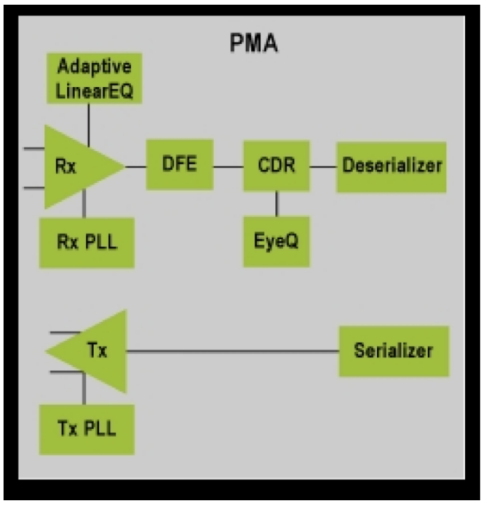

Figure 2.10: *Altera PMA block.*

2.3 Electrical and optical backplane solutions

In the previous section the best backplane configuration (horizontal coupled striplines) and the best match between I/O card and matrix card has been described. In this section a comparison between this achievable electrical backplane and an optical fiber-based backplane in terms of power consumption and capacity will be discussed.

2.3.1 Performances/limits evaluation of copper-based electrical backplane

For the electrical solution analysis the transceiver of Altera, Stratix V GT 28Gb device described in [63] have been taken into account. The Physical Media Attachment (PMA) block is shown in Fig. 2.10 and includes serialization and de-serialization operations, pre-emphasis, Clock Data Recovery (CDR) and equalization. PMA is 1.2 V supplied and the absorption depends on the operating frequency. The core chip is 0.9 V supplied. The last block of transmission buffer is 1.5 V supplied and the absorption depends only on the output swing. The reported absorption power is referred to the entire PMA block. We considered the received power as the minimum power to guarantee error free in all the bandwidth of the receiver. In figure 2.11 we report the power analysis of the electrical solution in two cases: without and with equalization (note that the equalization function is not optimized to work at low frequencies). At low frequencies (up to 3.9 GHz) the equal-

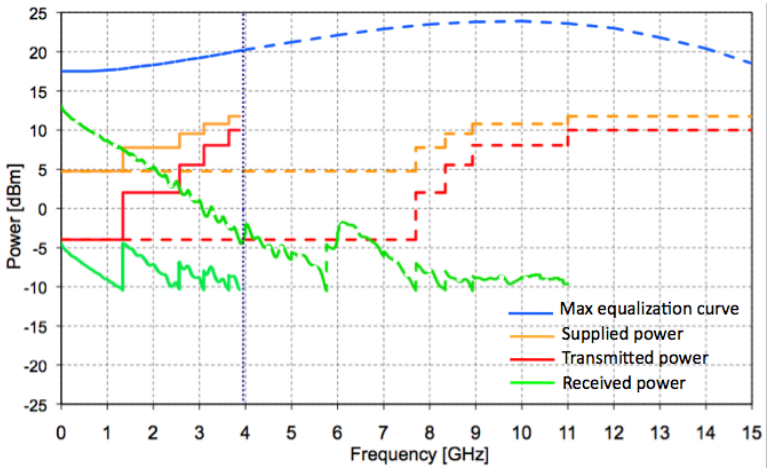

Figure 2.11: *Power analysis of electrical solution.*

ization function can be switched off (the transmitted, supplied and receiver power are represented by continuous curves). To increase the useful bandwidth is necessary to activate the equalizer (blue dotted line) to compensate the distortion introduced by the copper link, so you can reach about 11GHz bandwidth, which means approximately 20-22Gb/s transmission rate. The transmitted, supplied and received power, in case of equalization is working on, are represented by dotted lines in the picture. The results of the simulations constitute the best performance achievable nowadays with the most advanced solutions in terms of capacity and power consumption. This performance represents the reference for the solution based on optical interconnection proposed in the Section 2.3.2.

2.3.2 Analysis of an optical fiber-based backplane

In order to achieve a comparison with the optical solution in terms of power consumption an optical backplane have been ideally designed by replacing (see Fig. 2.12) the Cu-based interconnection line with silica optical fiber (for example standard multi-mode fiber); the output buffer of electrical line driver with a VCSEL source; at last, the first input stage of receiver buffer with a photodiode. In the fiber link we have considered fully optical connectors. The attenuation of the optical link includes insertion losses at the interfaces between Tx/Rx and optical fiber (about 0.5 dB respectively), insertion loss of 0.5 dB between ferrule-ferrule of the connector and a further loss due to the male-female connectors alignment. Hence, the total loss due to the optical link is about 4 dB. In the designed optical backplane it has

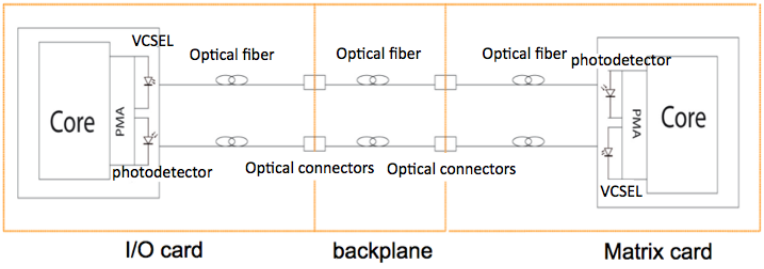

Figure 2.12: *Optical solution scheme: optical fibers based interconnections*

been considered an optical fiber less than 1-m long, so losses due to the fiber attenuation and losses depending on the transmission frequency are negligible. Optical single mode and multimode VCSEL sources have taken into account. VCSELs are already considered a very attractive solution for data communications as explained in detail in Section 1.3.1. They are capable to deliver highest modulation speeds beyond 40Gb/s [64]. At the same time they consume small amounts of power and can be mass fabricated at very low cost. In order to realize energy-efficient high-speed performance, large resonance frequencies must be achieved at a low drive current [65]. Recently, large progress on energy-efficient VCSEL was made at different bit rate [66]. For this analysis we have referred to data and performances from the present literature. For example, a very efficient single-mode 850-nm VCSEL with 56fJ dissipated energy for 25-Gb/s operation have considered. The threshold current is 0.15 mA and the bias current is about 1 mA to achieve error-free transmission [67]. The achievable transmittable power is about -3 dBm. If a commercial device to directly modulate the VCSEL is considered, with a 3.3V supply the power consumption for the VCSEL is 5.56 dBm. Instead, if a multimode 850-nm VCSEL is used the power consumption of the VCSEL is 6.68 dBm. The transmittable power is about 0 dBm. A V-I-Systems D30-850M photodetector can be employed with sensitivity about -9.5 dBm (BER =10^{-12} at 25 Gb/s) and the received power remains always higher than sensitivity value. Hence, for very short distance typical of optical interconnects, the transmitted frequency is not limited by the backplane implementation realized by means of optical fiber, but only by the bandwidth of the exploited optical TX/RX devices. In this analysis the performance of only commercially available devices have been considered.

In Table 4.5 are summarized the results in both solutions taken into account. In the electrical solution with no equalization we observe an upper

Table 2.2: *Comparison between electrical and optical solution.*

	Absorption power [dBm]	Max bit rate [Gb/s]	Power consumption [mW/Gb/s]	References
Cu-based interconnections (no equalization)	12.5	6-7	2.26	[63]
Cu-based interconnection (equalization)	12.5	22	0.81	[63]
Optical interconnection multimode 850-nm VCSEL (I_{bias}=1.41 mA)	6.68	25	0.19	[67]
Optical interconnection single mode 850-nm VCSEL (I_{bias}=1 mA)	5.56	25	0.132	[67]
Optical interconnection single mode 850-nm VCSEL (I_{bias}=1.5 mA)	6.95	28	0.18	[66]
Optical interconnection multimode 850-nm VCSEL (I_{bias}=5 mA)	12.17	40	0.41	[68]

limit of 6-7 Gb/s. With equalization it is possible to reach about 22 Gb/s, paying in terms of complexity and costs of the interfaces. It is a matter of fact that for the Cu-based electrical solution the main limitation remains the backplane line losses. In the optical solution we report the absorption power achievable in case of different VCSEL sources taken into account at different bit rate. For the comparison a V-I-Systems photodetector described above was used, with a -3dB bandwidth of 30GHz and the consumed power to achieve error free transmission is considered. Regarding the transmission up to 25 Gb/s, from the calculated results for the optical design taken into account, using the data reported in Table 4.5 and by the comparison with the results for the electrical solution, it's deduce that considering the same power budget, the optical solution can easily reach 25 Gb/s only depending on the transmitter /receiver bandwidth characteristics, consuming almost a quarter of power with respect to use electrical interconnections. As example in Table 4.5 also the performance of a multimode 850-nm VCSEL working at 40 Gb/s are reported [68]. Half power consumption per Gb/s is obtained doubling the bit rate with respect to electrical condition. Furthermore, to minimize the total power consumption in case of optical interconnection it is necessary to work on driving electronics besides the single transmitter and receiver bandwidths. Significant works continue to be done in this direction, promoting an increased chip-level of integration [2]. Anyway, in fiber-based optical solution there is no limita-

tion due to the backplane line.

In conclusion, simulations carried out in this work have allowed to evaluate the best performance of the optimized configuration of a Cu-based backplane exploiting the technology available today and subseguently A power analysis to compare the electrical solution with respect to a possible future optical solution based on a full optical fiber-based backplane has then been presented. In the electrical solution with equalization at a bit rate lower than about 20-22 Gb/s we achieve that the power consumption per Gb/s is higher than 0.8 mW. It is a matter of fact that for the Cu-based electrical solution the main limitation remains the backplane line losses. Using the same power budget and considering the performance of optical Tx and Rx devices, the optical backplane can easily reach 25Gb/s only depending on Tx/Rx bandwidths. Considering the characteristics of VCSEL sources and optical receivers presented in literature, the power consumption per Gb/s is achieved lower than 0.2 mW, almost one quarter than the above explained electrical solution. There is no limitation due to the backplane line if constituted by optical fiber. In the next future, it is expected significant evolution in terms of performance, power consumption and costs as soon as the optical backplane will be accepted by the industry and become widely used, accelerating the ability of the backplane to scale towards higher and higher capacity with low power consumption.

2.4 Optical fiber-based backplane realization

The backplane is the main board that interconnects other boards in the telecom and datacom applications (see Chapter 1). All information and telecom apparatus are organized in boards or blades and it's very important that the backplane guarantees both interconnection and power supply. Referring to the Fig.1.3 in the section 1.2 the S_3 link type determines whether the backplane is considered electrical or optical. A backplane is "all-optical" when all S_3 link types on the backplane are optical. Likewise, a backplane is "all-electrical" when S_3 link types are electrical. Hybrid opto-electrical backplanes are possible, in which some S_3 link types are optical while others are electrical. For each type, the link medium can be printed traces or cables. For the electrical link type, the link medium can be copper traces on a PCB or copper cables. Likewise for an optical link type, the link medium can be printed optical waveguides or optical cables (optical fibers). In practice, only printed traces are considered for electrical S_1 and S_2 links since electrical cables are not used for short chip-to-chip links [5].

In this work of thesis we have decided to implement a prototype of an optical backplane, exploiting optical fibers in S3 e S1 links, rather than integrated waveguides technology, as in recent published works [69] - [71]. In the following section some aspects (choice of proper optical fibers, design of new optical connector and definition of the best topology of optical fiber in the backplane) related to the implementation of a fiber-optic based backplane will be discussed.

2.4.1 Choice of the optical fiber: single-mode or multimode

In choosing the type of optical connection of the backplane different parameters have been taken into account and compared:

- density of connections (ports/cm^2);
- alignment tolerances in fiber-to-fiber and fiber-to- transmitter/receiver coupling;
- bending tolerances;
- cost and availability on the market.

In Table 2.3 are summarized some examples of potential solutions for the realization of optical connections and the relative encumbrance in terms of area and number of connections per cm^2. Both solutions already available on the market, such as single mode fiber (SMF), multimode fiber (MMF) or polymer fibers, and with technologies recently proposed in the literature or still in prototype phase are listed. The latter can then be taken into account to further increase the capacity transmission of the optical backplane. Silica-based waveguides are not usually taken into consideration due to their main problems of alignment among the waveguides, the laser transmitter and the receiving photodiode (because their small core dimensions the alignment is difficult and expensive). The polycarbonate polymer waveguides have recently been used to make optical connections to 1Gb / s on PC motherboards [72] (see Fig.2.13) and it has also been shown that the polycarbonate has the same mechanical properties of the FR4, the material used to make printed circuit boards, and can therefore be easily replaced for example for the realization of the panel of the optical backplane. In terms of occupied space, that means number of connections per cm^2, the use of optical fibers, single mode or multimode, is definitely to be preferred compared to polymer guides, especially in the realization of a backplane in which you want to guarantee a full-mesch interconnection between all

Table 2.3: *Some of optical connections types.*

Technology	**Hypotesis**	**Area [cm^2]**	**1/Area [1/cm^2]**
polymeric optical fiber	1mm diameter	7.9 e^{-03}	126
polymeric waveguide	500μmx500μm	2.0 e^{-03}	500
Silica-multimode optical fiber	50μm core, 125μm cladding	1.2 e^{-04}	8300
Silica single-mode- optical fiber	10μm core, 125μm cladding	1.2 e^{-04}	8300
Silica-silica waveguide	3μm core, 30μm cladding	0.09e^{-4}	111111
Silicon-silica waveguide	200nm x 480nm core, 3μm cladding	0.0081e^{-4}	1.23e^{6}
multicore optical fiber	7 core in 125μm cladding	1.7 e^{-05}	58100

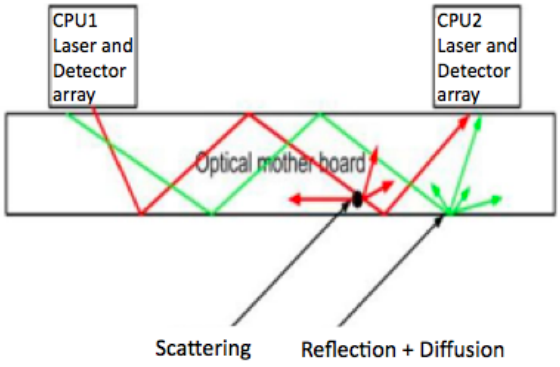

Figure 2.13: *Unguided optical communication bus*

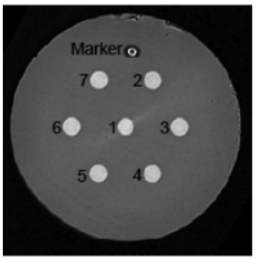

	Fibre A	Fibre B
Core Δ	0.38%	
Core 1 diameter	8.9 µm	8.1 µm
Core 2-7 diameter	9.4 µm	
Core-to-core distance *D*	30 µm	
Cladding diameter	125 µm	

(a)

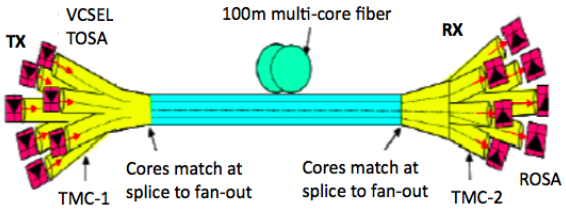

(b)

Figure 2.14: *Multicore optical fiber examples. a) multicore fiber section. b) 7 x 10 Gb/s transmission system over 100m multicore fiber (7 cores) with VCSEL sources and PIN receivers.*

boards connected one to each others via backplane. Recently, in literature, 70Gb/s fiber-based multi-core connections have been reported [73], [74] which with the same occupied area of a single fiber (external cladding diameter of 125μm as standard fibers) can contain up to 7/8 core as it's shown in the examples in Fig 2.14 (a) and Fig.2.14 (b). However, the effects of crosstalk between the different cores in dependence of the bending radius are still under study that may prove to be a limit to the applicability of this solution into an optical backplane.

Based on these considerations and the data reported in Table 2.3, we decided, to consider as possible alternatives for the realization of the optical backplane, standard single-mode or multimode fibers.

As shown in Table 2.3, multimode fibers have the same occupied space of single mode fibers (external cladding equal to 125 μm) but they have a core 5 times (area $\approx$50μm) larger than single mode fibers (area $\approx$10μm). The larger size of the multimode fiber core, helps in decreasing power losses at joints/connections point between MMF-to-MMF fibers, and the optical power losses induced by misalignments when interfacing transmitter / receiver-to-MMF and with other types of fibers, both in "direct coupling" mode and through the use of optics (lenses). Table 2.4 and Table 2.5 show

Table 2.4: *Coupling tolerances in case of: TX-to-MMF, MMF-to-RX and MMF-to-MMF connection.*

IN/OUT	Coupling tolerances		
	Direct coupling	Lenses	45° mirror
TX/RX	n.a.	7μm for 1dB loss	to be tested
MMF	7μm for 1dB loss	\	\

Table 2.5: *Coupling tolerances in case of: TX-to-SMF, SMF-to-RX and SMF-to-SMF connection.*

IN/OUT	Coupling tolerances		
	Direct coupling	Lenses	45° mirror
TX/RX	1μm for 1dB loss	2.5μm for 1dB loss	to be tested
SMF	2.5μm for 1dB loss	\	\

the coupling tolerances relative to MMF and SMF, respectively, both in the case of interfacing transmitter or receiver with a fiber and in the case of a fiber-to-fiber connection. For this analysis a single mode VCSEL with a 8μm mode field diameter (MFD) has been considered as a transmitter. The coupling efficiency with a MMF is very low due to the small size of the output beam of the VCSEL and a lenses is usually used. For the same power loss of 1dB, it's observed how the MMF is more tolerance than the SMF (respectively, 7μm against 2.5μm), also in case of a direct connections between two optical fibers.

Another critical factor is power loss due to the fiber bending. Stresses set up in the bent fibers induce change of the refractive index of cladding and coatings of the fibers. This in turns causes a less confinement of the light that propagates in the fiber which leaks away reducing the signal strength. Depending on the layout, that is how the fibers are distributed in the backplane, the optical fibers are subjected to very small bending radii, mostly close to in/out connectors in the backplane, due to very high density of optical fibers present in the backplane and the size of the FR4 layer used for the backplane (e.i. its thickness). It's note how for similar bending radii (7.5mm and 5mm) the power losses in the multi mode fiber are in the same order of magnitude respect to the single mode fibers. In our case, if the measured losses due to the bending are excessive for the available power budget, then there are some types of optical fibers, called "bend insensitive" where the power losses depending on bending decrease respect with standard optical fibers [75] - [77]. For instance, for a 15mm radius the power

losses decrease from 1dB to 0.1dB if a bend insensitive Corning fiber is used. OFS, Corning and Draka are the major company producing optical fibers.

Cost is another determinant factor affecting the choice of the optical fiber. Actually, the distances in a backplane are very shorts (within 10 meters) and the costs per meter for single mode and multi mode fibers are very similar. Hence the big impact in terms of cost is the transmitter/receiver module to interface the optical fiber. The VCSEL optical source we have decided to exploit for the backaplane it is characterized not only by low power consumption level but also by low fabrication cost, due to mainly the avaiability of array of VCSELs. Especially it's notice that a TX/RX module with a multimode 850nm VCSEL interconnected with a multimode fiber are present on the market (Finisar, Avago, Luxetera) with prices reduced by 50% compared to DFB - single mode optical fiber based solutions [78], [79]. Also, multimode connectors cost less than single-mode connectors due to the more stringent alignment requirements of single mode fiber. In data center, pre-terminated solutions continue the overall cost advantage of multimode over single mode fiber, enabling the use of low cost 850 nm parallel transmission. Here, even with the cabling cost advantage of single-mode for longer links, the much lower cost electronics make multimode much more cost effective. Beyond 150 meters at 100 Gb/s (or 550 meters at 10 Gb/s), it is necessary to utilize single-mode fiber. The network designer or end user who specifies multimode fiber for short-reach systems still must choose from two types - 50 μm or 62.5 μm. 50 μm multimode fibers were first deployed in the 1970s for both short and long reach applications. 62.5 μm multimode fiber, introduced in 1985, supported campus applications up to 1990s, with the introduction of the VCSEL laser light source, saw a shift back to 50 μm fiber. Today, 50 μm laser-optimized multimode (OM3/OM4) fiber offers significant bandwidth and reach advantages for building applications, while preserving the low system cost advantages of 850 nm-based multimode fiber. In new installations, only 50 μm OM3/OM4 laser-optimized fiber is recommended for today's high-speed enterprise networks and data centers. 62.5 μm (OM1) fiber, or older 50 μm (OM2) fiber, is not recommended. For existing installations with OM1 fiber or OM2 fiber, users should carefully weigh the costs of re-cabling their network against the limited benefits of extending the current infrastructure. The ability to support high speed 10 Gb/s applications that are becoming common in enterprise networks is a key advantage of OM3/OM4 fiber. Since optoelectronic make up a large percentage of total

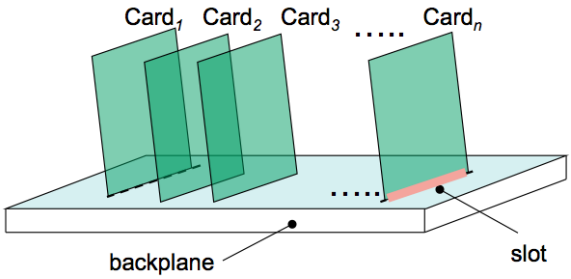

Figure 2.15: *An example of cards inserted in a backplane in their related slots.*

system cost, the most economical solution for multigigabit transmission in the enterprise is 50 μm OM3 or OM4 fibers designed and manufactured for use with inexpensive VCSELs.

This research has underlined how multimode fibers are comparable in terms of encumbrance, flexibility and bending tolerance with respect to the single mode fibers. Nevertheless multimode fibers guarantee major tolerances in transmitter/receiver- fiber and fiber-to-fiber connections, allowing easier mechanical design of the connectors used to interface optoelectronic boards to backplane. Therefore in the design of our backplane a solution based on VCSEL sources combined to standard multimode fiber has been considered.

2.4.2 Optical backplane characteristics

The complete system consists of a subrack, with a backplane, object of this research, which allows the interconnection between the various cards, both at the electrical (control signals, power, alarms, etc.), and at the optical level (traffic signals at high speed, 10Gb / s and beyond). The two types of signal will be distributed in different parts of backplane, redesigned from the solution currently present. In Fig.2.15 a simple scheme including cards, slots and backplane structures is shown. Slot is the dedicated space to the insertion of the card in the backplane (pink slice in the figure). The system is designed to have a bandwidth of at least 100 Gb / s per slot, with a full mesh architecture between all boards. This means that such architecture requires, a connection capacity of at least 100 Gb / s from any board to each others, including itself (see Fig.2.16). The full-mesh architecture has a higher number of connections compared to a dual star configuration, but avoids the central switching unit, decreasing the system costs, when it is under-used. In fact, in the apparatus with full mesh architecture, each card

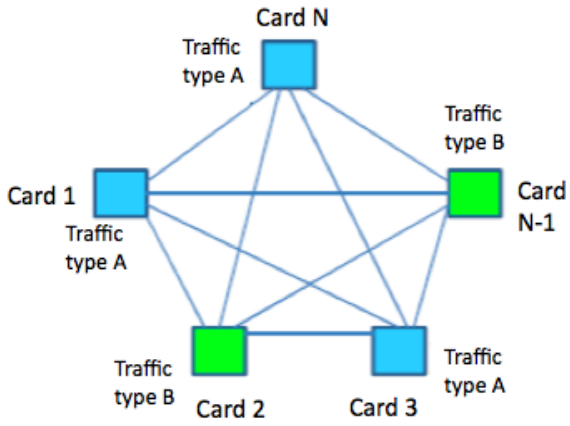

Figure 2.16: *Full-mesh architecture.*

has a portion of the switching capacity (the boards are all the same) and the apparatus can be initially configured with a minimum number of interfaces, to increase them successively according to the requirements (”Pay as you grows” concept). Furthermore, the full-mesh architecture allows the complete transparency of the system to the type of format and bit rate of the signal, or the coexistence of different sub-systems in the same sub-frame. Such architectural solution, taking advantage of the high transmission capacity of optical fibers used for the backplane, allows further increases the total bandwidth, simply by increasing the bit rate of the transmitted signals, using high-order modulation formats or Wavelength Division Multiplexing (WDM), without changing the backplane. A reference system architecture for the development of the optical backplane has been identified to be competitive in terms of transmission capacity, energy dissipation and cost compared to existing electrical backplane and in the meantime has to keep similar dimensions to be easily integrated in test real environments already in use. The main characteristics of the optical backplane are summarized below (assuming to use an optical fiber as a connection):

- full-meshed interconnection network;
- systems with variable configuration (flexibility);
- availability for direct line-to-line connections in order to be transparent to any type of complex transmission format (coherent) and bit rate
- no active devices on the backplane (neither electrical or optical);

- whole power consumption (including electro-optical (EO) and opto-electrical (OE) interfaces) lower than the present one
- very high reliability
- full compatibility with the existent production line
- costs lower or comparable with the present costs (Cu-based backplane: 700-1000$; for a batch of 20 pieces)
- 8 slots to non-default function;
- 8 optical connector for each slot;
- 12 optical fibers for each connector;
- bidirectional connections;
- 12Gb/s per fiber (10Gb/s useful traffic) with possible evolutions to 24Gb/s (10Gb/s payload to 20Gb/s);
- total thickness of the backpanel <15mm;
- occupied space in depth from the connectors <25mm;
- maximum acceptable error rate = 10^{-12}

A scheme of the overall configuration of the system, including the optical backplane and related electro-optical connections of the cards, is shown in Fig.2.17. It consists of 8 horizontal slots. Each card has 8 transmitter optical connectors and 8 receivers optical connectors plus a connector for electrical signals. In the first prototype of the optical backplane, the intention is to use a subrack already in use in Alcatel Lucent (Fig.2.18), taking advantage of the power supply and ventilation part, but, of course, this requires additional constraints on the layout of the backplane with respect to a complete re-design of the drum and the backplane. In an actual backplane (Fig.2.18) the 2 last lower slots are dedicated to matrix cards and the rest for interface boards. The new system, instead, has 8 boards (full-width) all equal among them, because the full-mesh architecture doesn' t require any centralized matrix cards. Therefore, the pitch of the cards have been changed in order to adapt the area for 8 equal spaces. The pitch is now 34.4 mm, the total width of the card is 353.2 mm, while the distance between the optical connectors in horizontal is equal to 37.5 mm. The two lateral sides have been changed. Currently the side wall is a metal grid that also contains the sliding guides of the cards. The grid has been redesigned, as

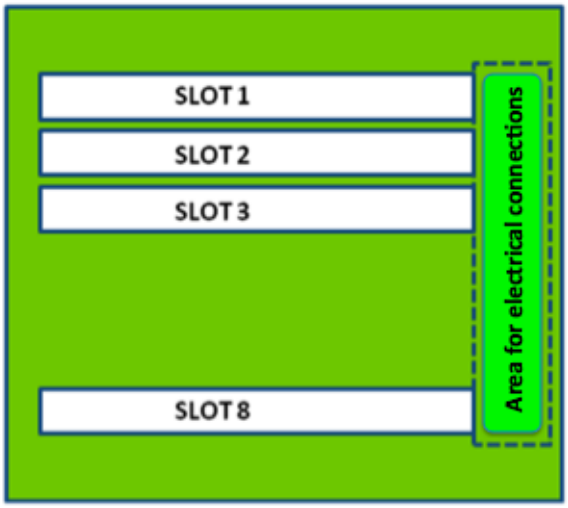

Figure 2.17: *Scheme of a complete configuration of the system.*

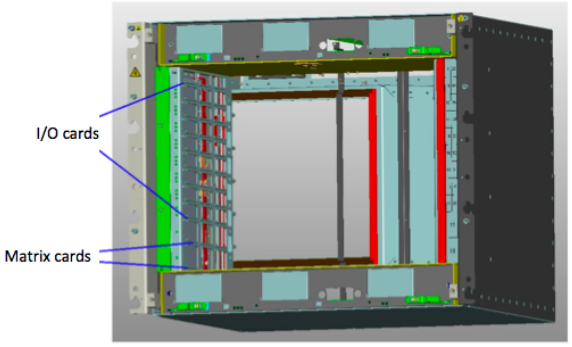

Figure 2.18: *Actual subrack used by Alcatel-Lucent.*

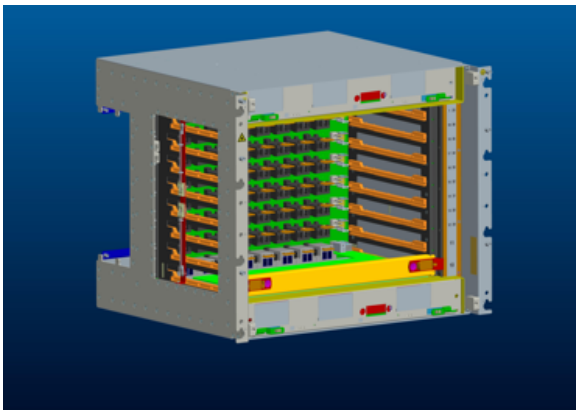

Figure 2.19: *New subrack.*

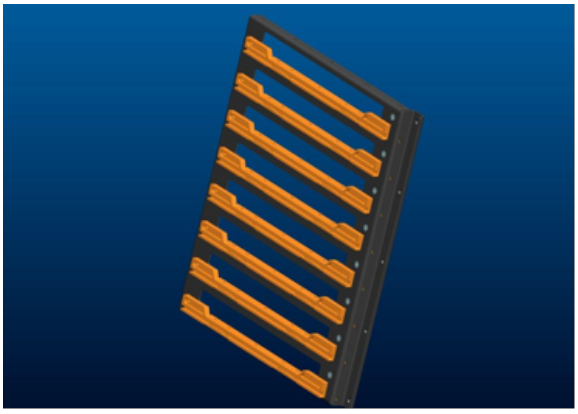

Figure 2.20: *Details: grid and sliding guides of the card.*

can be seen in Fig.2.19, eliminating the central part containing the guides for the sliding of the card, which have been replaced by plastic guides (the detail of the grid side and the guide is shown in Fig.2.20), hooked in holes placed at the two front and rear ends of the side.

Furthermore, it has been necessary to modify the profile of the upright side panel to allow proper working of the extraction lever of the card, see Fig.2.21. The final layout will have the characteristics shown in Fig.2.22 where 8 optical connectors and power connector for each slot are visible on the backplane. Each optical connector interfaces multimode fiber ribbons.Indeed the hypothesis of using individual fibers to be placed in the backplane has been discarded for the difficult in the management of placing 640 optical fibers. The ribbon are terminated with Mechanical Transferable (MT) ferrules and Multifiber Push-On (MPO) connectors. Developed in the

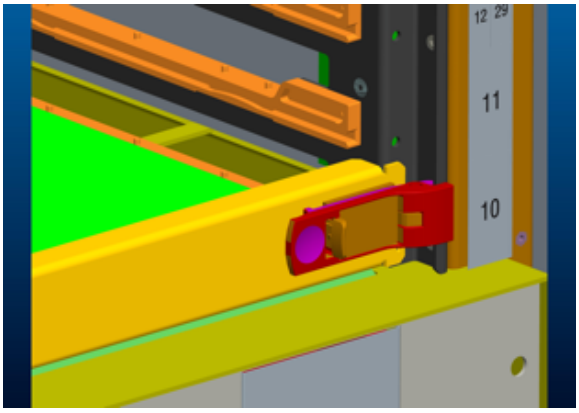

Figure 2.21: *Extraction lever of the card.*

Figure 2.22: *Hypothesis of final backplane layout.*

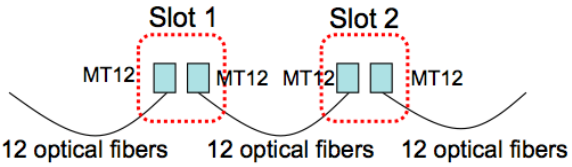

Figure 2.23: *12 optical fibers ribbon from/to TX/RX MT ferrule.*

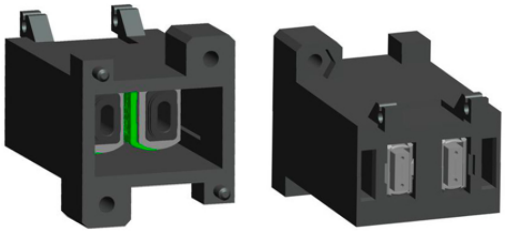

Figure 2.24: *Optical connector 3D-view for backplane: (a) back view; (b) front view.*

late 1980s by NTT, the MPO connector can be fitted with ribbons of 12 to 72 fibers [80]. The connector was first deployed to aggregate fibers and alleviate fiber congestion. Now, the demand of low loss and high density optical connector for high speed and high density transmission system is increasing. To respond to such a demand, suppliers have started to develop very low loss MPO connector, a push-pull, reconnectable connector which adopts MT connector ferrule. One MT ferrule with optical fibers attached is accommodated in each MPO connector [81]- [85]. The size of MPO connector (2.5 x 0.7 cm) limit the maximum number of connectors per slot. In order to obtain a full mesh connection 8 transmitters and 8 receivers on each card are required. If all 16 connectors were aligned, this would have required too much space. Hence, we had the idea to place together, side by side, in a single connector both the TX and the RX connectors as shown in Fig.2.23 with a custom solution. Each TX or RX connector interfaces a 12 fiber multimode ribbon. Recently, both connectors for backplane and card sides have been developed [86]. The final custom connector for the backplane is shown in Fig. 2.24. It complies with standard MPO - IEC 61754-7 and it's duplex.

We decided to use as much as possible commercial components and connectors, in order to minimize the cost of the project. For both connectors a protective housing has been designed and some samples are also available. In Figure 2.25(b) is represented the protective housing for the backplane connectors with a clip system to connect properly each card with the

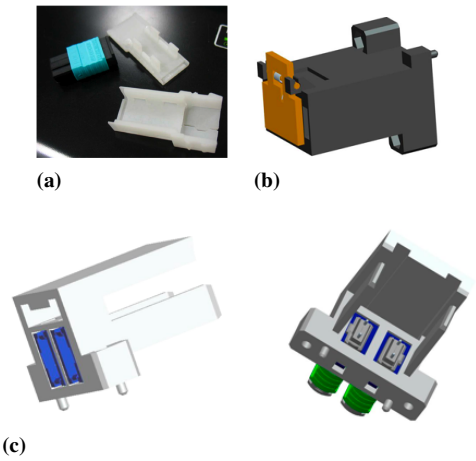

Figure 2.25: *(a) First samples of clip-housing for backplane connector.(b)Protective housing to put on backplane connector. (c) 3D-view of optical connector for the card.*

backplane to guarantee protection by external contaminating agents. The custom component called ”clip-housing” has been realized by 3D printing (rapid prototyping, STL by Compel). Figure 2.25(a) shows some first samples. Clip-housing and connector comply with the specifications of the standard MPO about mechanical tolerances which guarantee minimized power losses in the alignment between connectors on the card and backplane sides (see Fig.2.25 (c)).

2.4.3 Topology of the optical connections on the backplane

As explained in the previous subsection the goal is achieving an optical full-mesh interconnection using optical fibers. If 8 slots are considered and for each slot there are 8 connectors, and each connector has to deal with two 12-optical-fibers ribbons (TX+RX), in total 64 twelve-optical-fibers ribbon must be managed. Different optical fibers routing solutions have been studied and and one in particular has been chosen to be realized. Right now the patent of the new proposed layout is under evaluation. Hence only a general overview and the requirements we fulfilled for a preliminary realization of the optical backplane will be presented. Following, a summary of the characteristic of this routing logic:

- N slot with M connections from each slot to any other slots (in our case N=8 e M=64);
- no overpass between connections to avoid power losses;

- a minimum number of layers used in order to minimize production costs;
- no specialization imposed by the optical backplane to the slots (i.e. the cards) of the apparatus, to achieve maximum flexibility;
- the interconnection matrix can be developed "line-by-line" independently of other connections. In this way it adds an element of modularity (rows) and "scalability" (you can also add rows later) to the solution
- a simplification of the physical structure of the backplane with respect to the actual ones;
- guarantees a complete, neat and clean interconnection, without bypasses and crossovers;
- optimization of resources because it provides modularity, i.e. a subdivision into the backplane is possible.
- an increase in the transmission capacity;
- is not limited to a specific technology, but is applicable to any type of interconnection. In particular fits perfectly with the use of optical fibers or cables;
- a ”cylindrical” logic developed on a plane, facilitating the management, the process of building, supporting energy savings and a reduction in production costs.

The backplane must connect each slot to each other slot providing the same number of potential connections (connection full-mesh). The backplane must not impose any qualification to the slots of the apparatus, in order to achieve maximum flexibility. In this context, the interconnection between card and backplane must obviously be "blind", that means it must be connectable fully automatically with the deeply insertion of the card into the subrack. The information must travel from a transmitter to the receiver via backplane interconnection. At the beginning we planned to follow three possible solutions:

- to dig slots into the FR4 backplane panel following the layout design and place the ribbon inside
- to use an external device, called "telaio" to distribute the fibers and fix them to the backplane panel.

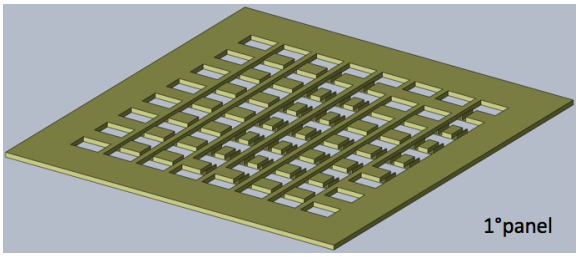

Figure 2.26: *An example of an FR4 panel.*

- to embed the fibers into the backplane panel

We have planned to dig or create ad hoc V-grooves (caves) with dimension about 3x3 mm, where optical ribbon are inserted. Holes are also realized in the panel, with size approximately 25x18 mm, to allow insertion of the connector. In Fig.2.26 some view of the backplane design in CAD software in which cave and holes can be seen. It has also been decided to place the connectors on the back of the backplane panel in correspondence of the through holes. In this way the ribbon with the MT ferule, during the fabrication stage of the backplane do not float in the air but are positioned and remain inside the connector (black rectangular in Fig. 2.27). In first analysis we have been taken into consideration the possibility to use both round ribbons and flat ribbons. The size of round ribbon are 3mm x 3mm and the flat one has dimensions of $\sim$ 1mm x 3mm. Each optical fiber is a standard OM2 multimode fiber with a core diameter of 50μm and a cladding diameter of 125 μm. Due to the space available between slots and connectors we studied different implementations in the case of using round ribbons and flat ribbons. In the first case, due to the incumbrance of the round ribbon, it has been proposed to implement the backplane on two layers, that means using two panels of FR4 and then, when the fiber ribbons have been placed in the right position according to the routing logic, put together both panels to complete the backplane. Some section of these panels are shown in Fig.2.27. Some channels have been dug out to put the ribbon inside. When the ribbon is into the corresponding connector area, the idea is performing a sort of "buttonhole" in the slot, so that there is sufficient play to hook the ferrule. It's also important dimensioning the distance between the inputs of the two ferrules in the connector ensuring that the ribbon in the ducts doesn't block the input/output of the ferrule to/from the connector. Another issue that it has been taken into consideration is related to the depth of the panel. It's important to be sure there is enough space to rotate and manipulate the ribbon with MT ferrule within the "connector area" and

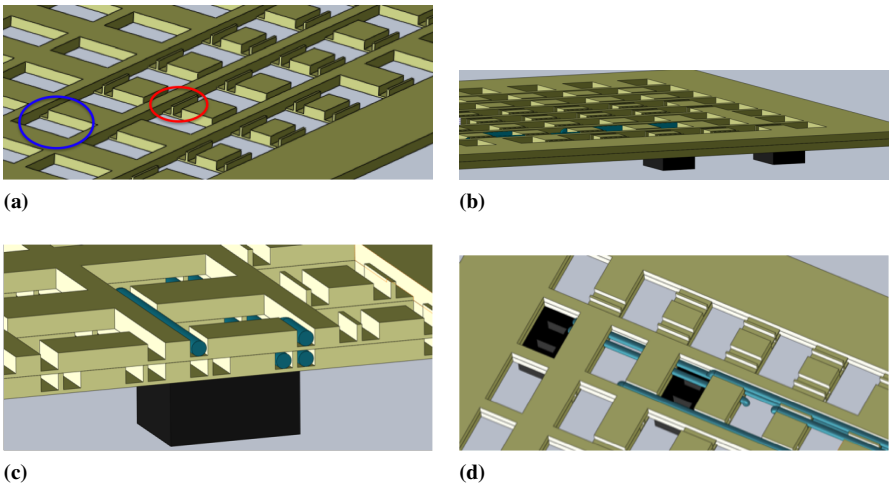

Figure 2.27: *Details of the optical backplane. a) Holes for connectors (blue circle) and ducts (red circle); b) connectors attached on the back of the backplane. c) Section of the backplane with two panels. It's possible to see connectors (black box), round ribbons placed in the duct and some empty ducts. d) Top view of a detail of the backplane.*

correctly insert the ferrule in the MPO connector. Preliminary characterizations performed on test panels have been used to define the minimum height of the panel. The topology of round ribbon deployment can not be shown as it is in the process of patenting right now. However it can be said that the topology found permits to have all connection on just two levels of FR4 and well-ordered arrangement of ribbons that allows a easy and fast deposition process. Moreover the handling of round ribbon performed by an automated robot, results easier with respect to flat ribbons and have less loss criticity from a point of view of bending. A possible disadvantage is due to maintenance service, because if there is something that does not work or broken in the bottom panel, it is necessary to disconnect all the ribbons on the top panel to fix the damage. For this reason we have decided to consider the solution based on flat ribbon, as in this case the topology we have been found would require only one FR4 panel. Flat ribbons are placed orthogonally to the plane of the backplane to be sure to have enough space to put all ribbons needed. In Figure 2.28 are shown some details of this solution: the thin red and green foils represent the flat ribbons inserted in the ducts orthogonally to the plane. The idea is to line up several parallel ribbons. There are several possible configurations of excavation of grooves to lay the ribbon and make easier the process of laying. If you have a look at the layout, the most critical case is when there are more than two par-

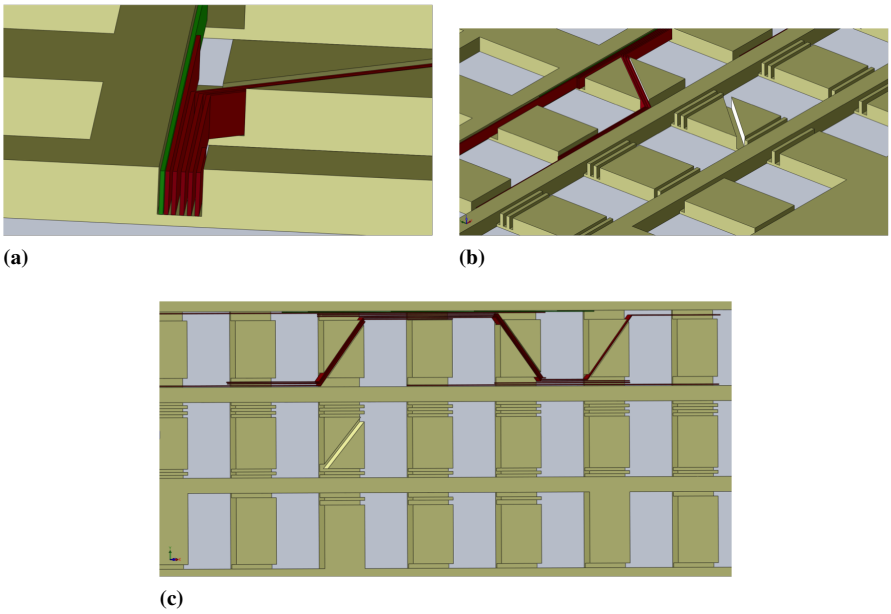

Figure 2.28: *Details of a flat ribbon-based optical backplane. Flat ribbons (red) have placed orthogonally to the backplane in the apposite caves.*

allel ribbons passing at the same time in the space between two adjacent connectors. It's possible to have one slot containing all ribbons together or more slots where the ribbons are shared. Some tests have been carried out by the ITIA group (Institute of Industrial Technologies and Automation) to identify the practical and simpler method to place them in the right position by an automated robot (Fig.2.29). For the automatization process the main difficulty is the vertical placing of parallel ribbons in the narrow milled grooves. As an alternative solution ITIA has proposed a sort of "ad hoc" auxiliary tool, called "telaio", made in plastic or other easily printed and economic material, that avoid to place the ribbons directly into the FR4. In this case all ribbons are connected in air, that is, are left floating, and only in the end this external structure, called "telaio", fixes and blocks all connections. From the assembly point of view, this solution has resulted to be the simpler one.
The direct embedding of fibers in FR4 is still under study as first experiment proves very high optical power loss along the embedded fiber due to high thermal and mechanical stress taking place during FR4 preparation.
In all proposed solutions the routing takes place without having crossing of the fiber ribbon which would give too high power loss along the connection. The main source of optical loss in the proposed solutions is the bending of

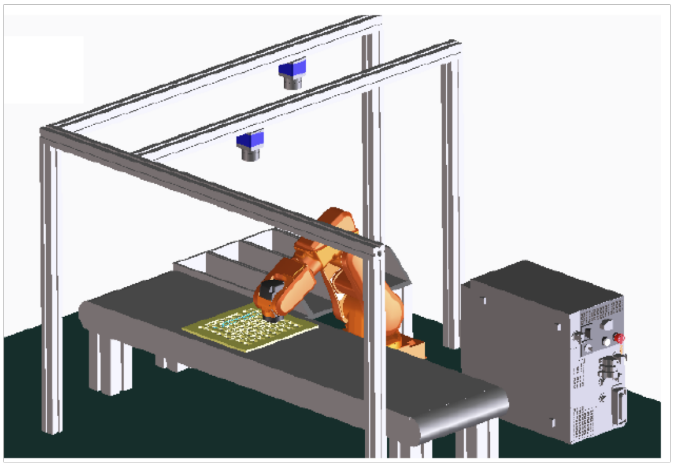

Figure 2.29: *Robot manipulation of the optical fibers in the backplane panel.*

the ribbon, especially inside the connectors. Some experimental tests have been carried out to quantify the losses due to fiber bending and to evaluate the minimum accetable radius of curvature of the MM fiber and verify the feasibility of the proposed solution.

Experimental setup to measure bending losses in MMF

As described in previous subsection, one of the critical aspects of the layout chosen for the routing of the optical fibers on the backplane is represented by the bending that the fiber ribbons must perform both inside the backplane and in input/output operations from the holes dedicated to the optical backplane connectors. Very small radii of bending may, in fact, introduce optical power losses to degrade the transmission performances in the backplane. Therefore, it has been considered necessary performing an experimental evaluation of the minimum radius of curvature able to guarantee an error free transmission, and, contextually, acceptable power losses related to the power budget aspects. In particular, to emulate and replicate same operating conditions that will realize in the backplane, a setup where a multimode 850nm VCSEL source is coupled into a standard multimode fiber have been realized and the power penalty introduced by the MMF bending have been evaluated. A 10Gb/s multimode 850nm VCSEL from RayCan with output power (P_{out}) about 1mW have been used (Fig. 2.30). The VCSEL is a LC-TOSA package and can be directly coupled to a fiber with LC connector. To drive the VCSEL a Finisar Evaluation Board 10GEBSWA (EB) have been used. Unfortunately the MM VCSEL

Figure 2.30: *Raycan pigtailed VCSEL with LC connector.*

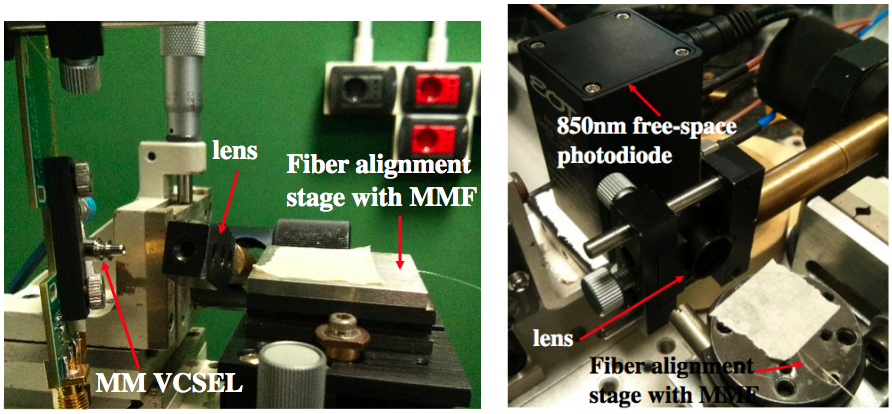

(a) (b)

Figure 2.31: *Some setup pictures: (a) free-space coupling between MM VCSEL and MMF at the transmitter side. (b) Focusing of the optical output signal from MMF to the photodiode area (60μm^2)*

has been provided without connector LC from MM fiber, so a free space coupling has been realized, using focusing lenses in both input and output at the multimode fiber as shown in Fig.2.31. The 50μm multimode fiber is about one meter long. For the optical-electrical conversion of the received signal an amplified photodiode EOT has been used with 9GHz bandwidth at 850nm. To test the penalty introduced by the bending, the MMF has been curved with different radii. In particular, the penalty has been evaluated in terms of optical power loss and Bit Error Rate (BER). In Fig.2.32 is shown the trend of the received optical power at the photodiode as a function of the diameter of curvature of the multimode fiber. Significant losses start to occur for diameters around 4-5 mm. At 3 mm diameter there are losses of 50% (-3dB). As will be explained in the next section, the commercial module of AVAGO, which will be used on the cards to be connected to

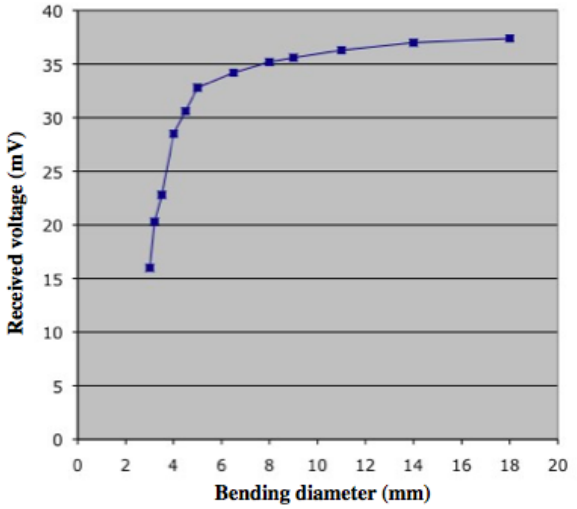

Figure 2.32: *Receiver side. Received voltage with respect to the MMF bending diameter.*

the backplane, has a power budget of 4.8 dB. Thus it is necessary that in correspondence of connectors the MMF bending has to be above 5mm. In Figure 2.33 are shown the BER measurements in function of the diameter of curvature of the MM fiber and, therefore, correspondingly as a function of optical received power. These measures are referred to the directly modulated NRZ-OOK VCSEL at 2.5 Gbit/s. In the absence of curvature, the 2.5 Gb/s transmission is error free (BER $<10^{-12}$). Significant penalties are visible with the BER worsening, when the bending diameter is close to 3-4mm. The BER measurements performed at 10Gb/s, shown in Fig.2.34, confirm the presence of a sort of ”knee” in BER curve in correspondence of 3-4 mm diameter of MMF bending. The measurements have provided at first indication of the bending radius beyond which the penalty of the multimode fiber transmission are no longer tolerable according to the specifications of the system. This information has been used for proper optimization of the size of the holes and connectors developed by the project team.

2.4.4 First prototype of an optical backplane subsection

By exploiting the solution called ”telaio”, a subsection of the optical backplane has been produced, including 8 double connectors TX/RX. In Figure 2.35 the ”telaio” is the white-plastic structure that embeds 8 connectors and 8 twelve-fiber-multimode ribbons. In order to individually analyze every connection, an adaptor (fan-in/out) has been placed to connect every TX/RX couple to each fiber of each ribbon. The target is verify that, using

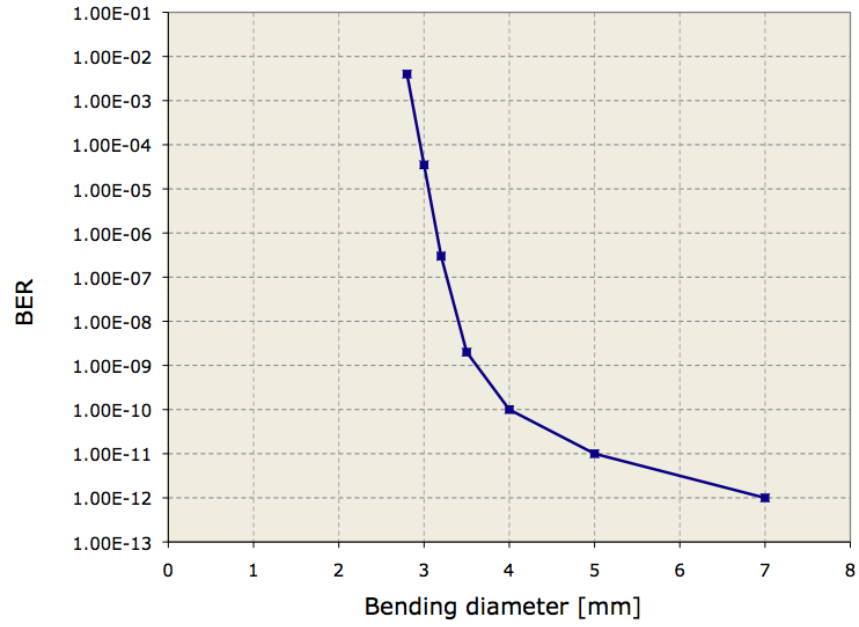

(a)

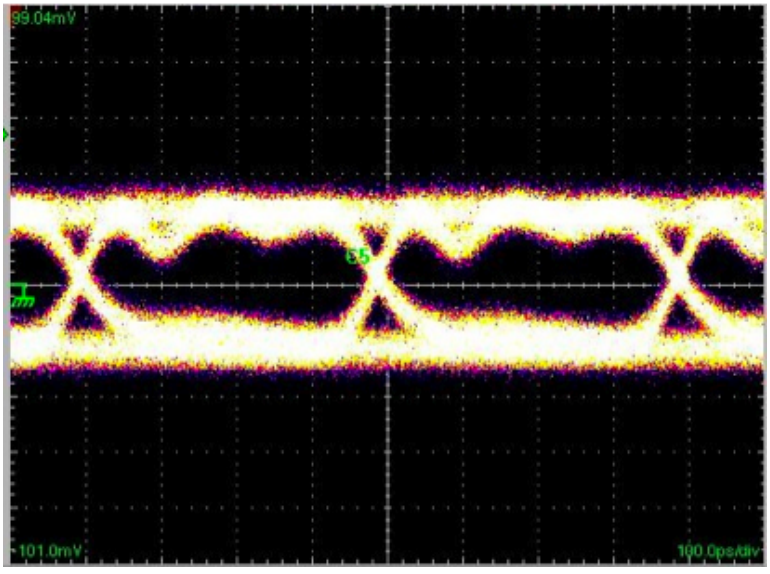

(b)

Figure 2.33: *(a) BER measurements at 2.5Gb/s vs MMF bending diameters. (b) Eye diagram at BER=10^{-12} for 2.5Gb/s NRZ-OOK signal.*

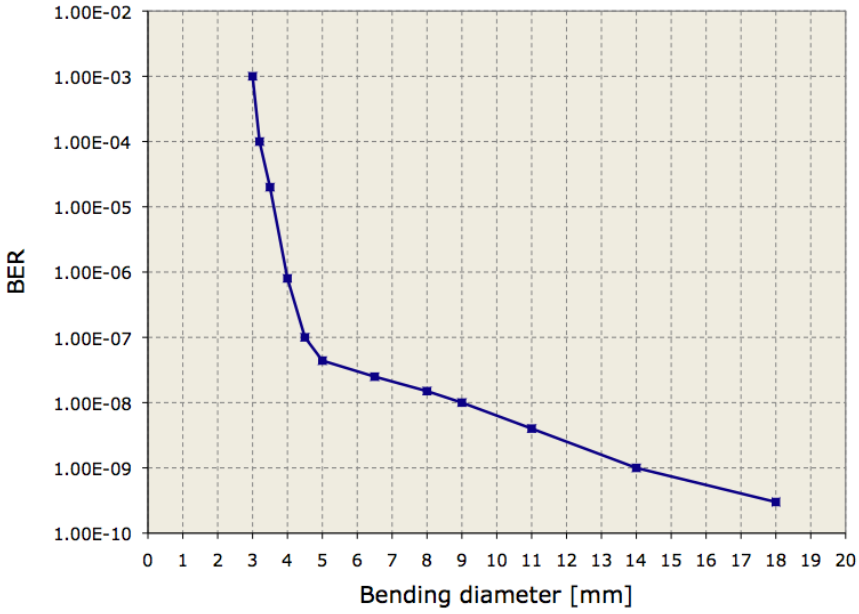

(a)

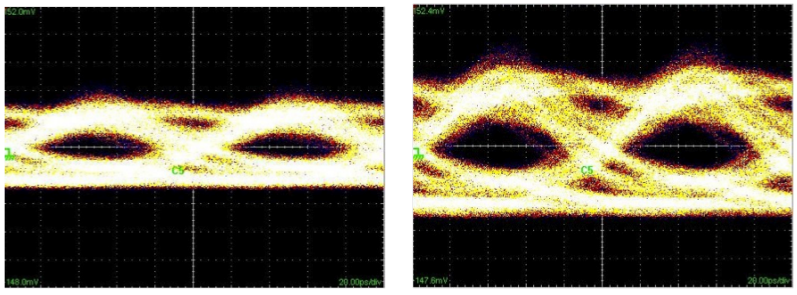

(b) (c)

Figure 2.34: *(a) BER measurements at 10Gb/s vs MMF bending diameters. (b) Eye diagram at BER=10^{-3} for 10Gb/s NRZ-OOK signal. (c) Eye diagram at BER=10^{-9} for 10Gb/s NRZ-OOK signal.*

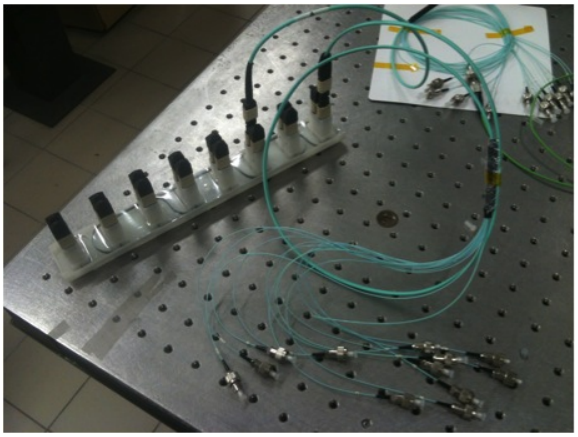

Figure 2.35: *Subsection of the backplane with "telaio".*

a standard multimode fiber ribbons, the losses are acceptable in the power budget of the system. The same experimental setup, previously described to characterize the loss of a single fiber, has been used to quantify losses due bending for each of the 8 connections of the subsection of the backplane. The only difference is that now, the VCSEL is directly fiber-coupled and connected to a port of the fan-in. A RayCan MM @ 850 nm VCSEL has been used with a P_{out} = 0 dBm. The VCSEL is modulated up to 10 Gbit/s through a Finisar evaluation board. At the receiver a free-space EOT 850nm photodiode (bandwidth= 9GHz, sensitivity at 10^{-12} is -10dBm) is connected to a BER tester. To evaluate the real bending problem the connections have been characterized in terms of power losses and BER. The measurements have been carried out in two configurations, with and without pressing on fan-in/out, as shown in Fig.2.36. In the second case, that emulates when the boards have to be hook to the backplane, the measured power loss on the most bending ribbon is variable, due to the different excited modes depending on the exercised pressure. In Figure 2.37) some results between connections are shown. The fibers enumerated from 1 to 6 are the more internal ones and are subjected to more bending. The maximum loss for all 12x8 connections are minor than 2dB (including 0.35dB and 0.15dB respectively of fan-in and fan-out insertion losses). In the more external fibers, where the bending is minor, the power losses are on average lower than 0.5dB. Then, we have taken into consideration the connections with maximum (2.28dB) and minimum (1.44dB) loss and we measured the BER. In both cases the error-free transmission (BER< 10^{-12}) is guaranteed. Finally, to emulate all possible real working backplane conditions,

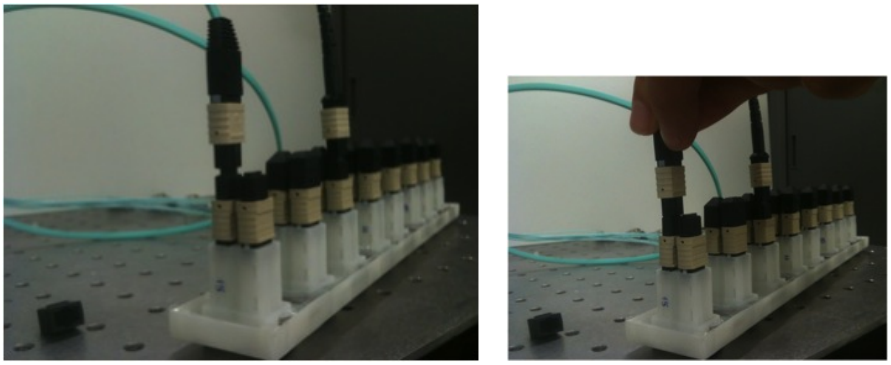

(a) (b)

Figure 2.36: *(a) Fan-in/out MPO connected to TX/RX MPO without pressing. (b) Fan-in/out MPO connected to TX/RX MPO with manual pressing.*

we checked the power losses in case of a single mode fiber is connected to the multimode fiber of the ribbon. Minor losses are observed (< 1dB) with respect to the MMF-MMF ribbon connection, because only two fiber modes are excited at 850nm. Moreover, the loss is more dependent on the bending type (see Fig. 2.38). By concluding, the ”telaio” solution designed by ITIA ([87]) allows to stay in the estimated power budget (4.8dB) for the entire link (from TX to RX via fiber-based backplane). Further test will be made on the entire backplane prototype.

2.4.5 Card design

To test the feasibility of the backplane it has also been necessary, as part of the project, to design a test card, in collaboration with Compel Electronics S.p.A.. This board should have the same features of a real card processing traffic, and thus should preserve the main performance, which are:

- at least bandwidth of 100 Gb / s per card.
- system architecture of full-mesh type.
- optical interconnection for high-speed traffic signals, as for the actual electric-based cards.
- electrical connections for residues signals and power supply

It was very important to identify the electro-optical unit to be placed on the transmission board and the opto-electrical unit to be placed on the receiver board. We have decided to use commercial devices available on

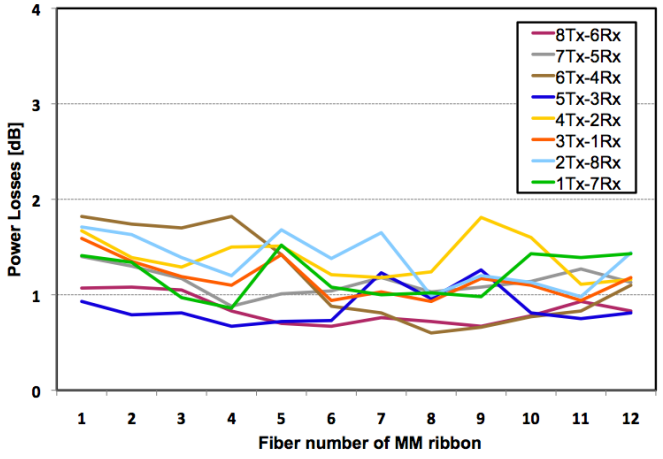

(a)

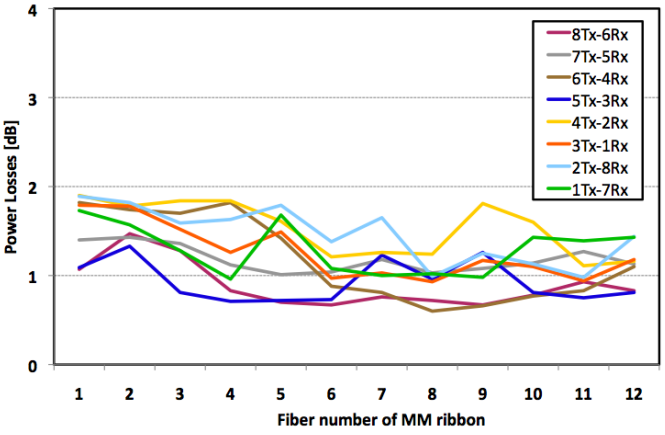

(b)

Figure 2.37: *Power losses in case of connections between a multimode fiber and a multimode fiber of the ribbon obtained with pressure. Minimum losses (a) and maximum losses (b).*

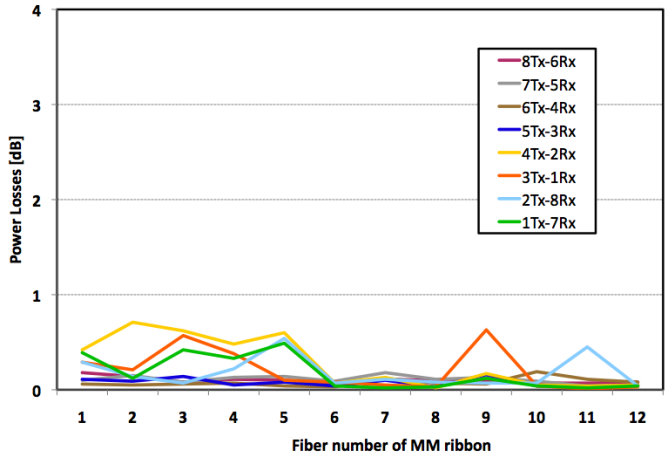

(a)

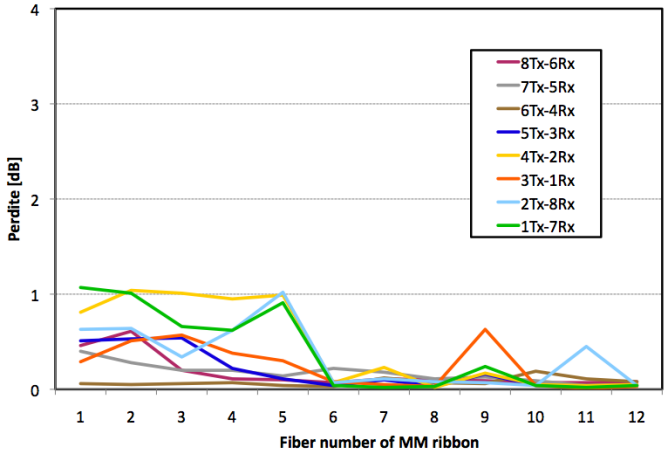

(b)

Figure 2.38: *Power losses in case of connections between a single mode fiber and a multimode fiber of the ribbon obtained with pressure. Minimum losses (a) and maximum losses (b).*

Figure 2.39: *MiniPOD Tx and Rx optical modules.*

the market nowdays. Many module at 10 Gb/s per channel with 12 optical channels have been evaluated, in terms of cost and performances. After this preliminary analysis we decided to use AVAGO miniPOD (Tx AFBR-811FH1Z, RX AFBR-821FH1Z) Twelve-Channel Transmitter and Receiver Pluggable, Parallel-Fiber- Optics Modules (see Fig.2.39), because of more mature technology compared to other modules, smaller and cheaper, since it does not require the design of $ad\text{-}hoc$ mechanical interface for the heat sink device and the connecting system for a ribbon cable [88]. For the interface between electro-optical converters and card connector, a flat ribbon cable with 12 fibers is used called cable PRIZM^{TM} (designed for AVAGO MINIPOD modules). Two different ribbon cables are used: one for the transmitter module and the other one for the receiver module. The other end of the connector is a MPO and hooks up into card connector, as described in the subsection 2.4.2. The connector PRIZM^{TM} LightTurn^{TM}, designed as a miniature connector for removable parallel optical modules on high speed cards, offers a passive alignment with innovative characteristics of the retention mechanism, which allows coupling into perpendicular direction with respect to the printed circuit board (PCB). The connector consists of a multi-fiber ferrule with an array of lenses with total internal reflection (TIR) that allows the alignment of the fibers with the relating housing and provides an excellent coupling with parallel optical modules

at high bit rate. The typical insertion loss is about 1.45dB at 850nm and the minimum return loss value is major than 20dB at 850nm. The european supplier is SYLEX (Sylex spol. s. r.o). Real traffic processing boards for real ICT apparatus are quite complex from a point of view of the managment and routing of electrical signals and typically an Field-Programmable Gate Array (FPGA) [89] and microprocessor-based software platform are exploited to run out all these functions. The design and realization of such a card, in this first stage of the project, would have been to complex and expensive. Thus it has been decided to develop simpler tests cards, with the minimal functionalities required to test the optical backplane transmission. In particular the objective has been focus on:

1. the development of a pure interconnect card (called the interconnect board), to test the quality of optical backplane connections and make preliminary checks on the mechanical characteristics of the connector and the card;

2. the development of a card realized with less complex components (no FPGA, no on-board microprocessor, but control of the functions via an external PC)

In Figure 2.40 it is schematically shown the architecture of the test card to be realized. The main functional blocks are:

- XFP module that includes an optical source and a receiver. It receives signal from a generator tool / traffic analyzer for the test stage;
- a cross-point switch with 16 I/O at 10 Gb/s, that performs signal routing between the XFP signals and the 12 input/output of the MINIPOD AVAGO TX and RX;
- AVAGO MINIPOD modules (Tx:12 channels 850nm VCSEL array + Rx: 12 channels PIN photodetectors array);
- optical connectors to the backplane;
- function check (cross- connections , amplitude levels , enabling pre-emphasis and equalization) via I2C bus, managed by an external PC (RJ45 connector at front) ;
- power supply, for the voltage battery conversion - 48V (or 60V) , towards all necessary voltages : 5V, 3.3V , 2.5V , (1.8V provided for the use of future XFP modules , although not required by XFP modules currently used);

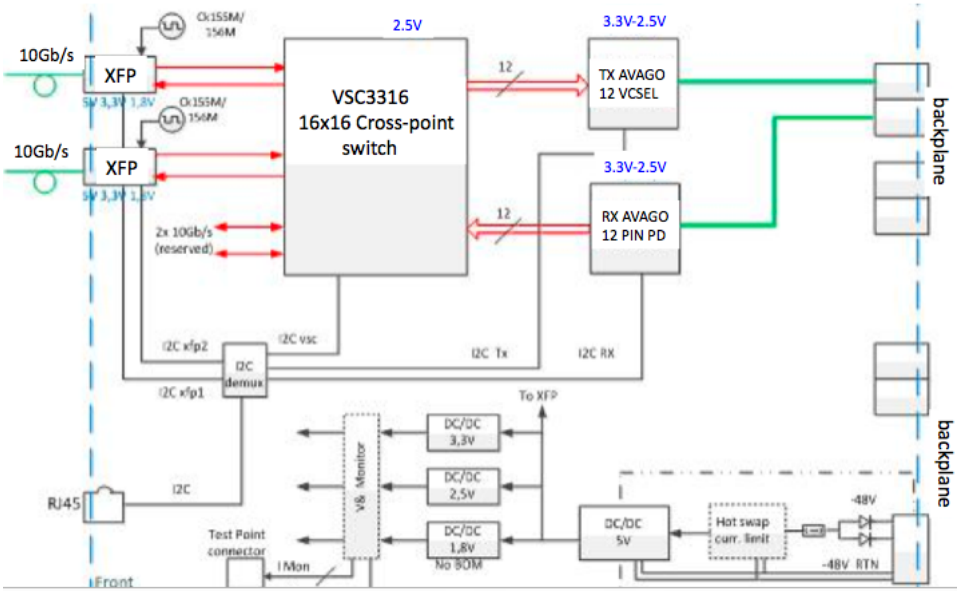

Figure 2.40: *Test card architecture*

- voltages and currents analog circuit monitor (that means no Analog/Digital converter on the board, but direct reading through an external digital voltmeter).

This type of card also allows simultaneously test on different types of signals, both for texture and format (SDH/OTN/10GBE), for bit-rate (up to maximum of 10.7Gb/s) thanks to the traffic transparency guaranteed by the asynchronous cross-point.
An important aspect will be the power dissipation evaluation of the optical backplane and TX-RX cards. It will be possible to monitor each power supply, monitoring on a external digital voltmeter (via a dedicated connector on PCB or at the front) the voltages and currents analog measurements. It should be pointed out that it will be possible to measure just the power consumption of each power supply and it will not be possible to divide the contribution due to individual transmitter and receiver from a complex transceiver like Avago module and due to the buffer of the cross-point. The evaluation of the power consumption of the buffer can be made by difference: a comparison can be done in case of absence of transmission, transmission to the maximum level or intermediate levels of amplitude, equalization or pre-emphasis.

Once realized, the test card will be used to prove the feasibility of the proposed full-mesh optical backplane. In this first stage, the optical ribbons of the MINIPOD AVAGO will be switched to all the TX-RX connectors of the card to test all connections. In a second step the design and ingegnerization of a complete card with 12 TX-RX modules will be considered.

CHAPTER 3

Center-launching technique in backplane-based applications

In this Chapter we focus the attention on one of the characteristic of the optical backplane: the transparency to the modulation formats and bit rates. The optical backplane also has to provide rounting of external signals coming from external network on single mode fiber, without electro/optical conversion. Since these signals can be modulated with intensity or/and phase, it's necessary to keep the single mode propagation also through the fiber-based optical backplane. Center-launching technique appears as a promising method to allow single-mode propagation in multi-mode fibers, guaranteeing full transparency to the transmitted optical signal also for applications in board-to-board and data server interconnects. In this Chapter, a brief introduction to the optical-guided modes into an optical fiber will be given and then an experimentally demonstration of 1.3 μm VCSEL-based transmission in legacy standard multimode fiber (MMF) by using the mode-field matched center-launching technique will be presented. Transmission bit-rate of 12.5 Gb/s is realized at 1.3 μm by direct modulation of VCSEL suitable for high speed applications. Performances without significant penalties, also compared with single mode fiber (SMF) propagation,

are measured up to 10-km MMF coils, simply connected by fusion splicing, without SMF patchcords. Finally we verify the robustness of this technique to mechanical perturbations up to about 1 kHz, demonstrating that the vibrations do not affect the transmission performances. Different experimental configurations are tested in order to exclude multimode propagation and to confirm the only fundamental mode propagation. A theoretical discussion comments the experimental results.

3.1 General theory of modes of optical waveguides

In this section is reported a simple method for determining the modes of an optical waveguide with a cladding refractive index n_{cl} that differs only slightly from the maximum refractive index of the core n_{co}. This method, said the $n_{co} \cong n_{cl}$ method, has been introduced by Snyder and Young in 1978 and it's normally used to obtain the propagating modes of a generic optical waveguide of arbitrary cross section and arbitrary profile grading [90]. The analysis does not require the waveguide to be multimoded or the refractive index profile to vary "slowly". However, a complete description of propagating modes of cylindrical dielectric waveguides in terms of transverse components, cut-off conditions, modal notation and characteristics is exposed by Snitzer in [91]. Anyway, we decide to follow Snyder's treatment because it focuses on the propagation constants β of the higher-order modes and their stability during propagation in a cylindrical waveguide and in an elliptical space using simple simmetry considerations. The $n_{co} \cong n_{cl}$ method synthesizes the vector modal fields from linear combinations of solutions to the scalar wave equation. The appropriate linear combinations are dictated by properties of the $\nabla\epsilon$ terms in the vector wave equation, where $\epsilon(x, y, z)$ is the permittivity of the waveguide and ∇ is the operator expressed by

$$\nabla = \frac{\partial}{\partial x}\hat{\mathbf{x}} + \frac{\partial}{\partial y}\hat{\mathbf{y}} + \frac{\partial}{\partial z}\hat{\mathbf{z}}. \tag{3.1}$$

where $\hat{\mathbf{x}}, \hat{\mathbf{y}}$ and $\hat{\mathbf{z}}$ are unit vectors in he x, y, z directions. Failure to account for the $\nabla\epsilon$ terms, however small, will in general lead to "pseudo-modes" with the property that their cross sectional intensity and polarization pattern changes as the modes propagates [92].
It's important to review several fundamental concepts required for the following analysis: when the permittivity $\epsilon(x, y)$ of the medium has cylindrical (not necessary circular) symmetry the modal electric $\mathbf{E}$ and magnetic $\mathbf{H}$

vector fields have the form

$$\mathbf{E}(x,y,z) = \mathbf{e}(x,y)\exp(i\beta z) = (\mathbf{e}_t + \mathbf{e}_z)\exp(i\beta z), \tag{3.2a}$$

$$\mathbf{H}(x,y,z) = \mathbf{h}(x,y)\exp(i\beta z) = (\mathbf{h}_t + \mathbf{h}_z)\exp(i\beta z), \tag{3.2b}$$

assuming an $\exp(-i\omega t)$ time dependence. The fields $\mathbf{e}_t$ are solutions of the reduced wave equation

$$\nabla_t^2 \mathbf{e}_t + (k^2 + \beta^2)\mathbf{e}_t = -\nabla_t(\mathbf{e}_t \cdot \nabla_t \ln\epsilon), \tag{3.3}$$

where

$$\nabla_t = \nabla - \hat{\mathbf{z}}\left(\frac{\partial}{\partial z}\right), \tag{3.4}$$

∇_t^2 is the transverse vector Laplacian [93], $k(x,y) = 2\pi n(x,y)/\lambda$, $\epsilon = \epsilon_0 n^2$ and ϵ_0 is the permittivity of free space. The remaining field components are determined from $\mathbf{e}_t$ using Maxwell's equations. The allowed values of β result by demanding only that solutions of equation (3.3) be bounded, since effects of any discontinuity in ϵ are fully contained within the $\nabla_t(\ln\epsilon)$ term. For bound modes β is real and restricted to the range [94, 95]

$$k_{cl} \le \beta \le k_{co} \tag{3.5}$$

where $k_{cl} = 2\pi n_{cl}/\lambda$, $k_{co} = 2\pi n_{co}/\lambda$, n_{co} is the maximum refractive index of the core and n_{cl} is the refractive index of the cladding. Because of the $\nabla_t \ln\epsilon$ terms in vector wave equation, the modal fields are in general hybrid, possessing both $\mathbf{e}_z$ and $\mathbf{h}_z$ components.

3.1.1 The $\mathbf{n_{co}} \cong \mathbf{n_{cl}}$ method for deriving modes

In this section are derived the approximations for modal fields and their propagation constants on waveguides with $n_{co} \cong n_{cl}$.This approximation begins considering the calculus of the modes of a $n_{co} = n_{cl}$ waveguide (paragraph 3.1.1), that are the "building blocks" needed for obtaining the approximated results for a generalized $n_{co} \cong n_{cl}$ waveguides (paragraph 3.1.1). In the following the fields of optical waveguides will be expressed in terms of the parameters:

$$\sin\theta_c = \left(1 - \frac{n_{cl}^2}{n_{co}^2}\right)^{1/2} \cong \theta_c \tag{3.6a}$$

$$V = R(k_{co}^2 - k_{cl}^2)^{1/2} = k_{co} R \sin\theta_c \tag{3.6b}$$

where the first is the critical angle θ_c, the second is the well-known dimensionless waveguide parameter V and R is the characteristic dimension of

the waveguide cross section, i.e. the core radius for circularly symmetric waveguides.

TEM modes of the $\mathbf{n_{co} = n_{cl}}$ waveguide (LP modes)

Snyder and Young begin by finding the modes of optical waveguides in the artificial limit when the maximum refractive index of the core equals that of the cladding refractive index, i.e. when $n_{co} = n_{cl}$. By itself, this condition would appear to assume that the medium is homogeneous and incapable of guiding energy. However, to avoid the trivial consequences of this assumption, it's imposed the constraint that the guiding properties of the structure remain unchanged, i.e. the waveguide parameter V be an arbitrary constant [96].
Because bound modes are restricted to the range of values in equation (3.5), the limit $n_{co} = n_{cl} = n$ demands that

$$\beta = k_{co} = k_{cl} = k = \frac{2\pi n}{\lambda}. \tag{3.7}$$

This condition is satisfied only by a z-directed transverse electromagnetic (TEM) wave, i.e. by a wave for which the electric and magnetic field vectors lie in a plane that is transverse to the axis of the waveguide. Accordingly, the modal fields components on the $n_{co} = n_{cl}$ waveguide are

$$\tilde{\mathbf{h}}_z = \tilde{\mathbf{e}}_z = 0 \tag{3.8a}$$

$$\tilde{\mathbf{h}}_t = \left(\frac{\epsilon}{\mu}\right)^{1/2} \hat{\mathbf{z}} \times \tilde{\mathbf{e}}_t \tag{3.8b}$$

where μ is the magnetic permeability of the medium and the $\tilde{}$ is used to indicate quantities to be associated with the scalar wave equation.
Because $n_{co} = n_{cl}$, all polarization-dependent properties of the structure are removed. Since the $\nabla_t \ln \epsilon$ term in the vector wave equation (3.3) is solely responsible for the polarization properties of modes, it is omitted solving for the $\tilde{\mathbf{e}}$ fields of the $n_{co} = n_{cl}$ waveguide. In other words, the $n_{co} = n_{cl}$ fields are solutions to the scalar wave equation. These vector modal fields can then be expressed in rectangular coordinates as

$$\tilde{\mathbf{e}}_x = \psi\hat{\mathbf{x}},\ \tilde{\mathbf{e}}_y = \psi\hat{\mathbf{y}}, \tag{3.9}$$

where ψ is a solution of

$$(\nabla_t^2 + k^2 - \tilde{\beta}^2)\psi = 0. \tag{3.10}$$

The solutions ψ must be bounded everywhere and have the property of the scalar wave equation that ψ and its normal derivative are everywhere continuous. These constraint lead to an eigenvalue equation from which the allowed values of $\tilde{\beta}$ are found, where $\tilde{\beta}$ is distinguished from β being an eigenvalue of equation (3.10) rather than equation (3.3).
It's important to notice that the $n_{co} = n_{cl}$ waveguide is an unphysical condition. Nevertheless, as shown in the next sections, the fields of the $n_{co} = n_{cl}$ waveguide are the building blocks for the $n_{co} \cong n_{cl}$ waveguide. The modal fields of step profile waveguides with circular symmetry are often called LP (linearly polarized) or uniformly polarized modes.
In the next section is shown how the solutions of the scalar wave equation $\tilde{\mathbf{e}}$ and $\tilde{\beta}$ can be used to construct accurate representation of $\mathbf{e}$ and β, which are themselves solutions of the vector wave equation (3.3).

Modes on the $\mathbf{n_{co} \cong n_{cl}}$ waveguide

The significant consequence of having n_{co} different from n_{cl} is that the waveguide has polarization properties. The polarization properties are contained within the $\nabla_t \epsilon$ term of the wave equation. The modes of such a waveguide must exhibit these properties and, therefore, they must be solution of the vector equation (3.3). However, since the term $\nabla_t(\mathbf{e}_t \cdot \nabla_t \ln \epsilon)$ is zero when $n_{co} = n_{cl}$, it must have a small, but nevertheless a very important effect for $n_{co} \cong n_{cl}$. The modes of the $n_{co} \cong n_{cl}$ waveguide can then be approximated by linear combinations of the modal fields $\tilde{\mathbf{e}}$ of the $n_{co} = n_{cl}$ waveguide. The proper linear combinations are dictated by the symmetries of the waveguide which are fully contained within the $\nabla_t \epsilon$ term of the vector wave equation. The method of constructing the linear combination introduced by Snyder and Young is reported in section 3.1.2.
Because $\beta \cong k$ on the $n_{co} \cong n_{cl}$ waveguide, the transverse fields obey the approximate relationship

$$\mathbf{h}_t \cong \left(\frac{\epsilon}{\mu}\right)^{1/2} \hat{\mathbf{z}} \times \mathbf{e}_t. \tag{3.11}$$

The longitudinal fields are then found from Maxwell's divergence equations, leading to

$$\mathbf{h}_z = \frac{i}{\beta} \nabla_t \cdot \mathbf{h}_t \tag{3.12a}$$

$$\mathbf{e}_z = \frac{i}{\beta} \nabla_t \mathbf{e}_t + \nabla_t \ln \epsilon \cdot \mathbf{e}_t \cong \frac{i}{\beta} \nabla_t \cdot \mathbf{e}_t \tag{3.12b}$$

The propagation constant β for the $n_{co} \cong n_{cl}$ modes nearly equals $\tilde{\beta}$ determined from equation (3.10). To include small polarization effects one uses a standard method presented in [90], leading to

$$\beta - \tilde{\beta} \cong \frac{\beta^2 - \tilde{\beta}^2}{2k} = \frac{\int_{A_\infty} \tilde{\mathbf{e}}_t \cdot \nabla_t (\mathbf{e}_t \cdot \nabla_t \ln \epsilon) dA}{2k \int_{A_\infty} \tilde{\mathbf{e}}_t \cdot \mathbf{e}_t dA}, \tag{3.13}$$

where $k = 2\pi n/\lambda$, $\tilde{\beta}$ and $\tilde{\mathbf{e}}_t$ are defined by equations (3.9) and (3.10), $\mathbf{e}_t$ and β are defined by equations (3.3) and A_∞ is the infinite cross section. The small correction to $\tilde{\beta}$ obtained by equation (3.13) is necessary to separate the erroneous degenerate $\tilde{\beta}$'s found by solving the scalar wave equation rather than the vector wave equation. For example, equation (3.13) includes the small polarization dependent effects necessary to distinguish the β of a TM from a TE wave.

3.1.2 Vector modal fields

In this section is reported the method of constructing approximations of the vector modal fields by linearly combining the $n_{co} = n_{cl}$ fields. The philosophy of the method is based on the fact that modal fields must satisfy the symmetry properties of the waveguide. These symmetry properties are contained within the $\nabla_t \epsilon$ term of the vector wave equation and therefore they are automatically included in solutions of this equation. However, it is often possible to guess the appropriate symmetry conditions without solving the vector wave equation (3.3), as explained in the examples of circularly symmetric waveguide (paragraph 3.1.2) and waveguide with two preferred axes of symmetry (paragraph 3.1.2).

Waveguides with circular simmetry

The $n_{co} = n_{cl}$ modes are given by equation (3.9) in terms of the scalar function ψ. By virtue of the circular symmetry, there are in general two solutions of the scalar wave equation (3.10) for each allowed value of $\tilde{\beta}$. One solution, ψ_e, has even symmetry, while the other, ψ_o, has odd symmetry:

$$\psi_e(\rho, \phi) = f_\ell(\rho) \cos \ell\phi, \ \psi_o(\rho, \phi) = f_\ell(\rho) \sin \ell\phi. \tag{3.14}$$

In equation (3.14), ϕ is the azimuthal coordinate and $f_\ell(\rho)$ is a solution of

$$\left(\frac{d^2}{d\rho^2} + \frac{1}{\rho} \frac{d}{d\rho} + k^2(\rho) - \tilde{\beta}^2 - \frac{\ell^2}{\rho^2} \right) f_\ell(\rho) = 0. \tag{3.15}$$

and, for an optical fiber with a step profile of the refractive index, it assumes the form

$$f_\ell(\rho) = \frac{J_\ell(\tilde{U}\rho/R)}{J_\ell(\tilde{U})} \qquad \rho \le R \tag{3.16a}$$

$$f_\ell(\rho) = \frac{K_\ell(\tilde{W}\rho/R)}{K_\ell(\tilde{W})} \qquad \rho \ge R \tag{3.16b}$$

where the notation $\tilde{}$ indicates that they are derived from the scalar wave equation, J_ℓ is a Bessel function and K_ℓ is a modified Hankel function and $\tilde{U}$ and $\tilde{W}$ are related to the parameter V of equation (3.6b) by $V^2 = \tilde{U}^2 + \tilde{W}^2$.

Thus, the $n_{co} = n_{cl}$ waveguide of paragraph 3.1.1 has four modes for each allowed value of $\tilde{\beta}$, i.e.

$$\tilde{\mathbf{e}}_{xe} = f_\ell(\rho)\cos(\ell\phi)\hat{\mathbf{x}} \tag{3.17a}$$

$$\tilde{\mathbf{e}}_{xo} = f_\ell(\rho)\sin(\ell\phi)\hat{\mathbf{x}} \tag{3.17b}$$

$$\tilde{\mathbf{e}}_{ye} = f_\ell(\rho)\cos(\ell\phi)\hat{\mathbf{y}} \tag{3.17c}$$

$$\tilde{\mathbf{e}}_{yo} = f_\ell(\rho)\sin(\ell\phi)\hat{\mathbf{y}} \tag{3.17d}$$

When $\ell = 0$, there are only two $n_{co} = n_{cl}$ modes, $\tilde{\mathbf{e}}_{xe}$ and $\tilde{\mathbf{e}}_{ye}$. These fields exist at all frequencies and depend only by the radial coordinate ρ. By virtue of the circular symmetry, any linear combination of these two fields must be a modal field on the $n_{co} \cong n_{cl}$ waveguide. Also, from circular symmetry, the $n_{co} \cong n_{cl}$ waveguide has two fundamental modes with equal $\tilde{\beta}$'s. We can take one mode to be polarized in the x direction ($\mathbf{e}_x$) and the other to be polarized in the y direction ($\mathbf{e}_y$):

$$\mathbf{e}_x = f_0(\rho)\hat{\mathbf{x}},\ \mathbf{e}_y = f_0(\rho)\hat{\mathbf{y}} \tag{3.18}$$

where $f_0(\rho)$ is the solution of equation (3.15) with $\ell = 0$.
The two fundamental modes of the circular symmetric $n_{co} \cong n_{cl}$ waveguide are exceptional in that they are the same as the fundamental modes on the $n_{co} = n_{cl}$ waveguide, i.e. they are uniformly polarized throughout the cross section and have the same β's.

Unlike the fundamental modes, none of the $n_{co} = n_{cl}$ fields for $\ell \ge 1$ are individually modal fields of the $n_{co} \cong n_{cl}$ waveguide. This can be proved from symmetry considerations together with equation (3.13) [90]. Thus,

we require linear combinations of $\tilde{\mathbf{e}}_{xe}$, $\tilde{\mathbf{e}}_{xo}$, $\tilde{\mathbf{e}}_{ye}$ and $\tilde{\mathbf{e}}_{yo}$ to form the higher-order modes.

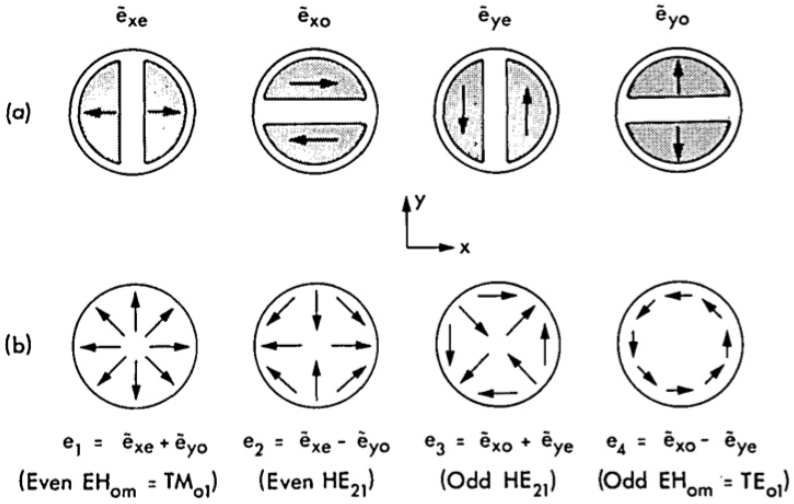

Figure 3.1: *First-order modes. (a) The $n_{co} = n_{cl}$ or LP modes for $\ell = 1$. The $\tilde{\mathbf{e}}_{xe}$ and $\tilde{\mathbf{e}}_{yo}$ are symmetric under reflections in the x and y axes, while $\tilde{\mathbf{e}}_{xo}$ and $\tilde{\mathbf{e}}_{ye}$ are antisymmetric. If any one of the above fields is rotated through an arbitrary angle it transforms into a linear combination of all four. (b) The $n_{co} \cong n_{cl}$ modes for $\ell = 1$. Under an arbitrary reflection and rotation, $\mathbf{e}_1$ and $\mathbf{e}_4$ are unchanged, while either $\mathbf{e}_2$ and $\mathbf{e}_3$ transform into linear combinations of $\mathbf{e}_2$ and $\mathbf{e}_3$ themselves.*

To form the correct linear combinations, we combine those modes which have the same properties under a rotation of $90°$ and under reflections in the x and y axes. It may help to consider the specific example of $\ell = 1$ modes shown in Figure 3.1(a). Thus, $\tilde{\mathbf{e}}_{xe}$ is combined with $\tilde{\mathbf{e}}_{yo}$ because one rotates into the other, while $\tilde{\mathbf{e}}_{xo}$ is combined with $\tilde{\mathbf{e}}_{ye}$ because one rotates into minus the other. Taking symmetric and antisymmetric combinations lead to the 4 modes of the $n_{co} \cong n_{cl}$ waveguide:

$$\mathbf{e}_{t1} = \tilde{\mathbf{e}}_{xe} + \tilde{\mathbf{e}}_{yo} \tag{3.19a}$$
$$\mathbf{e}_{t2} = \tilde{\mathbf{e}}_{xe} - \tilde{\mathbf{e}}_{yo} \tag{3.19b}$$
$$\mathbf{e}_{t3} = \tilde{\mathbf{e}}_{xo} + \tilde{\mathbf{e}}_{ye} \tag{3.19c}$$
$$\mathbf{e}_{t4} = \tilde{\mathbf{e}}_{xo} - \tilde{\mathbf{e}}_{ye} \tag{3.19d}$$

Using conventional nomenclature [97, 98] modes 1-4 refer to the even $EH_{(\ell-1,m)}$, even $HE_{(\ell+1,m)}$, odd $HE_{(\ell+1,m)}$ and odd $EH_{(\ell-1,m)}$ modes re-

spectively. Figure 3.1(b) illustrates the modes for $\ell = 1$. These combinations can be shown to be consistent with the symmetry properties of the waveguide. By placing $\mathbf{e}_{t1}$ in equation (3.13) for $\mathbf{e}_t$ and $\tilde{\mathbf{e}}_{xe}$ for $\tilde{\mathbf{e}}_t$ we obtain β for mode 1 and similarly for the other three modes. In general, the β's of the EH and HE modes differ from one another. This difference gives rise to a beat phenomenon causing a rotation of the $n_{co} = n_{cl}$ or LP patterns as the mode advances. The stability of the LP mode patterns is set by the difference $|\beta_{HE} - \beta_{EH}|$ in the propagation constant of the two different mode types that form an LP pattern. If $\beta_{HE} = \beta_{EH}$, the $n_{co} = n_{cl}$ modes could be also modes of the $n_{co} \cong n_{cl}$ waveguide. However, the LP modes are not modes of a $n_{co} \neq n_{cl}$ waveguide. The reason is that each LP mode is formed by combining two proper modes, an $HE_{(\ell+1,m)}$ and $EH_{(\ell-1,m)}$ modes, and these proper modes have different propagation constants, β_{HE} and β_{EH}. Because of the beat phenomenon, when $|\beta_{HE}-\beta_{EH}| \neq 0$, the modes appear to rotate or fade into each other [99].The greater $|\beta_{HE} - \beta_{EH}|$, the shorter the beat length and hence more rapidly the LP modes fade into one another. As explained by Snyder and Young [90], the condition $|\beta_{HE} - \beta_{EH}| \neq 0$ is always satisfied by modes with $\ell \geq 2$: these LP modes are never modes of the circularly symmetric waveguide. Furthermore, the greater ℓ, the greater $|\beta_{HE} - \beta_{EH}|$, so the less stable the LP modes. It's important to notice that, apart from $\ell = 1$, the four modes can be divided into two couples of modes, HE and EH. The modes of each set have the same propagation constant, i.e. the even and odd HE modes have the same β_{HE}, while the even and odd EH modes have the same β_{EH}. The situation for $\ell = 1$ is more complicated, because the EH modes are the TE and TM modes that present different propagation constants β_{TE} and β_{TM}, while the HE modes share the same constant β_{HE}. The relation between these two propagation constants and β_{HE} are shown in Figure 3.2.

Waveguides with two preferred axes of simmetry

Many structures of practical interest have a pair of preferred orthogonal axes of symmetry, i.e. the ellipse that can represent the core of a real optical fiber endowed with birefringence. When $n_{co} \cong n_{cl}$, the modes of these waveguides can be formed by linear combinations of the $n_{co} = n_{cl}$ modal fields.

It's intuitive that the fundamental modes, which propagate for all values of frequency, have electric fields that are polarized along one of these two axes of symmetry. Thus, the $n_{co} = n_{cl}$ modal fields are the proper approximations of the fundamental fields of the $n_{co} \cong n_{cl}$ waveguide only if the $\hat{\mathbf{x}}$ and $\hat{\mathbf{y}}$ directions of equation (3.9) are aligned with the direction of the

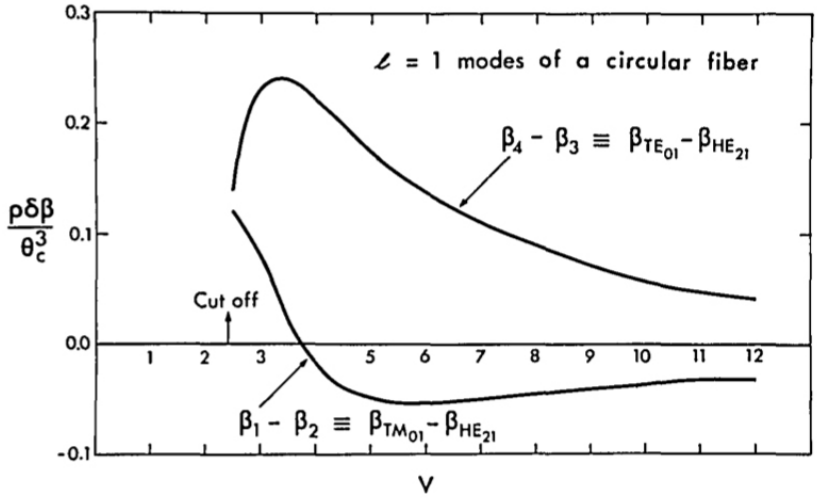

Figure 3.2: *The difference in $\tilde{\beta}$'s for $\ell = 1$ modes of the circular symmetric, step profile waveguide.*

symmetry axes. Therefore the fundamental mode has vector fields of the form

$$\mathbf{E}_x = \mathbf{e}_x \exp(i\beta_x z) = \psi \exp(i\beta_x z)\hat{\mathbf{x}} \tag{3.20a}$$

$$\mathbf{E}_y = \mathbf{e}_y \exp(i\beta_y z) = \psi \exp(i\beta_y z)\hat{\mathbf{y}} \tag{3.20b}$$

where ψ is the fundamental solution of the scalar wave equation (3.10). The modal propagation constants β_x and β_y are found by substituting into equation (3.13) $\mathbf{e}_t = \tilde{\mathbf{e}}_t = \mathbf{e}_x$ and $\mathbf{e}_t = \tilde{\mathbf{e}}_t = \mathbf{e}_y$ respectively. It's important to notice that in an elliptical space $\beta_x \neq \beta_y$, i.e. the two fundamental modes have different phase velocity. So, if the fiber is illuminated by linearly polarized light at $45°$ to the optical or symmetry axes, then both fundamental modes are excited equally and the wave becomes elliptically polarized as it propagates. Because of the beat phenomenon, the $\mathbf{E}$ vector appears to rotate. The length of a $360°$ rotation is $2\pi|\beta_x - \beta_y|^{-1}$.

The fields of higher-order modes, instead, are more complicated than the fundamental modes. It is clear that for a sufficiently large eccentricity the field of any particular $n_{co} \cong n_{cl}$ mode is represented by equation (3.20), so that the only difference between it and a fundamental mode is in the values of ψ and β. However, it is equally clear that for a sufficiently small eccentricity, the same mode resembles a modal field of a circular symmetric waveguide, with $\hat{\mathbf{x}}$ and $\hat{\mathbf{y}}$ parallel to the symmetry axes of the ellipse. This

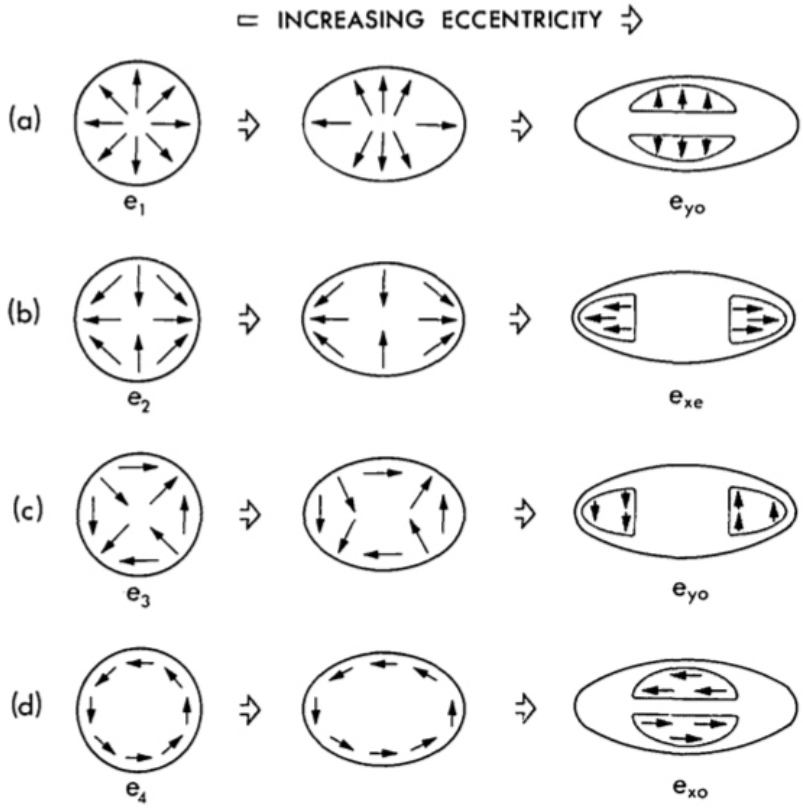

Figure 3.3: *Transition from circle to ellipse modes for $\ell = 1$ modes. An electric field vector maintains its orientation to the interface, i.e. if it was initially perpendicular it remains perpendicular, as the eccentricity increases. Using this heuristic principle one can anticipate the way in which a particular circle mode changes as the eccentricity increases.*

transition is sketched in Figure 3.3. We can associate each ellipse mode with the fields of a distorted circle mode. For example, the ellipse mode that corresponds to distorting either $\mathbf{e}_{t1}$ or $\mathbf{e}_{t2}$ of Figure 3.1 is formed by a linear combination of $\tilde{\mathbf{e}}_{xe}$ and $\tilde{\mathbf{e}}_{yo}$, where these $\tilde{\mathbf{e}}$'s are now solutions to the scalar wave equation in elliptical geometry. Consequently, the fields of the ellipse modes $\mathbf{e}_{t1}$ and $\mathbf{e}_{t2}$ are

$$\mathbf{e}_{ti} = a_i \psi_e \hat{\mathbf{x}} + b_i \psi_o \hat{\mathbf{y}} = a_i \tilde{\mathbf{e}}_{xe} + b_i \tilde{\mathbf{e}}_{yo} \tag{3.21}$$

where $i = 1$ or 2, ψ_e and ψ_o are solutions of the scalar wave equation in elliptical geometry and are analogous to ψ_e and ψ_o given by equation (3.14) for the scalar wave equation in circular cylindrical geometry. Figure 3.4

provides an example of ψ_e and ψ_o. The propagation constants associated with ψ_e and ψ_o are denoted $\tilde{\beta}_e$ and $\tilde{\beta}_o$ respectively. These $\tilde{\beta}$'s are different; the difference increases as eccentricity increases.

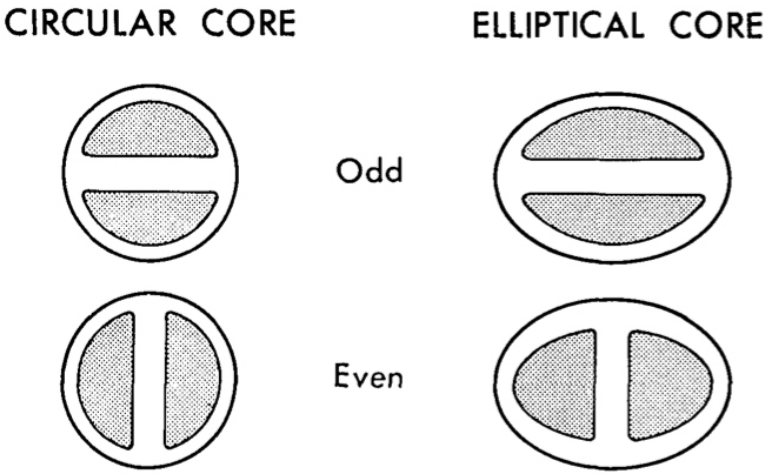

Figure 3.4: *An example of a solution of the scalar wave equation corresponding to the $\ell = 1$ mode. The $\tilde{\beta}$'s of the even and odd circle modes are identical unlike the $\tilde{\beta}$'s for the even and odd modes of the elliptical core.*

At the end of paragraph 3.1.2, it has been stated that the rate that LP modes rotate into one another depends upon $|\beta_{HE} - \beta_{EH}|$, where β_{HE}, β_{EH} are the β's of the circular waveguide. When this difference is zero, the LP modes are stable, i.e. they are proper modes of the $n_{co} \cong n_{cl}$ waveguide. The stability of circle modes on an ellipse depends upon $(\tilde{\beta}_e - \tilde{\beta}_o)$, where $\tilde{\beta}_e, \tilde{\beta}_o$ are the $\tilde{\beta}$'s for the ellipse determined from the scalar wave equation. Consequently, the parameter Λ is influential in determining the limiting behavior of ellipse fields, where

$$\Lambda = \frac{(\tilde{\beta}_e - \tilde{\beta}_o)}{(\beta_{EH} - \beta_{HE})}, \tag{3.22}$$

where $\beta_{EH} = \beta_1$ and $\beta_{HE} = \beta_2$ for the particular ellipse modes $\mathbf{e}_{t1}$ and $\mathbf{e}_{t2}$ given by equation (3.21). When $|\Lambda| \gg 1$, the fields of the ellipse are uniformly polarized, while when $|\Lambda| \ll 1$ the ellipse modal fields are the fields of modes of a circularly symmetric waveguide.

3.2 Center-launching technique

Optical data links should guarantee also a complete transmission transparency in the interconnection with the external network, i.e. a travelling signal must be allowed to pass through the backplane network on a determined internal link without any need of opto-electronic and electro-optic conversion and processing. This hypothesis should allow transferring very high bit rate optical signals also with complex modulation formats and multiplexing (for example in wavelength [100] or in polarization [101]). In this configuration, the connected input/output signal is presumably travelling into a single-mode fiber (SMF) coming from and going to the external network. The employment of MMF in the interconnect link between two SMFs might be critical because of the introduction at the output interface of power losses and modal noise, which cause undesired link loss fluctuations and can have a strong detrimental impact on the quality of the received signal [102]. Hence, the optical backplane should be composed by multimode fibers for their advantages but, in the meantime, allowing the transit of complex signals from the external network without introducing any impairment or exploiting optoelectronic conversions. Recently, for MMF propagation the mode-field matched (MFM) center-launching technique has been proposed, in which the beam profile of the incident light is precisely matched to the fundamental mode (LP_{01} mode) of the MMF [103]. Exploiting this technique, since only the fundamental mode of MMF is excited, it is possible to directly connect the input SMF to the MMF ensuring the transparency to the transmitted signal and SMF-like propagation [104], [61].

To explain the operating principle of the mode-field matched center-launching technique, first it is important to evaluate the launching condition required for exciting only the fundamental mode of MMF. For this purpose, it is necessary to calculate the coupling efficiencies of a few lower order LP modes of MMF as a function of the mode-field diameter (MFD) of the incident beam. In this calculation, we assumed that the incident beam had a Gaussian profile and was launched at the center of the MMF. For example is we consider an OM2 MMF (diameter: 50 μm) when the MFD of the incident beam was 14.5 μm, we could achieve an ideal mode-field matched condition as most of the launched power ($> 99\%$) was coupled into LP_{01} mode (see Fig. 3.5). The result also shows that this coupling efficiency is not sensitive to the minor variation of MFD from its optimum value of 14.5 μm. However, as the MFD of the incident beam deviates far away from this optimum value, the incident power tends to be coupled into higher or-

der modes (i.e.,LP_{0x} modes). For example, when the MFD of the incident

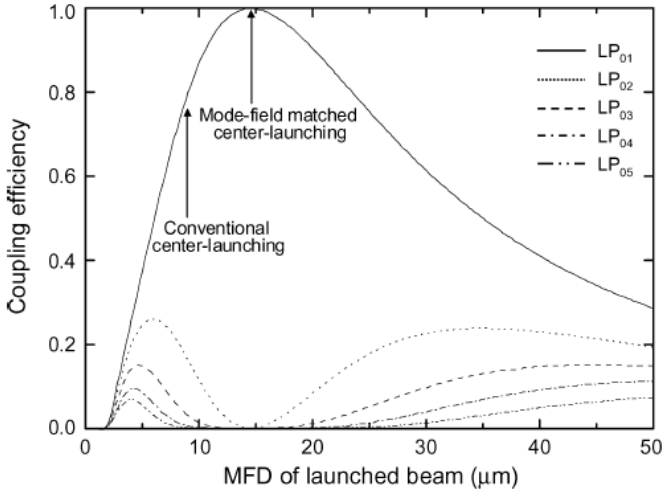

Figure 3.5: *Coupling efficiencies of a few lower order LP modes calculated as a function of the MFD of the incident beam for 50 μm graded-index MMF (λ=1304nm).*

beam was set to be 9 μm (to be same as the MFD of the conventional SMF at 1.3 μm), the total power of the excited higher order modes exceeded 20%. This condition (i.e., using SMF at the input of MMF transmission fiber) has been referred as "center-launching" in many previous literatures [105] - [107]. In fact, the so-called "center-launching" has been used for a wide range of launching conditions with large variations of the MFD and lateral offset of the incident beam.

3.2.1 Center-launching into MMF from VCSEL

In order to achieve center-launching condition into the MMF, a single-mode VCSEL source pigtailed by a standard step-index SMF has used as transmitter. The mode field pattern coming from the SMF matches very well with the fundamental mode of the standard graded-index MMF (OM2 with 50μm core diameter), allowing the excitation of just the fundamental mode LP_{01} in the MMF. In case of VCSEL emission directly coupled into the MMF by using a lens, owing the low mode field diameter (about 6 μm) and the high Numerical Aperture (NA) of the MMF, mode-field mismatch occurs and the higher-order modes starting from LP_{11} mode are excited into the MMF with a power comparable with that of LP_{01} mode. To evaluate the center-launching technique feasibility, some experiments have been carried

out. The power losses of the signal as a function of the lateral launch offset between the input SMF and the output MMF have been measured. The optical radiation coming from the SMF was butt-coupled into the MMF, and the offset between the two fibers was adjusted with step of 1 μm. At the receiver side the coupling between the MMF and the final SMF provides the mode filtering, allowing the measurement of the power lost by the fundamental mode and given to the other superior modes. In Fig.3.6 the experimental data are compared with the results of simulations realized by a suitable simulator (ModeSys) describing modes propagation in fiber. According to the simulations, when the lateral offset between SMF and

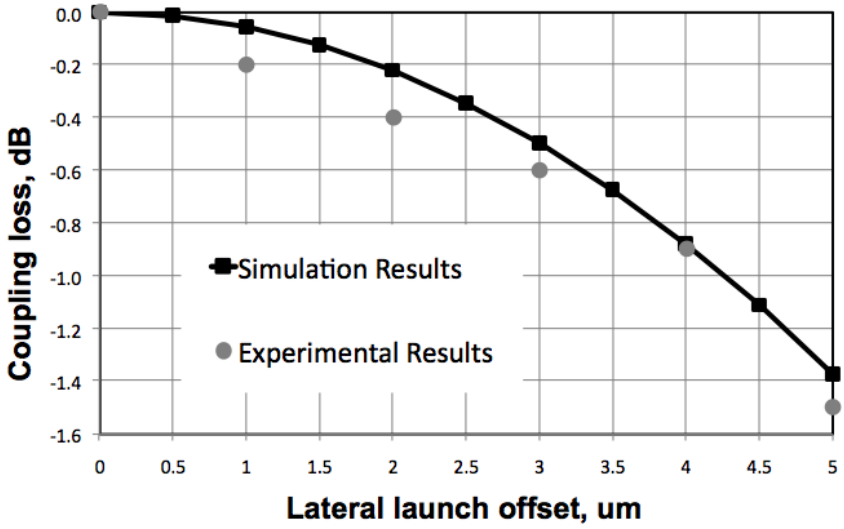

Figure 3.6: *Power lost from the MMF fundamental mode vs.the lateral launch offset between SMF and MMF.*

MMF is less than $\pm 1\mu$m, 96% of the optical power in the SMF is coupled into the fundamental mode of the MMF, while with a lateral offset of about $\pm 4\mu$m 80% of the optical power is still coupled to the LP_{01} mode. A simple fusion splice can maintain the misalignment under these values. Hence, in this experimentation center-launching condition by fusion splicing the SMF pigtailed with the VCSEL source and the MMF span has achieved.

3.2.2 Experimental results

The experimental setup used to characterize VCSEL-based 12.5-Gb/s propagation in MMF is shown in Fig. 3.7. The VCSEL source employed in the experimentation and suitable for high-speed applications was the same pro-

duced by VERTILAS described in [32]. The VCSEL was packaged into a pigtailed LC-TOSA: the output power was about 1 mW at 1335 nm with bias current set to 11 mA in uncooled conditions. Direct modulation at 12.5 Gb/s with NRZ-OOK data (2^{31}-1 PRBS pattern length) was performed. The

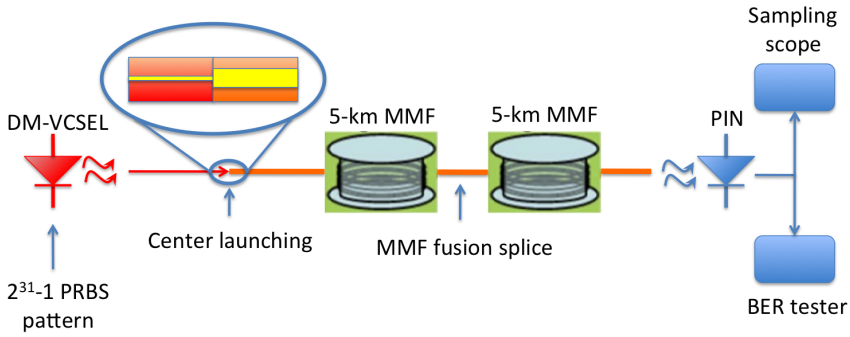

Figure 3.7: *Experimental setup.*

SMF pigtail was fusion-spliced with the MMF achieving center launching condition, as described previously. 12.5-Gb/s transmission performances were evaluated in case of propagation over both 5 km and 10 km of OM2-standard graded-index legacy MMF (50 μm core diameter), characterized by overfilled launch (OFL) bandwidth of 2000 MHz·km at 1310 nm. Therefore, it is worth to note that the maximum reach for 12.5-Gb/s transmission could be less than 160 meters. In this experimentation, the achieved center launching conditions guarantee a longer transmission distance than the maximum estimated from the OFL bandwidth. Moreover, operating around the null value of chromatic dispersion, no reach limitations due to chromatic dispersion are present. In case of 10-km propagation, we have employed two MMF spoils connected by standard fusion splicing. No addiction SMF patchcord is present between the two MMF spoils to filter the coupled-induced higher-order modes. At the receiver side the MMF optical output is directly detected by a free-space coupled PIN photodiode with a sensitivity of -13 dBm (@ BER = 10^{-9} with an extinction ratio of 12 dB). No SMF patchcord is present at the receiver in order to avoid mode filtering effects and polarization dependency. The PIN is then connected to the sampling oscilloscope or to the BER tester for the transmission performance characterization. By optimizing the amplitude modulation an extinction ratio of 6.2 dB is achievable at 12.5 Gb/s. In Fig.3.8 the BER curves as a function of the received optical power are reported. The figure reports the performance in back-to-back (BtoB) condition (black continuous line and full triangles), after 5-km (dashed line and open circles) and after 10-km

(continuous line and full circles) propagation over an unamplified MMF link (at 1.33 μm the attenuation is 0.45 dB/km and the dispersion is 2.5 ps/nm·km) without any dispersion compensation. It is interesting to note that no significant penalties are visible, both for 5-km and for 10-km propagation. Moreover, MMF performance are compared with the case of 10-km propagation (dashed line with open squares) over a standard step-index SMF (at 1.33 μm the attenuation is 0.35 dB/km and the dispersion is 2.5 ps/nm·km) and no significant differences are evident. The propagation over MMF does not cause serious impairments, demonstrating the capabilities of center launching technique to propagate at very high bit-rate.

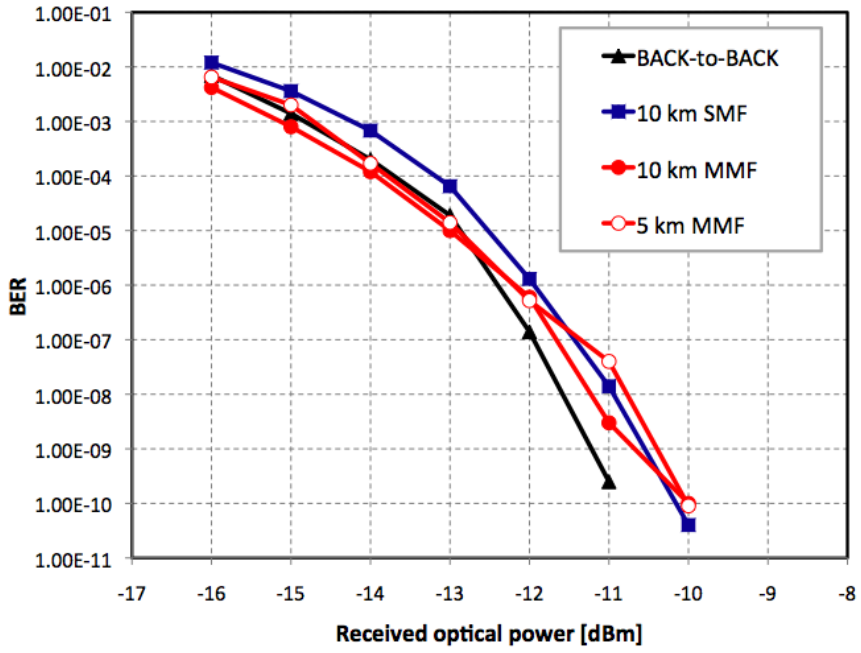

Figure 3.8: *BER curves vs. received optical power at 12.5 Gb/s.*

3.3 Robustness to mechanical perturbations

On the other hand, ETSI standards [108] recommend the robustness to mechanical perturbations required to the telecommunications equipment. If MMF center-launching condition is exploited, in case of external perturbations the system transmission performances could be deteriorated due to higher order modes excitation in MMF. Hence, it is mandatory to investigate the impact of mechanical perturbations on the performances of

these board-to-board MMF systems in order to guarantee error-free transmission [109].
In this section the analysis of the robustness of the center-launching technique in MMF in presence of mechanical vibrations up to about 1 kHz applied to the system will be presented.

Polarization analysis and transmission performances at 1-Gb/s bit rate are evaluated in case of propagation along 2 m of a standard graded-index legacy MMF, when the mechanical perturbation is applied. To reproduce different operating conditions in backplane applications, we have analyzed two experimental configurations: at first, the transmitted signal is received directly on a receiver, set on the board in the internal network; later, the transmitted signal is transferred into another external network in a transparent way passing through the MMF backplane. In the former configuration a simple free-space photodiode is adopted at the receiver side, while in the latter one a SMF pigtailed photodiode is used. Finally, we considered a 1-Gb/s transmission on a long MMF span (4.5-km length), e.g. when a large amount of modal dispersion could affect the performances if multimode propagation occurs in the link. This configuration emulates a direct connection between the backplane and a local area network in which the maximum transmission distance is not limited to 300 meters. As explained in the theoretical discussion, all these different experimental tests are necessary to exclude the generation of higher order modes in the MMF and to demonstrate the robustness of the center-launching technique to the applied mechanical vibrations.

3.3.1 Experimental validation in 2-m MMF link

The transparent connection achieved in a MMF by exploiting the center-launching technique was subjected to mechanical tests. The experimental set up used for the mechanical characterization is shown in Fig.3.9. The transmitter employed in our experimentation was a single-mode VCSEL source [32], [110] suitable for high-speed applications. The VCSEL was pigtailed by a standard step-index SMF; the output power was about 1 mW at 1335 nm with a bias current about 11 mA in uncooled conditions. Direct modulation at 1 Gb/s with NRZ data (2^{31}-1 PRBS pattern length) was performed.
In order to achieve the optimal center-launching condition into the MMF, the SMF pigtail was fusion-spliced directly to the MMF spoil of the length of 2m. The mode field pattern coming from the SMF matched very well with the fundamental mode of the standard graded-index MMF, which is

a OM2 fiber with 50 μm core diameter, characterized by overfilled launch (OFL) bandwidth of 2000 MHz·km at 1310 nm. If inaccurate SMF-MMF coupling is performed mode-field mismatch occurs and the higher-order modes are excited into the MMF with a power comparable with the one of the fundamental mode. The center-launching technique effectiveness was estimated without any applied vibration in presence of a free-space photodiode (PD) at the output. The measured power losses of the optical signal between the output of the pigtailed input SMF and the output of the MMF was about 0.4 dB. The intensity profile at the MMF output was monitored thanks to a CCD camera (in the inset of Fig.3.9 the detected light spot is shown). The very low power loss and the Gaussian intensity pattern visible after MMF propagation sustain the effectiveness of the realized center-launching technique.
Then, the MMF was fixed on the shaker, therefore the fiber does not move with respect to the shaker, when the vibration is applied, as shown in Fig.3.9. A sinusoidal signal at different frequencies (between 10 Hz and 800 Hz) was applied on a shaker to generate the vibration on the optical fiber. To verify the real mechanical transfer of the vibration to the MMF link, we chose to analyze the impact of the vibration on the state of polarization of the optical signal by means of a linear polarizer placed at the fiber output, before the free-space PD. In Fig.3.10 some examples of the signal at the output of the MMF are reported. Due to frequency response of the shaker checked by a suitable accelerometer the signal transferred to the MMF is very distorted at very low vibration frequencies. As the vibration frequency increases, it becomes more regular up to a good sine shape.

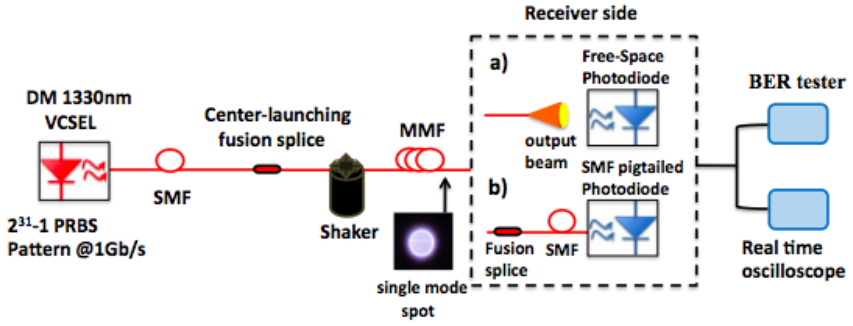

Figure 3.9: *Experimental setup in case of free-space PD detection (a) and in case of spatial filtering by SMF coupling before PD detection (b). In the inset the light spot at the MMF output after center-launching is shown.*

To check if the vibration affects the performances of the MMF intercon-

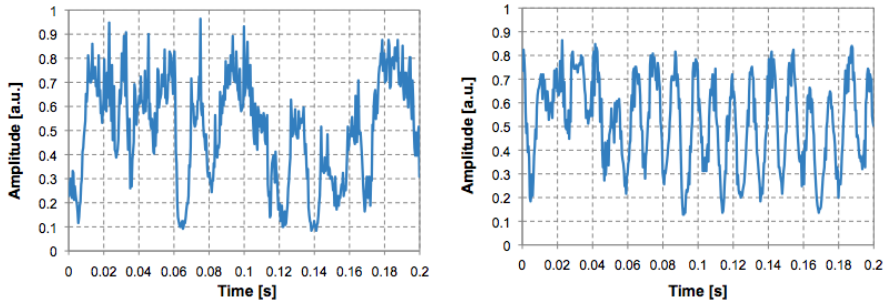

Figure 3.10: *Measured polarization response when a vibration of 18 Hz (a) and 38 Hz (b) is applied to the MMF. The range of amplitude values is normalized, with value 0 corresponding to polarization orthogonal to the analyzer and value 1 corresponding to polarization aligned to the analyzer.*

nect link, BER measurements were performed. The experimental setup was in this case without the linear polarizer used for the polarization analysis. At the receiver side, for the first round of measurement, the MMF optical output was directly detected by a free-space coupled PIN PD connected to the BER tester for the transmission performances characterization. The eye diagram of the received signal after 2-m MMF propagation is shown in Fig.3.11 in two different conditions: when no vibration and when a vibration of 97 Hz is applied (an extinction ratio of 6.2 dB was achievable optimizing the amplitude modulation). No visible distortions are present. The BER curves as a function of the received power are reported in Fig.3.12: The performances after 2-m MMF link at different vibration frequencies are shown. It is interesting to note that no significant penalties are visible, in spite of polarization changes previously measured.

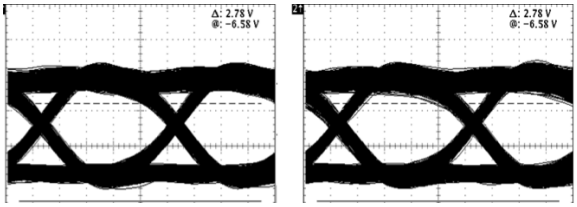

Figure 3.11: *Eye diagrams when no vibration is applied (on the left) and when a 97-Hz vibration is applied (on the right) on 2-m MMF.*

In order to verify the stability of the center-launching technique, a temporal BER analysis is carried out. The receiver power is fixed to be about

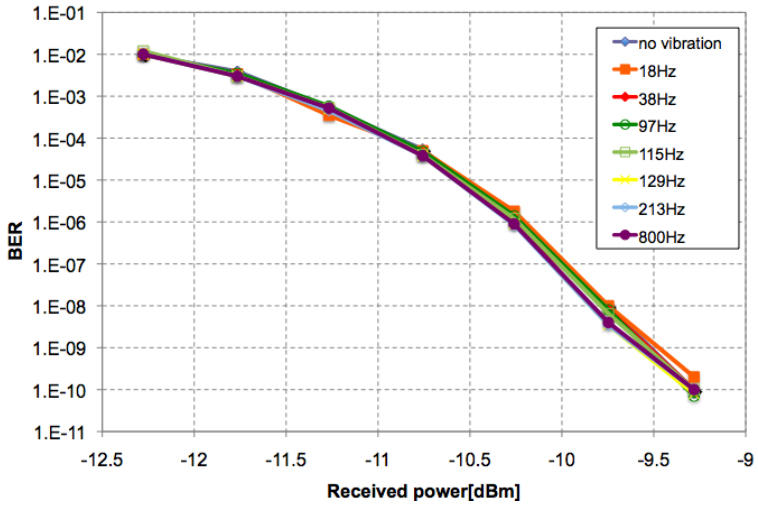

Figure 3.12: *BER measurements at different vibration frequencies in the free space configuration.*

-10.3dBm. Every 10 minutes the condition of the system was changed alternatively with no vibration and with vibration at different frequency. No significant BER variation around the value of 10^{-6} induced by the vibration is noticed Fig.3.13. BER fluctuations are limited in the normal error measurement range. These results demonstrate that the vibration does not modify the initial condition of the system and the polarization changes do not impair the system performances. As we will better explain in the theoretical discussion presented in subsection 3.3.2, the experimented absence of impairment in the propagation performances when mechanical vibrations affect the system does not entirely exclude the rise of higher modes in the under test MMF. Hence, BER measures were performed considering a second configuration at the receiver side: the end of the 2-m MMF was coupled with a SMF. In this configuration, the final SMF works as a spatial filter. If just the fundamental mode is propagating in the MMF, the mode matches with the single mode of SMF, showing fixed power losses for not-perfectly centered coupling. However, if higher order modes are excited in the MMF, they can couple with the fundamental mode of SMF, causing modal noise and affecting the system performances. Figure 3.14 shows BER measurements at different vibration frequencies in the case of SMF-coupling at the output of the experimental system before the receiver. A PD with a sensitivity of -17 dBm has been used. No visible degradation is present. The system performances do not change when the vibration is applied if the center launching technique is optimized. Finally, to check if the effects of

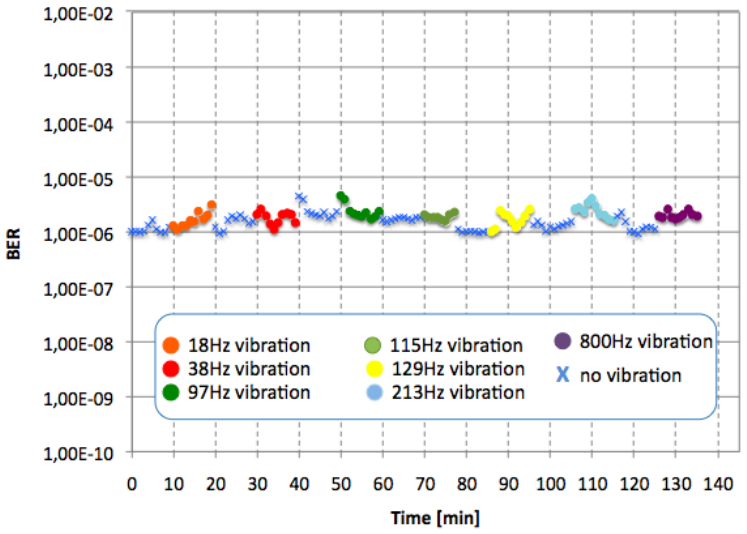

Figure 3.13: *Temporal BER measurements at different vibration frequencies and fixed receiver power in the 2-m MMF configuration.*

the vibration change for different positions of the applied vibration on the system, we placed the shaker on the first SMF span of the VCSEL pigtail. The measures were repeated in the same condition explained previously. Also in this case the vibrations do not affect the performances system.

3.3.2 Theoretical discussion

In the previous Section we have shown that an external vibration in the range 10-800 Hz does not introduce any significant impairment in 2-m MMF propagation when exploiting center-launching technique to excite just the fundamental mode in the MMF link. This result has been verified with and without the filtering effect achieved by coupling the MMF with a final SMF. It is important to know what value of frequency can induce the rise of high-order modes in the fiber. Generally, the external vibration produces an acoustic grating with a determined β_{eq}, which can permit the energy flow from one mode to the other [111]. To make possible this transfer the β_{eq} of the grating must be similar to the difference of the propagation coefficient $\Delta\beta$ between the two modes. More a mode is close to another one in terms of propagation coefficient, more the energy transfer between them is possible. Furthermore, in order to have a significant coupling efficiency, the spatial pattern of the perturbation must show the symmetry for matching one mode to another. For matching the modal beat length [111], [112]

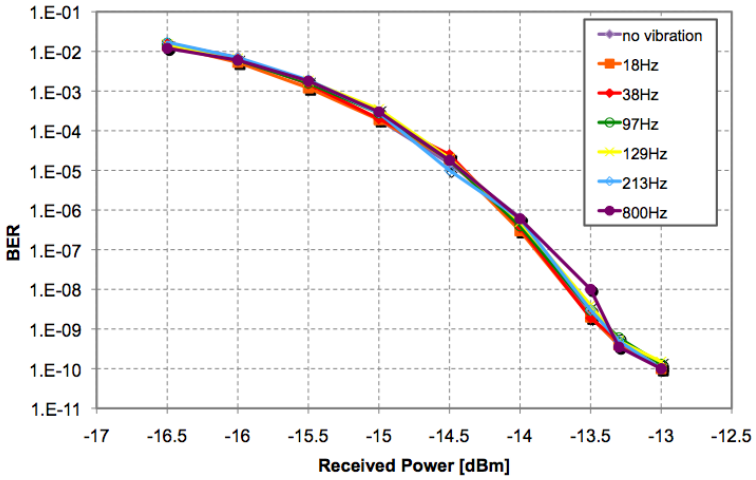

Figure 3.14: *BER measurement at different vibration frequencies in SMF-filter configuration.*

and inducing mode coupling, the frequency f of the external mechanical perturbation is related to $\Delta\beta$ as follows:

$$\Delta\beta = \frac{2\pi}{\nu} f \tag{3.23}$$

where ν is the velocity of an acoustic wave travelling in SiO_2. Since the system is based on the central launching technique, we can consider only the coupling between the fundamental mode and the higher order modes, neglecting the higher-order to higher-order coupling. The closest mode with respect to the fundamental one is the LP_{11} mode. From eq. 3.23 it is possible to estimate the frequency needed for matching the difference in the propagation constants of the LP_{01} and LP_{11} modes. Entering the geometrical parameter of the OM2 fiber, the difference $\Delta\beta_{01/11}$ has been evaluated by BeamPROP Tool, obtaining $1.18{\cdot}10^3$ m^{-1}, which corresponds to a beat length between LP_{01} and LP_{11} modes of 5.3 mm. Therefore, in order to obtain the coupling between the two considered LP modes it is required a spatially-periodic perturbation [112] with quite small pitch. Using Eq. 3.23 we obtain an acoustic frequency f of about 1 MHz. Due to this high frequency value, a realistic external perturbation can difficulty lead to a power transfer between the fundamental and a higher order mode. Moreover, it is important to notice that generally no penalties can be observed for very short propagation distance and free space detection after MMF propagating (without SMF filter) if the whole optical field is received by the PD. Also when multimode propagation occurs, thanks to the orthogonality of the dif-

ferent modes of a multimode fiber, no beating will be seen at the receiver if the whole spatial distribution of the output optical field is collected in the PD area. In fact, considering two generic modes in cylindrical coordinates, the electrical signal after the detector can be expressed as

$$\iint |E_1^*(\rho,\vartheta)e^{j\varphi_1} + E_2(\rho,\vartheta)e^{-j\varphi_2}|^2 d\rho d\vartheta = \iint |E_1(\rho,\vartheta)|^2 d\rho d\vartheta + \iint |E_2(\rho,\vartheta)|^2 d\rho d\vartheta + 2\Re\Big\{\iint E_1^*(\rho,\vartheta)E_2(\rho,\vartheta)e^{-j(\varphi_2-\varphi_1)} d\rho d\vartheta\Big\} = \\ = I_1 + I_2 + 2cos(\varphi_2-\varphi_1)\Re\Big\{\iint E_1^*(\rho,\vartheta)E_2(\rho,\vartheta) d\rho d\vartheta\Big\}, \tag{3.24}$$

where ρ and ϑ are the radial and azimuthal coordinates, respectively, $E_1(\rho,\vartheta)$ and $E_2(\rho,\vartheta)$ are the electric field distributions of two generic modes propagating in the multimode fiber and I_1 and I_2 are the associated intensity, while φ_1 and φ_2 are the generic phase terms due to propagation. If the receiver collects the whole spatial profile of the two modes or selects a circular section of the spatial field centered on the optical axis of the MMF the last integral in Eq.3.24 will vanish thanks to the orthogonality between the modes. In this situation, the performances of the system may be limited only by modal dispersion. Eq.3.24 can be generalized for n incident modes leading to the same results. When a spatial filter is introduced (for example by coupling the MMF with a SMF), instead, only a part of the spatial distribution at the output of the MMF can couple to the fundamental mode propagating in the SMF. Since the MMF to SMF alignment cannot be perfectly controlled, the presence of higher order modes is traduced in a reduction of the coupled power and in the generation of modal noise. Moreover, the arising of modal noise normally leads to an increasing of polarization dependence in the performances of the optical system. Hence, while short-reach free-space detection is robust also in presence of higher order modes generated in input or by an external perturbation, a SMF-MMF-SMF system demands strict requirements in terms of modal purity in the multimode section.

3.3.3 Experimental validation in presence of large modal dispersion

In subsection 3.3.1 also the SMF-MMF-SMF link exploiting center - launching in 2-m MMF has been demonstrated very robust to external mechanical perturbations. But, as explained in subsection 3.3.2, this configuration employing SMF filtering remains extremely sensitive to the presence of higher order modes in fiber. The experimentally measured absence of modal noise

in this measurement in Fig. 3.14 could be due to a particular splicing between MMF and SMF. A large amount of splicing with different offset should be tested to guarantee that no higher order modes are generated and so no modal noise can occur in case of spatial filtering due to fiber connections. To demonstrate that actually no higher-order modes are excited when vibrations affect the link exploiting center-launching, the propagation on a longer OM2 MMF span (4.5 km) have been analyzed. For this reach, operating at 1-Gb/s bit rate at 1335 nm, modal dispersion should be evident in case of multimode propagation (OFL bandwidth is 2000 MHz·km at 1310 nm). Moreover, this configuration suggests the capability of exploiting the center launching technique to transmit directly from the backplane to a LAN longer than 300 meters. Thanks to the center launching, in fact, the reach limitation due to modal dispersion will be greatly reduced. A complete integration between optical backplanes and local area networks could be mandatory in future short-reach networks for limiting costs, power consumption, guaranteeing greater scalability and simplicity. Both detection configurations analyzed for 2-m MMF propagation have been considered. By exploiting free-space PD configuration, it is able to eventually check the impact of pure modal dispersion in the BER measures; in case of SMF-filter configuration at the receiver side, also the penalties due to modal noise could be observed. The BER measurement at different vibration frequencies for both configurations are shown in Fig.3.15. For free-space configuration, no significant penalty is shown for the different vibration frequency. The slight spread of the curves at very low BER ($10^{-9} \div 10^{-10}$) is due to the absence of clock and data recovery and it is in the range of the measurement error. When the SMF filter is inserted, a slight spread can be observed for BER lower than 10^{-6} , i.e. a degradation due to modal noise is noticed. However, all the curves are enclosed in a range of about 0.5 dB and no error floor is visible, making the center launching technique suitable also for medium-reach local area networks.

In this Chapter it has been shown that the exploitation of center-launching technique guarantees an almost SMF-like propagation in MMF. The transmission of a 1-Gb/s NRZ OOK signal remains robust to mechanical perturbations as required by ETSI recommendations, demonstrating that no higher order modes are generated owing to the applied vibrations. No BER penalties have been obtained for vibrations with frequency up to about 1 kHz, both by directly detecting the optical signal at the MMF output by a PD and by coupling the MMF with a SMF in order to achieve a spatial filtering of the field propagating in the MMF. To confirm SMF-like propagation and to exclude multimode propagation in the MMF subjected to vibrations,

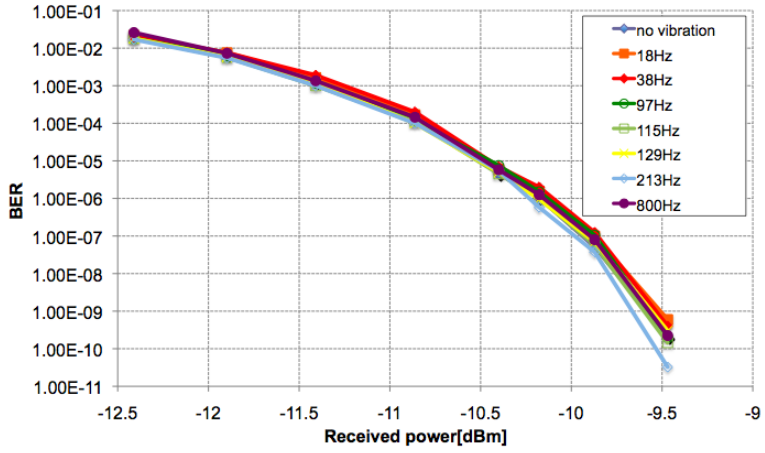

(a)

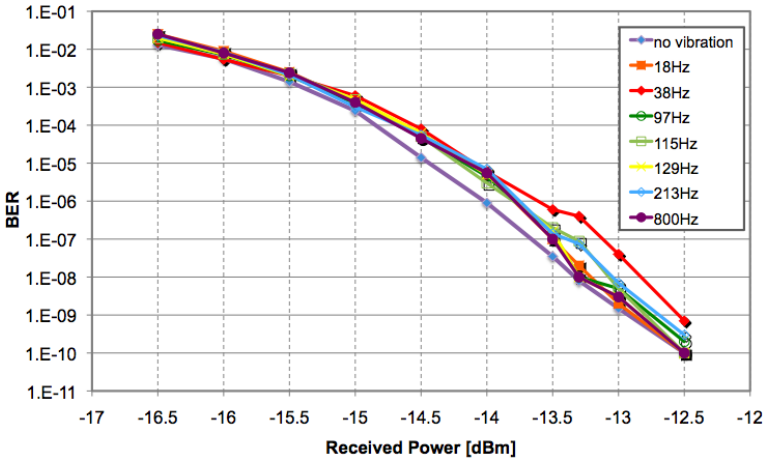

(b)

Figure 3.15: *BER measurements at different vibration frequencies after a propagation of 4.5 km in the MMF (a) and in the SMF-filter (b) configurations.*

also BER tests in case of a long MMF span in presence of a large amount of modal dispersion have been performed. The actual account of the mechanical perturbation frequency that can induce the generation of the first higher order mode has been achieved by suitable simulations, obtaining a frequency of about 1 MHz, much larger than the frequencies characteristic of the realistic environmental perturbations. Therefore, from the mechanical point of view, center-launching technique appears as a promising method to ensure full transparency to the transmitted signals for applications in board-to-board and data server interconnects.

CHAPTER 4

VCSEL and Silicon Photonics-based datacom optical links

In the previous Chapters we presented a comparison between an electrical and optical fiber-based backplane in terms of power consumption and capacity. A fiber-based optical backplane has been analyzed and some relevant aspects, like choice of optical fibers, type of connectors, material for mechanical support and layout have been taken into account to allow a realization of the optical backplane. Moreover, the design of the fiber-based optical backplane was carried out taking into account scalability of the system, low cost, transparency to modulation formats and bit rates, mechanical robustness and keeping the complexity of manufacturing as low as possible. In this Chapter, we address the most up-to-date technologies, like VCSEL and Silicon Photonics, for the electro-optical (EO) transceiver and their evolution for bakplane-based interconnections in order to increase the bandwidth and improving the power efficiency of the whole system. We will focus the attention on modulation formats as a way of increasing the link total capacity, maintaining the same number of optical interconnections. For both technologies, a performance analysis of standard On-Off-Keying (OOK) and M-Pulse Amplitude Modulation (M-PAM) is

reported. A power consumption comparison will be given between 4-PAM and Non-Return-to-Zero (NRZ) OOK and simulative results will be discussed in order to highlight the different performances and limitations for VCSEL-based and Silicon Photonics based links.

4.1 Introduction

The IEEE 802.3ba standard in definition by Ethernet Technology Summit, defines and regulates data communication links for short-reach applications. At the physical level, the adoption of EO transceivers is expected for high capacity links. In particular, the 100 Gb Ethernet standard either for short-reach VCSEL/MM-based optical links for less than 100 m or single-mode (SM) links serving over 10 km [113]. From the Ethernet Technology Summit, short-reach optical links should support 100Gb/s/fibre up to an aggregate data rate of 400Gb/s [114]. Figure 4.1 shows a scheme of a possible evolution of the link architecture for achieving this total capacity with implemented VCSEL-based transceiver (Fig.4.1(a)) or Silicon Photonics transceiver (Fig.4.1(b)). In order to increase the bandwidth of the data link, five possible solutions could be exploited:

- Increase the transmission frequency
- Increase the number of fibers
- Increase the number of modes (Mode Division Multiplexing- MDM)
- Increase the number of wavelengths per fiber (Wavelength Division Multiplexing-WDM)
- Increase the number of bits per symbol.

The first approach is to increase the transmission frequency of the electro-optical devices used in the optical transmission system. However, this involves high speed electronics and fast optical devices.
Enhancing the number of optical channels could be a solution to satisfy the higher bandwidth demand. However, the overall costs can grow because of the increasing of the optical interconnecting media: in fact, more complex ribbon connectors and layout are requested.
In WDM spatial links, different data channels can be propagated on a single optical fiber using multiple wavelengths. Commercial WDM mux/demux are currently deployed for long-reach applications and now are used also in

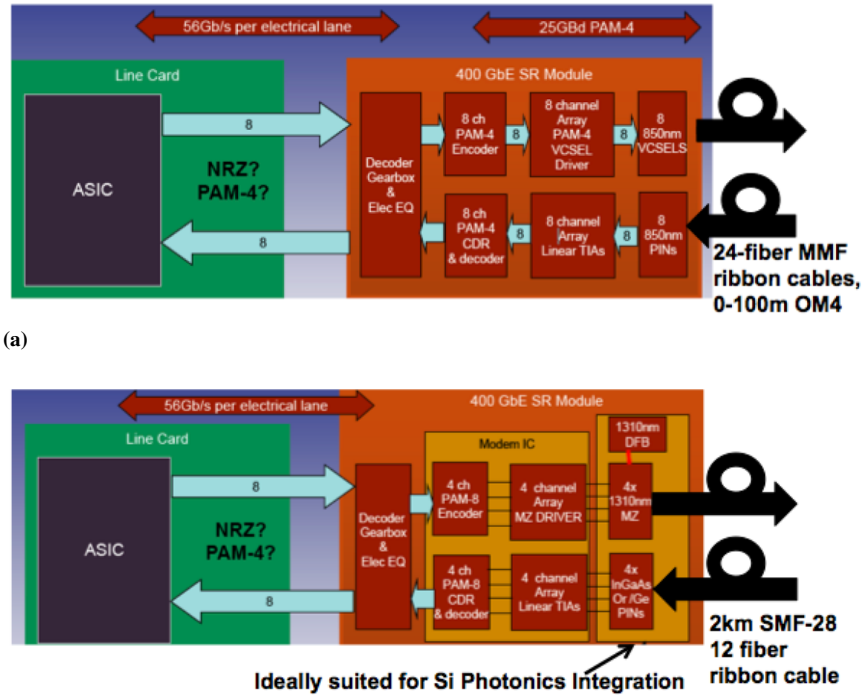

Figure 4.1: *Possible 400G system architecture. (a) 8 parallel full duplex 850nm 4-PAM operating at 25 Gbaud. Reduces cost, density and power, using existing cable plant. (b) 4 parallel full duplex 1310nm 8-PAM channels on a ribbon fiber operating at 35 Gbaud, only 1 DFB laser is required. Reduces cost, density and power using existing SMF ribbon cable plant.*

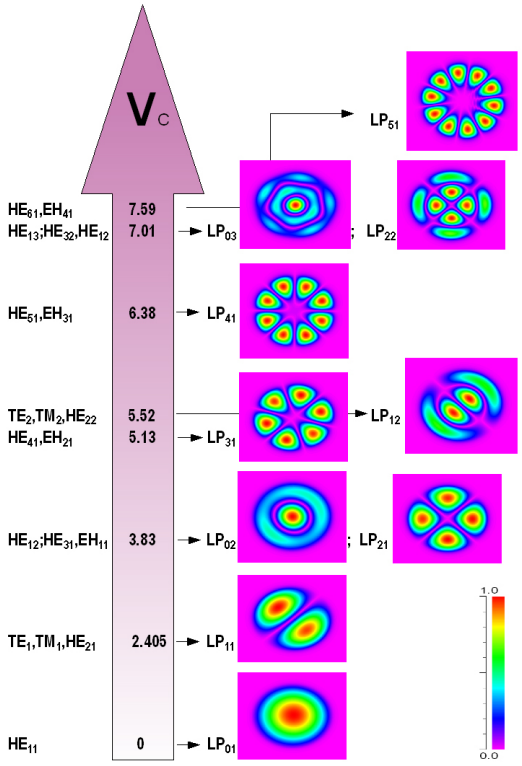

Figure 4.2: *Several modes can be excited and propagated into an optical fiber. The diagrams on the right represents the intensity distribution of the propagating mode in a given section of the optical fiber.*

metro optical networks [115]. The implementation of WDM technique requires dedicated components and design that can increase the cost of the EO transceiver. Mode division multiplexing (MDM) could be a suitable technique for multimode links. Choosing a suitable subset of propagation constants, independent signals can travel on different propagation modes as can be visualized in Fig.4.2 [116]. In the last years, some mode multiplexing and demultiplexing techniques have been experimentally validated. However, MDM technique is still far from integration into commercial products. On top of the high-speed requirements, these links must also comply with stringent power consumption, cost and size limitations. The introduction of multi-level modulation format can be an interesting tradeoff. For limiting cost and complexity, we will focus only on simpler amplitude modulation formats, such as M-PAM.

Also for electrical backplane-based applications M-PAM has been investigated to understand advantages and disadvantages with respect to OOK modulation format, in order to increase the bandwidth. 4-PAM does not have a demonstrated performance advantage over OOK for this set of backplanes. 4-PAM will perform better or worse than OOK based on channel design factors [117] - [120]. For optical fiber- based backplane use it is interesting to understand (e.g. from power consumption point of view) which modulation format is the most performant. As we have seen in the previous Chapter the optical fiber doesn't affect the transmission performances because the length is about 1 meter and the losses are negligible. The main contribution depends on the driver, type of the source and receiver circuits. In the next section, a brief review of the OOK and 4-PAM modulation format will be presented.

4.2 OOK and 4-PAM

The classical approach for the transmission of data over fiber-optic based link has been the use of OOK by binary encoding the zero and one bits into intensity modulation of the optical transmitters. An NRZ modulation format where the intensity of the light remains at its high level when consecutive "1" bits are transmitted, is the simplest modulation format under consideration, being simply PAM with two levels. This scheme is often used as a benchmark of the system performances. The main advantage of the NRZ-OOK modulation format is the low-complexity of the transmitter and receiver. The main disadvantage is the dependency on the speed of the eletro-optical transmitter. In fact, the electro-optical bandwidth of the devices is proportional to the bit rate. At the transmitter side, a directly modulated VCSEL or a DFB-laser external modulated utilizing Mach-Zehnder modulators (MZM) or electro-absorption modulators (EAM) are usually used. On the receiver side an intensity modulation direct detection (IM/DD) of the optical data through high speed photodiode is usually preferred in short-range optical network, instead of coherent detection, because of cost constraints. The data signal is detected by a high-speed photodiode and processed utilizing high-speed analog and/or digital electronics. For the realization of 100 Gb/s OOK systems the performance of high-speed electronic and opto-electronic components and as well as integration and packaging technologies have to be pushed to current technology limits. For example, due to limitations of the bandwidth of the devices, optical equalizers are applied to improve the signal quality at the transmitter output or at the receiver input [121].

The continuous demand of bandwidth for the data-link drives to consider more spectrally-efficient (i.e., the number of bits per Hz) modulation formats relative to the common NRZ OOK scheme. Many modulation formats have been considered. High spectral-efficiency modulation formats such as PAM, quadrature amplitude modulation (QAM), Quadrature Phase Shift Keying (QPSK), Differential QPSK (DQPSK), subcarrier modulation scheme (SCM) and Discrete multi-tone modulation (DMT), which is a multiple subcarrier scheme, were investigated [122]. Single-cycle or sub-cycle QAM modulation SCM have been demonstrated in links using VCSELs [123]- [125]. Also high speed data transmission of DMT signal using VCSELs has been demonstrated recently [126], [127] and a practical alternative such as carrierless amplitude and phase (CAP) modulation has been considered [128]- [130].
All these schemes require complex implementation and integration of digital/analog electronic conversion. This is an important limitation in the design of short-range data communication links. Higher complexity means higher power consumption, which is undesired in densely packed data centers. A relatively simple multilevel modulation format beyond the conventional OOK is M-PAM, encoding $log_2 M$ bits per symbol. For example, 4-PAM consists of two bits per symbol which allows transmission of an equivalent amount of data in half the bandwidth. The real-time transmission and reception have been demonstrated [131] - [134].
In order to decrease the power consumption of the system it is important to achieve a tight integration of electronics and optical technologies. Several efforts have been made to realize high data rates with low power dissipation, and recent breakthroughs have been made by deploying Complementary metal-oxide semiconductor (CMOS) technology for high-speed laser diode drivers (LDDs) and high-speed transimpedance amplifiers plus limiting amplifiers (TIA/LIAs). Nanoscale CMOS circuits offer good high-speed performance at power supply voltages below 2 V, enabling low-power operation. In contrast, high-speed circuits for optics using SiGe heterojunction bipolar transistors typically use power supply voltages greater than 2 V (often 2.5 V, 3.3 V, or 5 V), resulting in higher power consumption. In addition, nanoscale CMOS offers the possibility of integrating higher degrees of functionality into transmitter and receiver chips, such as equalization and clock and data recovery (CDR). The steadily decreasing channel length of CMOS transistors, also contribute to the trend of decreasing power consumption. At the circuit level, the downward trend in power supply voltages of advanced CMOS Integrated Circuits (ICs) accounts for much of the power savings. Additionally, at the device level, the shorter gate length

increases the bandwidth, which enables reductions in energy per bit consumption.
For the implementation of NRZ-OOK and 4-PAM based data-link two technologies were compared: VCSEL and the emerging Silicon Photonics.

4.2.1 VCSEL-based technology

The sources usually used for short range links are directly modulated lasers. VCSELs are popular because of their low cost, low power consumption and high efficiency. Moreover, the size and numerical aperture of multimode VCSEL allows efficient fiber coupling with multimode optical fibers. Recently very fast directly modulated VCSELs were developed and used with OOK modulation. It has been possible to achieve very high bit rate pushing their limits, using a pre-emphasis at the transmitter [135] and/or equalization at the receiver [136]. An optical interconnect has to be designed to meet the requirements of input and output electrical signals, such as a voltage amplitude and data rate [137]. The optical link consists of an EO transmitter, an optical interconnection channel and opto-electrical (OE) receiver. Mainly, the transmitter is composed by: a pre-amplifier, a laser diode driver (LDD) and a VCSEL source. The receiver consists in a photodiode, a Transimpedance amplifier (TIA), a limiting amplifier (LA) and an output buffer (OB).

The fastest demonstrated serial data rates that achieve error free transmission (commonly defined as BER < 10^{-12}) are: a 55Gb/s equalized [60] and 44Gb/s unequalized [64] VCSEL-based link at 850nm, 49Gb/s at 980nm (-10°C) [138], 40Gb/s at 1100nm [139], and 35Gb/s at 1550nm [31]. It is important to notice that many of the record VCSEL modulation results are obtained with test equipment in research labs. A complete link analysis (laser driver + VCSEL to photodiode + RX IC) has been reported in the paper [140]. Here it has been demonstrated that advanced VCSELs, combined with fast circuits and equalization, can operate above 50Gb/s and should continue to be part of the solution for future high speed serial links. To date, this reported data rate of 56.1Gb/s is the highest data rate for any VCSEL link, regardless of wavelength.
A VCSEL-based MM fiber optical links using 90 nm CMOS circuits that achieve sub-2 pJ/bit power efficiencies at data rates greater than 10 Gb/s was demonstrated [141] and a record optical link power efficiencies of 1pJ/bit at 25Gb/s and 2.7pJ/bit at 35 Gb/s using 32-nm SOI CMOS circuits [142] are achieved. VCSEL-based transceivers for commercial prod-

ucts are used in HPC system, for example the microPOD by AVAGO (see Chapter 1).
An alternative way of achieving a further increment of the total capacity of the system is to parallelize the transmission using VCSEL arrays as sources. Fully functional holey Optomodules with 24 TX and 24 RX channels operate up to 12.5 Gb/s/ch achieving efficiencies (including both TX and RX) of 8.2 pJ/bit [143]. The second generation consists in a 24 TX + 24 RX transceiver. All channels operate at 20 Gb/s (BER $<10^{-12}$, 7.3 pJ/bit) achieving record aggregate bidirectional bandwidth for parallel transceivers of 0.48 Tb/s [144].
Improvements on long-wavelength VCSEL array have been made [145]-[147] making them suitable for wavelength Division Multiplexing (WDM) or Coarse WDM (CWDM) applications.
4-PAM was extensively studied and implemented in VCSEL-based links [148]- [153]. This is in order to keep design and implementation of the VCSEL-based transceiver simple and to increase the spectral efficiency. An example of this technology will be simulated and assessed in the next section.

4.2.2 Silicon Photonics-based technology

Tremendous progress has also been made in efficient silicon photonic device development. Energy-efficient silicon photonic transmitters require high speed modulators with low parasitics that can achieve high extinction ratios with a low voltage swing. Similarly, energy-efficient receivers require high-speed photodetectors with low capacitance, low dark current, and high responsivity. Ring modulators and Ge-based photo-detectors achieve these qualities [154]- [156]. Usually, Silicon Photonics plays a main role for WDM and DWDM applications. To satisfy the bandwidth demands, the degree of WDM has to increase beyond the current four WDM channels of the 100 GbE standard. WDM technology can potentially provide the terabit bandwidth offered by an SM fiber, especially promising at relatively short distances of just a few kilometers where dispersion penalties do not yet play a significant role. However, the number of WDM channels and, correspondingly, the channel spacing will most likely be limited to less than 10 due to cost and power limitations associated with the technical solutions that can provide reliable uncooled operation and a high degree of integration [157], [158]. Integration of analog and mixed-signal circuits (AMS) together with optical components such as modulators, photodetectors (PD), and WDM filters is considered a viable approach for sig-

nificantly decreasing the cost of optical transceivers and for their massive deployment in large scale systems [159], [160]. In addition to efficient photonic devices, optical links also require low-power CMOS circuits to drive the modulator and to sense the photodetector current. Silicon photonics suggest monolithic integration with CMOS circuits and hence the possibility of minimized integration parasitics. However, special substrate requirements for optimized photonic device performance limit the choice of CMOS technology node; thus, CMOS platforms optimized for photonic devices are typically a few generations behind the state-of-the-art technology node. For optimized system energy efficiency, a better alternative is to decouple the photonic devices and CMOS circuits, and to take full advantage of low-power high-speed photonic devices and advanced circuit technologies simultaneously using hybrid integration.
Silicon Photonics components have been used to implement different high-order modulation formats [161]- [163]. Focusing on M-PAM, Silicon Photonics is a potential medium for PAM solutions: current modulators can be easily modified to act as PAM encoders. Minimal design alterations are required with no technology changes. A segmented Mach-Zehnder is used to implement M-PAM format [164] - [166] as detailed explained in the next sections. However, high power consumption, low link density and high cost seriously prevent traditional MZ from being the next generation of optical link technology. To fundamentally reduce the cost of MZ, it is highly desirable to make the process CMOS compatible with high efficiency, thus the modulation voltage, size, and power can be reduced to a level where advanced sub-1V CMOS circuits can be used as the driver. Two CMOS-MZ-based optical transmitters, OOK or configurable M-PAM (M = 4,16), featuring 20Gb/s data rate and sub-pJ/bit modulation energy (4-PAM) using a 1V supply have been demonstrated [167].

4.3 Link simulations

A comparison between VCSEL-based and Silicon Photonics-based link, in case of OOK or 4-PAM transmitted signals, will be presented. A simulative optical link has been designed. Then, the operating conditions to achieve error-free transmission have been found out. Based on these results, we analyzed the devices involved in the transmission and receiver part, quantifying their power consumption. These considerations have been done for short-reach applications (including backplanes). Moreover, propagation simulations (on standard single mode optical fiber) have been carried

out to understand the limitations of the two technologies at very high bit rate (beyond 25Gb/s).

4.3.1 4-PAM characteristics

As explained in section 4.1 the objective is to achieve an aggregate bit rate of the link of 400Gb/s using for example 8 channels at 50Gb/s. It is possible to use an OOK or 4-PAM modulation format for each channel. PAM is the transmission of data by varying the amplitude (voltage or power levels) of the individual pulses in a regularly timed sequence of electrical or electromagnetic pulses. The number of possible pulse amplitudes can be infinite (in the case of analog PAM), but it is usually some power of two so that the resulting output signal can be digital . For example, in 4-level PAM there are 2^2 possible discrete pulse amplitudes; in 8-level PAM there are 2^3 possible discrete pulse amplitudes and in 16-level PAM there are 2^4 possible discrete pulse amplitudes and so on. For a fixed total transmitted power and bit rate, 4-PAM (where four-level of the signal are transmitted obtained by encoding two consecutive bits into single symbol) allows to double the bit period at the expense of the reduction of the extinction ratio of two adjacent symbols. This tradeoff is attractive because short-distance optical link are constrained by data rate and power consumption, but typically they have enough received optical power to achieve error-free transmission. The bandwidth of M-level PAM is $1/log_2(M)$ of the OOK signal bandwidth at the same bit-rate, where M is the number of levels [168]. For 4-PAM, this means that the bandwidth is reduced by half, compared to OOK at the same bit-rate. Under assumptions that the noise is additive, white, and stationary, the optical power penalty for using a multilevel PAM, compared to OOK at the same symbol rate, in terms of the required optical power in dB to reach the same BER is

$$P_{ps} = 10log_{10}(M-1) \tag{4.1}$$

where M is the number of the PAM levels. This means that an additional 4.8 dB received optical power is required for 4-PAM at the same symbol rate of the OOK modulation format. The penalty is less when the bit-rate is kept fixed, because of reduced bandwidth. The optical power penalty for M-PAM, relative to OOK at the same bit-rate P_{pb}, is expressed in dB as

$$P_{pb} = 10log_{10}\left(\frac{M-1}{\sqrt{log_2(M)}}\right) \tag{4.2}$$

according to [168]. For 4-PAM this gives that an additional 3.3 dB optical power is required at the receiver, compared to the OOK signal at the same

Table 4.1: *Two labeling for M=4.*

Symbol	Natural	Gray
0	00	00
1	01	01
2	10	11
3	11	10

bit-rate to reach the same BER. The 4-PAM bit encoding into one symbol can be carried out using two different labeling: the natural and the Gray labeling as reported in Table 4.1. The BER is dependent on the labeling of the symbols. Gray labeling usually provides the best performance [169], though natural labeling is often used in lab experiments since easier to implement. Assuming that all M symbols are equiprobable, thermal noise is dominant, all symbol levels are equally spaced, and the decision thresholds are equidistant from adjacent symbols, the Symbol Error Rate (SER) can be expressed as:

$$SER = \frac{M-1}{M} erfc\left(\frac{I_{avg}}{(M-1)\sqrt{2}\sigma}\right) \tag{4.3}$$

where I_{avg} is the average photodetector current and $\sigma = \sigma_i$ for all i levels is the Root Mean Square (RMS) noise current. For high signal to noise ratios (SNRs), it can be assumed that only errors between adjacent symbols occur. In that case, the BER can be approximated as

$$BER_{approx} \approx d_{avg} \frac{SER}{log_2(M)} \tag{4.4}$$

where d_{avg} is the average Hamming distance (the number of bits which differ between two binary strings) between the labels of adjacent symbols. If natural labeling is used, the BER is still well approximated by Eq.4.4, where in this case

$$d_{avg} = \frac{\sum_{k=0}^{log_2(M)-1} (log_2(M) - k)2^k}{M-1} = 2 - \frac{log_2(M)}{M-1}. \tag{4.5}$$

Theoretical BER curves in case of natural labeling at 12.5Gb/s and 25Gb/s using OOK modulation format and PAM-4 are reported in [134].

Figure 4.3 shows the optical output power of a VCSEL versus its bias current in case of 4-PAM modulation format. Because VCSELs emit only for bias current greater than their treshold current, the first PAM level (lowest order symbol) must be generated at bias current sufficiently large compared

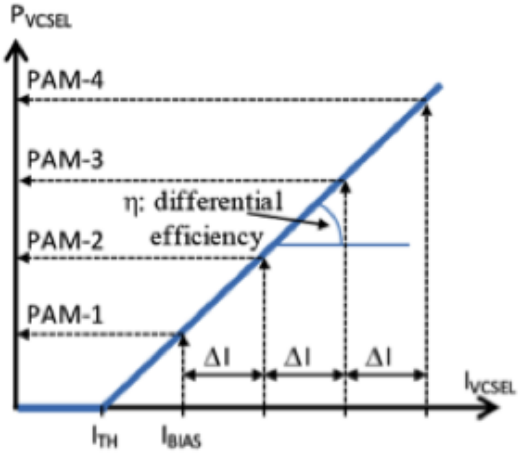

Figure 4.3: *VCSEL power vs current relationship in case of 4-PAM modulation format.*

to the VCSEL threshold. This bias current needs to be small enough to ensure sufficient modulation contrast. The other PAM symbols are generated by driving the VCSEL with an additional current ΔI per each PAM level.
4-PAM can also be implemented using Silicon-Photonics technology. In this case a segmented-Mach Zehnder as shown in Fig.4.4 is used. Since the output optical power is proportional to the MZ length, by cascading multiple MZ segments and driving them separately with inverters, multiple output levels can be realized, without using Digital-to-Analog Converter (DAC) [170]. An electro-optical modulator is formed to include a plurality of separate electrodes disposed along one arm, the electrodes having different lengths and driven with different signals to provide for 4-PAM signaling. By using separate drivers for each section, the number of sections driven at a given point in time will define the net phase shift introduced to the optical signal. The total length of the combined modulator sections is associated with a π phase shift (180°). Each section is driven by either a digital "one" or "zero", so as to create the multi-level modulation. An essentially equal change in power between adjacent transmitted symbols is accomplished by properly adjusting the lengths of each individual section. Hence, segmented MZ plus simple digital drivers provide built-in DAC function for PAM.

4.3.2 Simulation conditions

The OptSim ^{TM} software has been used to design and assess the optical link [171]. To modelize a correct behavior of the device, this software

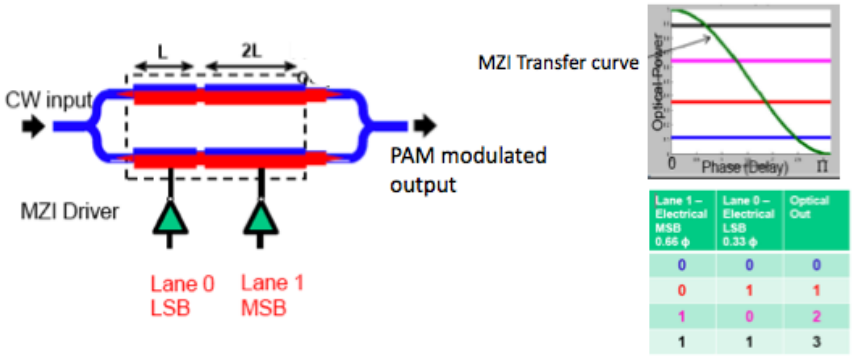

Figure 4.4: *Segmented Mach-Zehnder to generate a 4-PAM modulated signal.*

requires an accurate definition of the physical parameters of the devices involved in the simulation.
A simulative optical link for OOK and 4-PAM transmission signal has been designed. The theoretical OOK and 4-PAM BER curves have been used to set the correct parameters of the optical link.
In case of 4-PAM, three thresholds determine which symbol is received at the receiver. OptSim does not provide Bit Error Rate (BER) evaluation for a multi-thresholds system. For this reason and to have more degrees of freedom at the receiver side, a Matlab script was designed for the multi-level OE receiver. After propagation into the optical fiber and before to enter into a photodiode, the optical signal is acquired and processed in Matlab. Moreover, the noise (σ^2) is added at the receiver as a sum of three different contributions: the shot noise (σ_s),the thermal noise (σ_t) and the Relative Intensity Noise (RIN) [122], where

$$\sigma_t = 4KBTF_n \frac{B_{el}}{R_L}, \tag{4.6a}$$

$$\sigma_s = 2qI_{tot}B_{el}, \tag{4.6b}$$

$$RIN = RIN_{coeff} I^2 B_{el}. \tag{4.6c}$$

The values denoted by KB,T,F_n, B_{el}, R_L, q, RIN_{coeff} are, respectively, the Boltzmann constant, temperature in Kelvin, receiver amplifier noise figure, receiver bandwidth, load resistance, elementary charge, and average RIN spectral density. The total current (I_{tot}) at the photodiode is the sum of the dark current (current that flows without light) and the photocurrent. The photocurrent I is related to the optical power P as I = RP, where R is the responsivity of the photodetector. The photodiode dark current of the detector is small compared to the photocurrent and in a receiver where

thermal noise is dominating therefore it is ignored. Noise-equivalent power (NEP) is often used to quantify thermal noise and is defined as the minimum optical power per unit bandwidth required to produce Signal-to-Noise Ratio (SNR) equal to 1. In our simulator we used NEP to quantify the thermal noise [pW/sqrt(Hz)] and is expressed as:

$$\sigma_t = (eff/(h_{planck}c/\lambda))^2(NEP^2Bel_{el})Teq^2 \tag{4.7}$$

where eff is the quantic efficiency of the photodiode, h_{plank} is the Plank constant, c is the light speed and T_{eq} is the equivalent measurement time expressed as T_{eq} = $\frac{1}{2B_{el}}$.
Furthermore, we assume that the main noise contribution is the thermal noise at the receiver. The thermal noise is assumed to be Additive White Gaussian Noise (AWGN) [172]. The bandwidth of the receiver is defined by the use of an equivalent electrical filter. The filter can be modeled by a low-pass Bessel-Thomson of 4° order.
Once the signal is received the correct threshold and the optimum sampling point (where the minimum BER is achieved) have to be found. The BER of a fiber link is the most important measure of the faithfulness of the link in transporting the binary data from transmitter to receiver. The BER quantifies the rate of errors and is defined as the probability of an error occurring per transported bit. Typical benchmarks for the BER are rates of 10^{-9} and 10^{-12}, though with the use of Forward Error Correcting (FEC) codes, much lower rates can be acceptable. We implemented the semi-analytic method that allows to accurately evaluate the BER. Assuming a Gaussian distribution for the noise, the BER may be evaluated as:

$$P_e = \frac{1}{N}\sum_{i=1}^{N} P(e|V_i) = \frac{1}{N}\sum_{i=1}^{N}\frac{1}{2}erfc\left(\frac{|V_i - V_{th}|}{\sqrt{2\sigma^2}}\right) \tag{4.8}$$

where V_i are the received signal samples at the sampling instant, V_{th} is the decision threshold and σ^2 is the variance of the noise at the sampling instant i. For a more general introduction to BER estimation through semi-analytic techniques in communication systems, see for example [173]. This BER is calculated for NRZ-OOK modulation format, where there are just two levels to detect. For the 4-PAM modulation three decision levels are applicable, each of the levels being between a pair of two adjacent symbol levels. The total symbol error rate was derived from error rate measurements done on each of the 4-PAM threshold levels. Given that we have four symbols denoted as S_0, S_1, S_2 and S_3, there are three decision levels between the adjacent symbols: L_1, L_2 and L_3. A symbol error is detected

when a symbol S_i is transmitted and a symbol S_j is received, where i is not equal to j. The conditional probability of receiving S_j when S_i was transmitted is denoted with P_{ij}. In the high signal to noise ratio (SNR) case (which corresponds to low BER), when it can be assumed that only errors between the nearest neighboring symbols happen, and for natural bit to symbol mapping, the total BER is given by

$$BER = \frac{1}{8}(P_{01} + P_{10} + 2P_{12} + 2P_{21} + P_{23} + P_{32}) \tag{4.9}$$

The high SNR regime of operation is the most interesting one, because a practical link will be operated in this regime. Forward error correction would have to be implemented to enable operation in the low SNR region, which would probably be challenging in the targeted applications of short range optical links, because of costs and power consumption. The error rate measurements ER_1, ER_2, ER_3 at each of the consecutive decision levels L_1, L_2 and L_3 can be expressed in terms of P_{ij} as follows:

$$ER_1 = \frac{1}{4}(P_{01} + P_{10}), ER_2 = \frac{1}{4}(P_{12} + P_{21}), ER_3 = \frac{1}{4}(P_{23} + P_{32}) \tag{4.10}$$

The error rates at each of the levels were calculated. The aggregate BER can thus be obtained from

$$BER = \frac{1}{2}ER_1 + ER_2 + \frac{1}{2}ER_3. \tag{4.11}$$

To built the receiver model, real PIN parameters have been considered.

4.4 Performance evaluation

In order to find out the better solution for short-reach and medium-reach optical data link, in this section transmission performances have been evaluated. The analysis has been performed both for OOK and 4-PAM modulation formats.

4.4.1 VCSEL-based link

A multimode 850nm VCSEL-based link was simulated with OptSim. The VCSEL block is provided in OptSim as a built-in component, directly modulated with an electrical signal. The OptSim model computes the electrical current injected into the laser's optical cavity and solves the laser rate equations for the optical output. Important VCSEL behaviors such as spatial

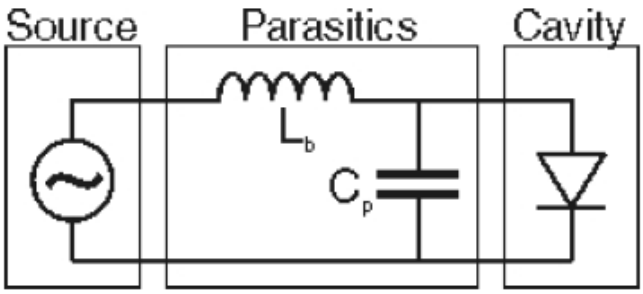

Figure 4.5: *Main components of the OptSim VCSEL model.*

hole burning, lateral carrier diffusion, thermally dependent gain, and thermal carrier leakage are all accounted for. The behavior of the model can be partitioned into three blocks, as shown in Fig.4.5. The driving source consists of the electrical signal input into the model. The parasitics consist of a bond inductance and shunting capacitance. Finally, the VCSEL cavity is modeled via a simplified current-voltage (IV) relationship and spatially independent VCSEL rate equations. To make the system closer to the real applications, a real high-speed VCSEL has been considered, referring to one of the most recent VCSEL [18]. In Fig.4.6 a screen-shot of the optical and electrical parameters used to modelize the VCSEL are shown. In Fig.4.7(a) the obtained output power vs injected current of the VCSEL at room temperature of 25°C, 55°C and 85°C is presented. In Fig.4.7(b) the small signal modulation response (S21) of the VCSEL model used in the simulations at bias current of 12 mA is reported. At room temperature the VCSEL reaches the maximum bandwidth of $\sim$ 25GHz and is suitable for high speed transmission. The threshold current is about 0.99mA and the maximum output power is 9.4mW at I_{bias}=16mA.
To drive the VCSEL an electrical signal model is used. To generate a 50Gb/s 4-PAM signal two De Bruijn electrical waveforms operating at 25Gb/s each have been used (see blocks called "PRBS2" and "PRBS1" in Fig.4.8). A k-ary De Bruijn sequence B(k, n) of order n is a cyclic sequence of a given alphabet A (in our case A= { 0,1}), with size k for which every possible subsequence of length n in A appears as a sequence of consecutive characters exactly once. Each B(k, n) has length k^n. One sequence is inverted and delayed with respect to the other by one symbol period, so that the two sequence are de-correlated. An electrical NRZ-OOK signal is generated using the specified rise time, fall time, and timing jitter (block called "ElecGen3" and "ElecGen1" in Fig.4.8). The signal rise and falls are ramped between the high and low levels. To optimize the eye diagram

VCSEL1

Parameter	Value	Units	Range	Std. Dev.	Distribution
effint	1.0	none	[0, 1e+032]	0.0	None
kf	7E-8	W	[0, 1e+032]	0.0	None
b	0.002	none	[0, 1e+032]	0.0	None
tp	1.5E-12	s	[0, 1e+032]	0.0	None
tn	2.5e-9	s	[0, 1e+032]	0.0	None
Go	80e3	1/s	[0, 1e+032]	0.0	None
ag0	-0.1	none	[-1e+032, 1e+032]	0.0	None
ag1	0.00147	1/K	[-1e+032, 1e+032]	0.0	None
ag2	7.65E-7	1/K^2	[-1e+032, 1e+032]	0.0	None

(a)

VCSEL1

Parameter	Value	Units	Range	Std. Dev.	Distribution
Drive_Scheme	"bias_tee"				
Rd	80	ohm	[0, 1e+032]	0.0	None
Von	1.4	V	[0, 1e+032]	0.0	None
voltage_equation	"I*80+1.4"				
Rs	100.0	ohm	[0, 1e+032]	0.0	None
Io	12e-3	A	[0, 1e+032]	0.0	None
Parasitics	"on"				
Lb	2e-9	H	[0, 1e+032]	0.0	None
Cp	70e-15	F	[0, 1e+032]	0.0	None

(b)

Figure 4.6: *VCSEL model used in the simulation. Optical (a) and electrical (b) parameters.*

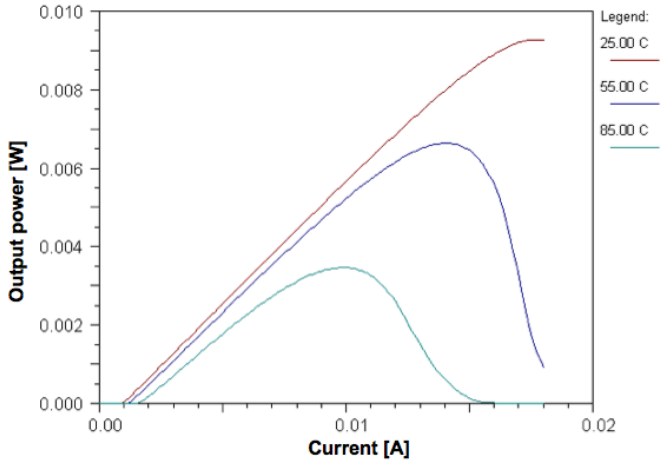

(a)

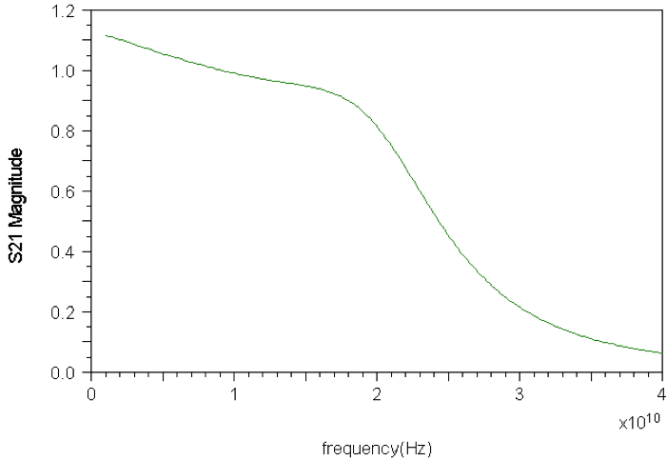

(b)

Figure 4.7: *Simulated VCSEL characteristics. (a) Output power vs current at 25°C, 55°C and at 85°C. (b) Normalized S21 at* I_{bias} *= 12mA.*

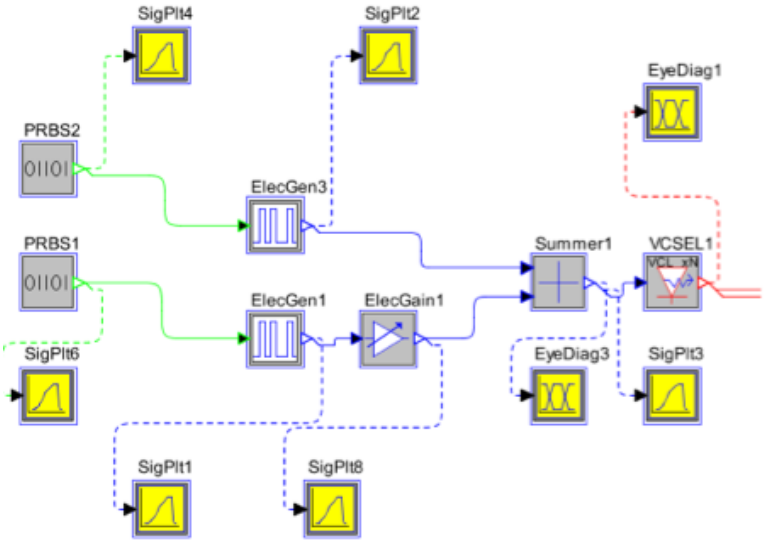

Figure 4.8: *4-PAM simulated transmission side.*

at the output of the VCSEL we changed the voltage amplitude and the rise time of the electrical signal to obtain a good open eye. The amplitude (V_{pp}) of each on-off ramped signal is 0.9V. In the simulation we used 2^7 bits for each sequence at 25Gb/s and 2^7 points per each bit. No electrical noise is added because as we explained in the previous subsection it will be taken into account in the total noise at the receiver side. To estimate the jitter we referred to the paper [140]. The total jitter consists in both deterministic and random components. For a 25Gb/s and 50Gb/s transmitted signal we respectively added 0.5ps and 3.3ps of jitter. The rise and fall time have been set to 8ps and 4ps respectively. Then, one of two waveforms is attenuated by 6dB (”ElecGain1”) in order to have half the peak-to-peak voltage value with respect to the other branch. The two signals are then combined. The resulting 4-PAM signal is fed to an electrical power coupler (”Summer1”) and is used to directly modulate the 850nm VCSEL. Figure 4.8 shows the scheme of the transmitter side of the optical link in OptSim. The driving amplitude voltage and the bias current of the VCSEL have been set to obtain the optimum extinction ratio and minimize the pulse overshoots at the output of the VCSEL.

In Fig.4.9 is shown the electrical 4-PAM signal eye to directly modulated the VCSEL and the optical eye diagram at the output of the VCSEL.

To generate a NRZ-OOK signal, a single De Brujin sequence at 50Gb/s has been used and the amplitude of the electrical signal to drive directly the

VCSEL is 1.35V.
At the 4-PAM receiver the signal has to be decoded. A New Focus 1484-

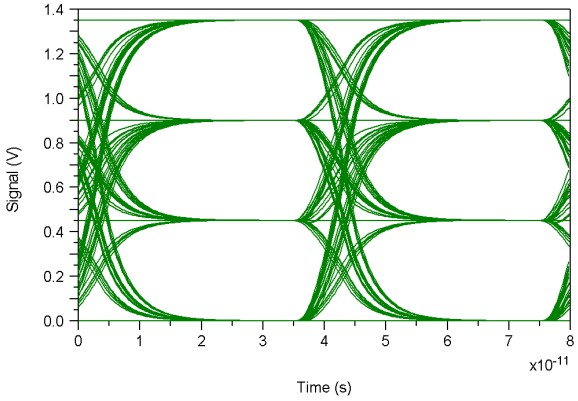

(a)

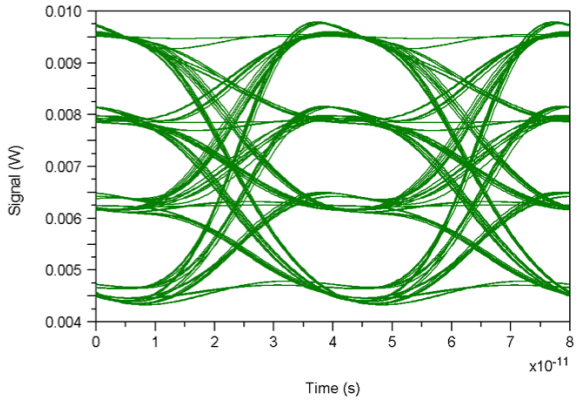

(b)

Figure 4.9: *Eye diagrams. (a) 4-PAM electrical signal to directly modulate the VCSEL. (b) Optical eye at the output of the VCSEL.*

A-50 device with a -3dB bandwidth of 22GHz, has been taken as reference for our Matlab receiver script. The receiver NEP is $38pW/\sqrt{Hz}$ with a photodiode responsivity of 0.45A/W at 850nm.
The complete simulated system for 4-PAM and OOK modulation format is represented in Fig.4.10. After the VCSEL block, the block called "NL-Fiber2" represents the standard multimode optical fiber. The blue dotted block represents the receiver part that has been implemented in Matlab.

In order to highlight the main limitations of the link, the system has been evaluated under a 50G/s and 60G/s OOK modulation format. At 60Gb/s is

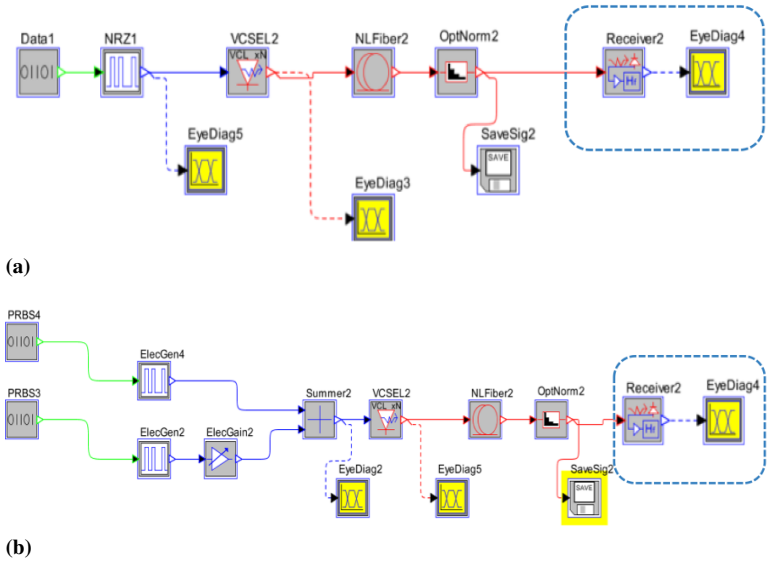

Figure 4.10: *Simulated optical VCSEL-based link. (a) OOK transmitted signal and (b) 4-PAM transmitted signal.*

no possible to achieve error-free transmission due to the bandwidth limitations of the devices, pushed up to their limits. Figure 4.11 shows the BER as a function of the received optical power in case of 50Gb/s and 60Gb/s OOK transmitted signal. In order to achieve higher bit rates, keeping the same VCSEL, a possible solution can be the implementation of a pre-emphasis pulse shaping technology [174]. In our simulative analysis, the pre-emphasis was implemented including in the model a "two tap" Feed Forward Filter (FFE) block. For OOK modulation format, even with the use of pre-emphasis a BER< 10^{-12} is not achieved, due to a large amount of jitter and the distortions caused by the limitations of devices used.
If a 4-PAM signal is transmitted, it is possible to achieve both 50Gb/s and 60Gb/s without use of pre-emphasis. Figure 4.12 shows the BER as a function of the received optical power in case of 4-PAM transmission at 50Gb/s, 60Gb/s and 80Gb/s. Since the -3dB bandwidth of the VCSEL is about 24GHz at a bias current of 12mA and the rate per symbol is 30Gsymb/s the device can support the signal. Increasing the bit rate up to 80Gb/s, BER< 10^{-12} is achieved using pre-emphasis with a 4dB of power penalty at receiver with respect to the 60Gb/s case. To find out this optimal working point, we tested different coefficients of the FFE and in this case we found the couple (0.9, -0.1) as the best choice to improve the performance. The eye diagrams at the output of the receiver at 80Gb/s with and without pre-

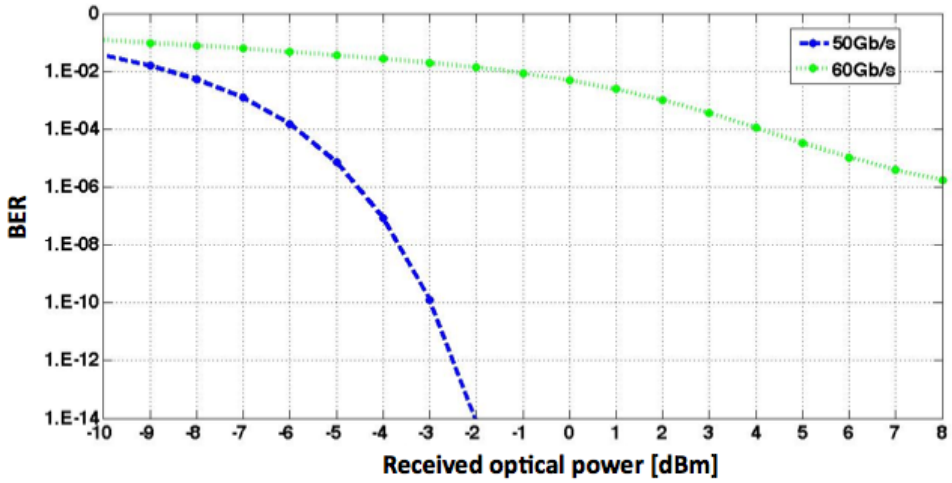

Figure 4.11: *BER vs received optical power in back-to-back condition for OOK modulation in case of directly modulated 850 nm VCSEL.*

emphasis are shown in the insets in Fig.4.12.
A comparison between the simulated analysis of the system and experimental results available in literature [175] shows some differences, due to the assumption we had to do in the simulations. Our model does not take into account some electrical bandwidth limits of all real used devices and some parasitic contribution. For this reason the simulative results differ from the experimental case of about 3dB. Hence experimental measurements are necessary to verify all simulative analysis which show that is possible to achieve 80Gb/s with BER< 10^{-12} with directly modulated VCSEL. The highest bit rate, never reached up to date.

The same simulative analysis, both for 4-PAM and OOK, was carried out considering also fiber propagation, in order to understand the performance limits of a VCSEL-based link. In this case a single mode 1550nm VCSEL was used. In OptSim the model has been built referring to the most recent high-speed VCSEL at 1550nm [36]. In Fig.4.13(a) is shown the static characteristic (output power against current curve) at 25 °C, 50°C and 85°C. In Fig.4.13(b) the dynamic characteristic (S21) at a bias current of 4.53 mA of the VCSEL is modeled. The maximum -3dB bandwidth of the VCSEL is around 15GHz. The maximum output power at 4.53 mA is about 2mW at room temperature. For that reason the electrical swing voltage (V_{pp}) to drive the VCSEL is lower than the 850 nm VCSEL case and it is 0.5V. The bit rate is 50Gb/s. The optical channel has been implemented with a standard single-mode Corning fiber with an attenuation of 0.2dB/km. Due

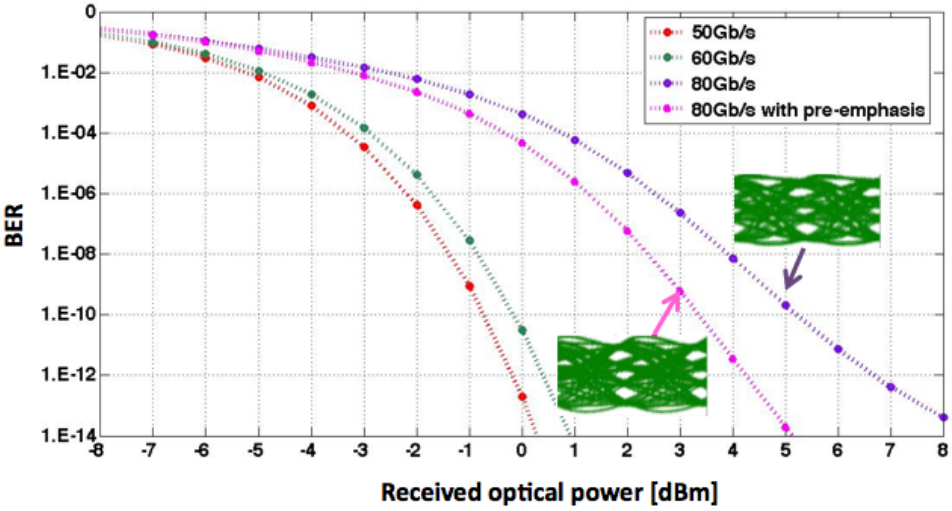

Figure 4.12: *BER curves vs received optical power in back-to-back condition for 4-PAM modulation in case of directly modulated 850 nm VCSEL. Simulated received eye diagrams at 40Gsymb/s with and without pre-emphasis are reported in the insets.*

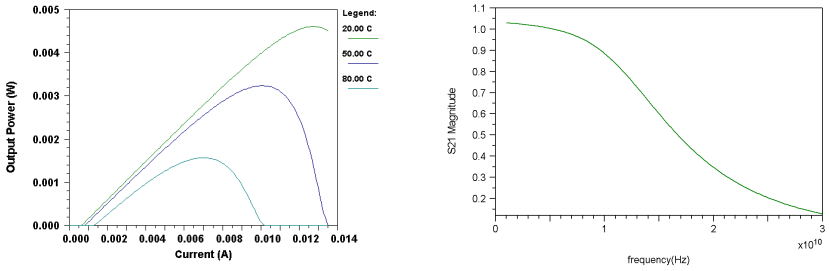

(a) **(b)**

Figure 4.13: *1550nm single-mode VCSEL model. (a) Output power vs current at three different operating temperatures, 20°C, 50°C and 80°C. (b) Normalized S21 at I_{bias}=4.53 mA at 20°C.*

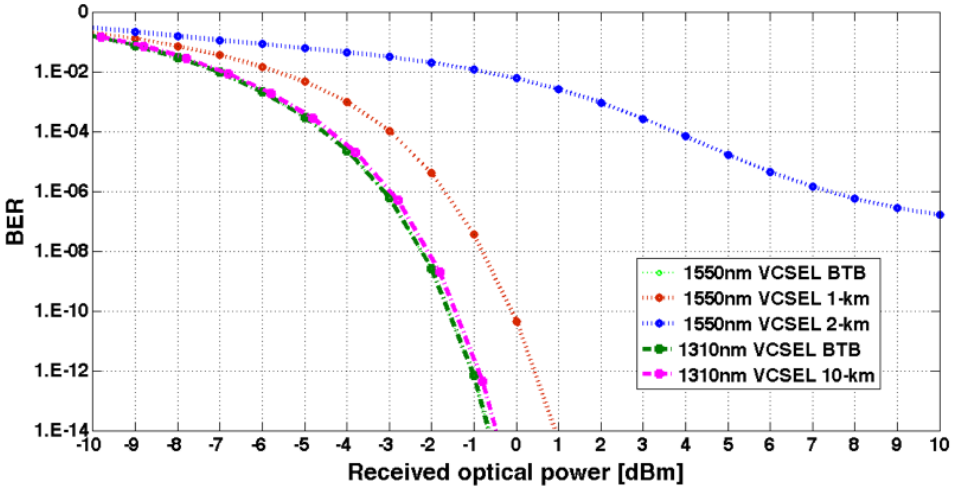

Figure 4.14: *BER curves vs received optical power for 50Gb/s 4-PAM modulation in case of directly modulated 1550 nm and 1310 nm VCSEL.*

to the VCSEL bandwidth limitation is not possible to achieve error-free for OOK transmitted signal. For 4-PAM transmitted signal the results are represented in Fig.4.14. The performances at BER= 10^{-12} in back-to-back (BTB) condition are similar in the case of using 850nm VCSEL. A 1dB improvement sensitivity is achieved due to the better responsivity of the photodiode (about 0.5 A/W) at such wavelength. The bandwidth of the receiver is 22GHz, the same in the previous case at 850nm VCSEL. The power penalty of about 1.5 dB after 1-km fiber propagation is due to the high value of the chirp (α >3) that combined with chromatic dispersion does not allow to reach error-free transmission for 2-km propagation.
Also a single-mode 1310nm VCSEL has been modeled. The VCSEL has similar characteristics than 1550nm one. If a 50Gb/s OOK modulation format is simulated it is not possible to achieve BER< 10^{-12} due the VCSEL bandwidth limitation (at 1310nm maximum bandwidth is 15GHz). If 4-PAM modulation format is used the transmission performances are limited only by the attenuation of the single mode fiber (SMF) (0.35dB/km at 1310 nm) and not by the chromatic dispersion, that is about zero at 1310 nm. Negligible power penalties (less than 0.5 dB) are visible with respect to back-to-back condition as shown in Fig.4.14, although the high symbol rate, as explained in [32]. In this case the maximum transmitted VCSEL power is 2 mW, allowing to reach 10-km propagation distance.

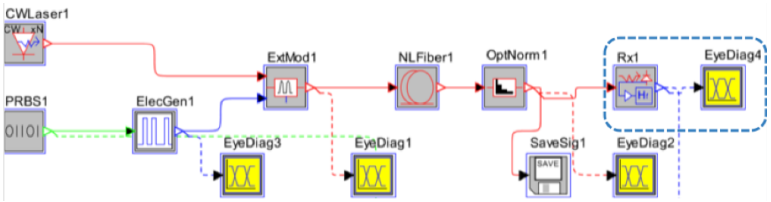

(a)

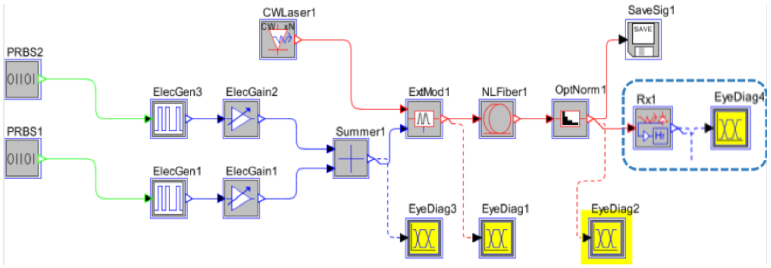

(b)

Figure 4.15: *Simulated system using Silicon Photonics technology for OOK (a) and 4-PAM (b) modulation format.*

4.4.2 Silicon Photonics-based link

The optical link considered in this context is similar to the VCSEL-based one. The difference is in the source and in the addition of an external modulator instead of the VCSEL. Figure 4.15 shows the simulated system in case of the use of Silicon Photonics technology for OOK and 4-PAM transmitted signal. Here a Distributed Feedback laser (DFB) externally modulated by a Mach-Zehnder modulator for 40Gb/s operation have been used [167]. The maximum output power of single-mode 1550nm DFB is 10mW. The RIN value is about -145dB/Hz. The Mach-Zehnder has: V_π L = 0.13V L, L=480 μm, extinction ratio (ER) = 20dB and Insertion Loss= 4.2dB. The V_{pp} of the electrical signal that drives the modulator is 0.9V. At the receiver side a Ge-photodetector has been modeled [155]. The optical-to-electrical -3dB bandwidth is up to 42GHz. The responsivity is 0.8 A/W in the 1500nm range and the dark current value is very low ($\sim <$ 18nA). To compare the performances with respect to the VCSEL-based link, where possible, all parameters have been set to the same values, used in the VCSEL-based link. The DFB optical power is set to 2mW as the VCSEL output power we previously simulated. The amplitude of the electrical signal (V_{pp}) to drive the Mach-Zehnder and the V_{bias} were set in order to achieve three equally spaced eyes at the output of the Mach-Zehnder (V_{pp} = 0.9V and V_{bias}=0.88V). In Figure 4.16 is shown the optical eye diagram at the output

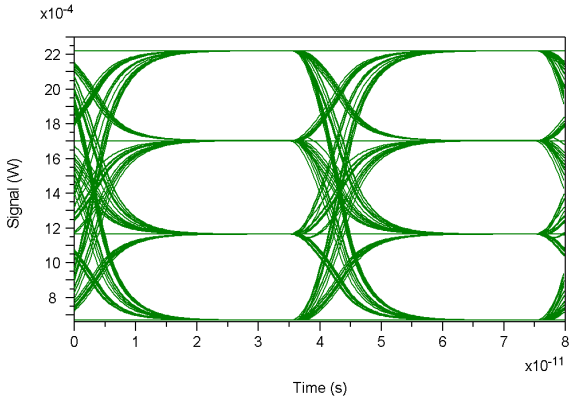

Figure 4.16: *Optical eye diagram at the output of the Mach-Zehnder.*

of the Mach-Zehnder. The simulation were carried out using two different bandwidths of the receiver (15GHz and 22GHz). A performance comparison between OOK and 4-PAM transmitted signal is obtained. If a 15GHz bandwidth receiver is used, only for 4-PAM transmitted signal a gain of 1dB on received power is observed. In OOK case, since the receiver bandwidth is too small with respect to the bit rate (50Gb/s) the performances are worst. Figure 4.17 shows the BER as a function of received optical power of OOK and 4-PAM at 50Gb/s, for 1-km, 2-km, 5-km and 10-km single-mode propagation in case of 22GHz bandwidth receiver. In case of OOK transmitted signal, the power penalties are negligible for 1-km fiber propagation and they are about 1 dB for 2-km fiber propagation. For 10-km fiber propagation, due to the chromatic dispersion, the BER $< 10^{-12}$ is achieved with a large amount of received optical power (around 6dBm) and this is not reasonable for real system, If a 4-PAM signal is transmitted, for 1-km, 2-km and 5-km fiber propagation there is no power penalties and there is a power penalty of about 2.3dB with respect to the back-to-back condition for 10-km fiber propagation. The power penalties are limited because the devices are working at 25Gsymb/s, thanks to the 4-PAM encoding, while still providing a total capacity of 50Gb/s. This implementation is suitable for datacom and Local Area Network (LAN) applications.

4.5 Power Consumption evaluation

The power consumption comparison of the different technologies used for high-speed data links is a relevant topic for the Research&Development

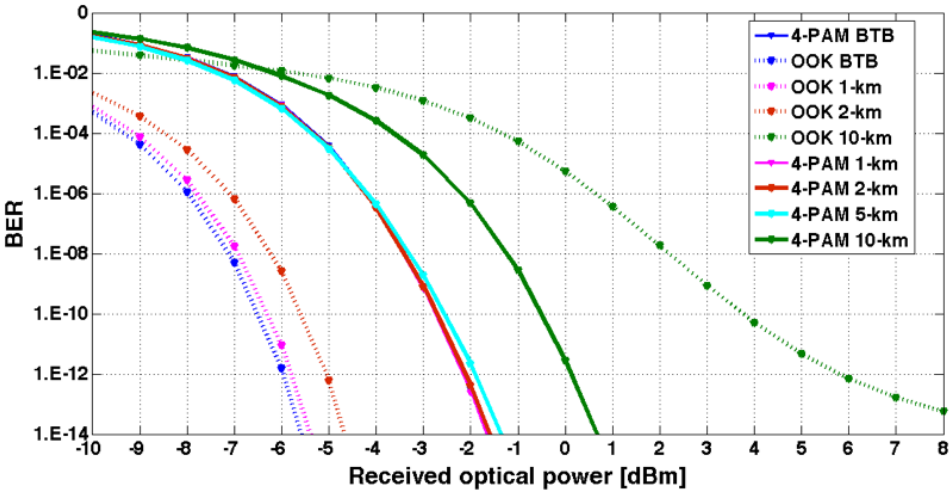

Figure 4.17: *BER curves vs received optical power for 50Gb/s OOK and 4-PAM transmitted signal at different propagation distances, using Silicon Photonics components.*

Table 4.2: *Experimental and commercial components considered in the power consumption evaluation (* Sometimes is included).*

	Signal generation	CDR	Encoder /decoder	driver	pre-emphasis /equalization	laser	external modulator (if needed)	Photodiode	TIA	Control function
experimental			X*	X	X	X		X	X	
commercial	X	X	X	X	X	X	X	X	X	

(R&D) community. In order to properly evaluated the power consumption of a specific link it is important to know which components are involved in. A technology comparison, using both VCSEL-based and Silicon Photonics-based technologies, has been carried out. In both cases information from experimental and/or commercial data were considered. For the first, only specific devices normally are considered, while for last ones a complete transmitter or receiver are evaluated. This means that all the requested standard capabilities like signal generation, clock signaling and Clock Data Recovery (CDR) are usually included. Table 4.2 summarizes the components included when experimental and commercial data are considered. Figure4.18 shows the block diagram of transceiver for OOK and 4-PAM formats. The great advantage of 4-PAM modulation is the very low complexity of the signal generation module, which consists in a 4-PAM encoder/decoder in addition to a standard OOK transceiver, as explained in [152]. The equalizer functions are usually implemented but they are optional. The ”LD” stands for Laser Driver. The power consump-

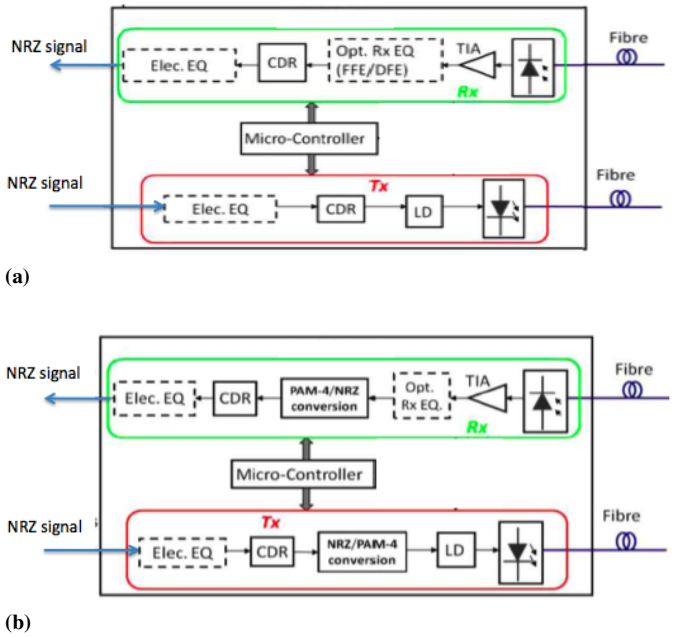

Figure 4.18: *Transmitter and receiver architecture for (a) OOK format modulation and (b) 4-PAM modulation format.*

tion of the optical link is related to the choice of the technology. Generally, the electronic circuitry is implemented using CMOS technology and it is involved in the generation of the signal, the clock, the driver, the pre-emphasis/equalization functions, TIA and eventually the encoding/decoding functions. Usually, a directly modulated VCSEL or a DFB externally modulated by a Mach-Zehnder modulator are considered.
Due to the very low threshold current (< 1mA), the energy per bit of present high-speed VCSELs is low (fJ/bit) with respect to the their driver [19]. A DFB laser usually consumes more power due to the higher threshold current (above 20mA). Normally, the pre-emphasis digital circuits are integrated on the same driver circuits, logical ports, delay lines and combiners, so its power consumption is negligible and it has not a significative contribution on the total power consumption. The encoder can be realized by an electrical circuit containing mainly delay elements, such as flip-flop, together with combiners in order to generate symbols with 4 levels. This circuitry consumes about 0.1pJ/bit. If the decoder is implemented using high resolution Analog to Digital Converter (ADC), the power consumption at receiver side is dominated by ADC. From [176] it's possible to calculate an approximate value of the power consumption of about 2 W, assuming

Table 4.3: *OOK and 4-PAM transmitters.*

Modulation format	Pre-emphasis	Bit rate [Gb/s]	Baud rate [Gsym-b/s]	Technology	product	Power con-sump-tion [mW]	energy effi-ciency [pJ/bit]	ref.
OOK	yes	20	20	40nm CMOS SOI	com. [2]	480	24	[167]
OOK	yes	25	25	90nm CMOS SOI	exp. [1]	46	1.84	[178]
OOK	yes	25	25	32nm CMOS SOI	com. [3]	180	7.2	[177]
OOK	yes	28	28	32nm CMOS SOI	exp. [1]	40	1.6	[142]
OOK	yes	28	28	32nm CMOS SOI	com. [3]	217	7.75	[177]
OOK	yes	56	56	IBM BiC-MOS8HP	exp. [1]	682	12.18	[140]
4-PAM	no	20	10	40nm CMOS SOI	com.[2]	446	22.3	[167]
4-PAM	yes	25	12.5	90nm CMOS SOI	com. [3]	102	4	[179]
4-PAM	no	56	28	65nm CMOS SOI	exp.[1]	32	0.56	[148]

an Effective Numbers Of Bits (ENOB) of 5 bits and the exploitation of 65nm CMOS technology. Almost 40% of the total power consumption is spent in data and about 56% in clock circuits, while the rest is in digital logic circuitry [177]. In Table 4.3 the most recent OOK and 4-PAM transmitters with related power consumption data are summarized. Note 1 means that the transmitter part was built for VCSEL-based applications, while note 2 means that the transmitter part was built for Silicon Photonics-based applications and note 3 means that the transmitter part was built for electrical-based interconnections. To give a more complete analysis of real power consumption commercial-level data should be considered. For transmitter side it has been possible, but for the receiver side we had to use experimental data to make a comparison between OOK and 4-PAM for both VCSEL-based and Silicon Photonics technology. Since at the time of writing, none "commercial-level" product that implements a 4-PAM driver especially designed for VCSELs exists, a 4-PAM driver initially developed for electrical-based interconnections has been taken into account. However, this assumption is generally correct, because the output electrical amplitude and the voltage supply of the "electrical interconnection-oriented" driver are compatible with the modulation amplitude of the VCSEL.
In Table 4.4 the most recent data about power consumption of receiver for OOK and 4-PAM modulation format are summarized.

Table 4.4: *OOK and 4-PAM receivers.*

Modulation format	Equalization	Bit rate [Gb/s]	Baud rate [Gsym-b/s]	Technology	product	Power con-sump-tion [mW]	energy effi-ciency [pJ/bit]	ref.
OOK	yes	25	25	90nm CMOS SOI	exp. [2]	121	4.84	[180]
OOK	yes	25	25	32nm CMOS SOI	exp. [1]	44.4	1.77	[142]
OOK	yes	56	56	IBM BiC-MOS8HP	exp. [1]	648	11.57	[140]
4-PAM	no	22	11	90nm CMOS SOI	com.[3]	228	10.36	[132]
4-PAM	no	25	12.5	90nm CMOS SOI	exp.[2]		∼5	
4-PAM	no	25	12.5	32nm CMOS SOI	exp.[1]		∼2	

Table 4.5: *Energy efficiency of VCSEL and Silicon Photonics based links.*

Technology	**OOK [pJ/bit]**			**4-PAM [pJ/bit]**		
	TX	**RX**	**total**	**TX**	**RX**	**total**
VCSEL	8.5	1.776	10.28	5.3	~ 2	~ 7.3
Silicon Photonics	24	4.84	28.84	22.3	~ 5	∼27.3

Assuming the same technology and bit rate, it clearly appears that the power consumption estimated from experimental-level data is lower than the commercial-level data. In both links, a simple receiver composed by three comparators (because of the three threshold of 4-PAM signal) can be used, avoiding the need of ADC. Usually, each comparator consumes about 0.1pJ/bit. The capability of exploiting this simple detector helps to save power. To estimate the power consumption for a 4-PAM receiver, the power consumption of the decoder is added to the OOK receiver relative to the specific bit rate. In the transmission side, VCSEL energy efficiency is included (I_{bias}=12mA, Voltage= 2.8V, 1.34pJ/bit). If 25Gb/s OOK and 4-PAM transmitted signal are considered, the total link energy consumption per bit [pJ/bit] is shown in Table 4.5. It's interesting to notice that for VCSEL-based link, at the same bit rate, the total energy consumption for OOK and 4-PAM signals is comparable, i.e. the increase in data transmission can be achieved without a significative enhancement of dissipated power. In this specific case, because of implementation choice of OOK transmitter, the consumption is more than 4-PAM of 3pJ/bit.

In Silicon Photonics-based link, the 4-PAM transmitter consume less than OOK transmitter, due to the choice of the encoder implementation. Since $P_{switching}$ = CV^2f, the switching frequency (symbol rate) must be reduced since C and V are relatively fixed for a given MZ length and CMOS process. By breaking one large MZ section into small pieces, further power saving is achieved because a smaller inverter can be used for a reduced segment capacitance and the effective capacitance is also reduced since not all segments are switching simultaneously with random input data. For a 4-PAM receiver, the power consumption is actually comparable with respect to the OOK transmitted signal, if an ADC is not employed. Both for VCSEL-based and Silicon Photonics link, the clock, digital control and driver have been implemented with the same CMOS technology. The significative difference in power consumption is due to different encoding design and in the laser source between VCSEL-based and SIlicon Photonics-based technology. The power consumption of VCSEL is about 30mW, for the DFB is around 100mW if OOK modulation format is used and more than 100mW if 4-PAM modulation format is considered.
Based on recent studies [181], the energy consumption per bit should decrease by increasing the bit rate and using a better technology. Sometimes when the CMOS technology is changed it is necessary to re-design the electronic circuitry to save power. Usually, for the same CMOS technology, the energy consumption vs bit rate stays constant up to a certain bit rate. Beyond this limit the energy consumption increases exponentially.

4.6 Conclusion

As reported in the previous section, both Silicon Photonics and VCSEL-based links guarantee error free transmission (BER< 10^{-12}) at almost the same receiver power in back-to-back configuration (-1dBm at 50Gb/s 4-PAM transmitted signal). To evaluate the propagation performances a 1550 nm source is used. Considering VCSEL-based link, the performances are limited by the VCSEL chirp and bandwidth, in addition to the chromatic dispersion. In this context Silicon Photonics technology combined with 4-PAM modulation format results more performing. It is possible to reach 10-km fiber propagation with 2dB of power penalty. When a 1310 nm source plus 4-PAM modulation format are used the performances are limited only by the attenuation of the SMF. Negligible power penalties are observed up to 10-km for both technologies.
From a power consumption point of view, for each technology, the power consumption of OOK and 4-PAM transceiver is comparable, depending on

the circuit design. If a VCSEL-based link is considered, 4-PAM results more energy efficiency ($\sim$ 7pJ/bit) with respect to OOK modulation format ($\sim$10pJ/bit). Silicon Photonics-based link consumes about 3 times more than VCSEL-based link. The main difference is in the power consumption of the source and drivers.
Moreover, in order to achieve more spectral efficiency, an increment of number of levels (i.e from 4 to 8 or 16) is desirable. Since VCSEL technology is clearly limited due to characteristic of the laser itself, the Silicon Photonics approach permits to achieve higher multi-level amplitude coding with simple implementation.
For short-reach applications (hence including backplanes) Silicon Photonics is more scalable, but less power efficient with respect to the VCSEL-based technology, which continues to ensure good propagating performances (combined with 4-PAM modulation format) at a wavelength of 1310 nm . Hence, VCSEL-based technology represents a good choice in data centers applications, where SMF typically operates at the 1310 nm wavelength.
Silicon Photonics combined with M-PAM modulation format is very promising for medium propagating distances where a long wavelength is used. Furthermore, using Silicon Photonics-based technologies, more functionalities can be monolithically integrated.

Conclusions

In this work we demonstrated the capability of replacing the current electrical copper-based backplane with a completely optical one, guaranteeing present and future bandwidth requests and low cost, low power consuption and simplicity requirements.

In the next years, when the data throughput in telecom equipment will increase, the electrical interconnections among the boards in a subrack will be a bottleneck for signal transmissions. For transmitting digital data at several tens of Gbps, a completely optical transmission layer will be needed. Here, optical boards will be interconnected in the same subrack by optical backplanes (see Chapter1). In this context, another issue arises, i.e. the power dissipation reduction. Power dissipation, in fact, is one of the main problems that directly limits the performance of chips and, currently, it is a significant factor in system economics and in the environmental impact of information technology. Hence, it would be very difficult to introduce new solutions for interconnects (such as optics) if more power is required, even if they lead to other advantages. Because of its impact on performances and reliability of future bacplane systems, great attention is spent on this topic.

First of all, a comparison between the best achievable electrical backplane and a fiber-based optical backplane is presented (see Chapter2). Using Hyperlinx simulator tool, the best achievable copper (Cu)-based electrical backplane has been designed, taking into account the best material and its roughness, low-loss electrical connectors, back drill vias and smart

design. The total loss of the electrical link from the Input/Output (I/O) board to the receiver side placed on matrix board has been characterized. At 8 GHz the attenuation of the link is about 30dB. From simulations, it appears clear that the best choice for copper-based backplanes is the horizontal coupled striplines backplane configuration; moreover, using an Altera Stratix V transceiver we estimated a link energy consumption per bit of about 0.8pJ/bit at 22Gb/s. The same power budget has been applied for an optical fiber-based backplane considering suitable transmitter (TX) and receiver (RX) devices. Since the propagation distance is less than 1 meter, negligible losses are present due to the optical fiber. The exploitation of multimode or single-mode Vertical Cavity Surface Emitting Laser (VCSEL) sources and the assumption of a total loss of about 4 dB (including insertion, alignment and connector losses) lead to a link energy consumption per bit of about 0.2pJ/bit at 25Gb/s. Considering the characteristics of VCSEL sources and optical receivers presented in literature, the energy consumption is almost one quarter than the best electrical solution. For the Cu-based electrical backplane, the main limitation remains the backplane line losses, while in the optical-based backplane the achievable bit rate is only depending on TX/RX bandwidths.

An optical backplane has to satisfy stringent requirements, as low cost, low power consumption, low complexity and always guarantees scalability, reliability and transparency. Since the target is an industrial product, all processes have to be compatible with the currently production line. In order to develop a real optical fiber-based solution, different aspects need to be analyzed in detail. For its greater tolerance to passive alignments, a standard multi-mode optical fiber, grouped in ribbons, has been considered. A new layout for optimizing the distribution of the optical fiber ribbon has been developed. The object is simplicity, avoiding crossing and too small bending. An experimental analysis has been carried out to quantify the loss due to multimode ribbon bending. Multimode 850nm 10Gb/s VCSEL sources have been used to characterize the link. The characterization has been performed using 8 couples of transmitter/receiver in MPO connectors connected with multimode 12-fiber ribbons, placed in a first prototype of the backplane. The maximum measured loss for all 12 x 8 connections is less than 2dB (including 0.5 dB insertion losses by fan-in and fan-out). Bending losses depend on the position of the fiber within the ribbon; anyway, the average power loss of the most penalized one is less than 0.5 dB with respect to the others, so bending impact on system performances is negligible. In order to reproduce all possible coupling configurations on

the board, before entering into the backplane, also a single-mode fiber is used before the multimode fiber ribbon. The loss is less than 1dB due to the only two modes excited into the multimode fiber at 850 nm. In all cases error-free transmission has been demonstrated. The optical fiber ribbons are orthogonally placed into the backplane via an automatized robot. An easy and smart way do not stress the fiber has been implemented. A new low-loss connector that includes TX and RX in the same housing has been designed and fabricated. At the time of writing the fiber-based backplane is very close to reach the final prototype version, almost ready to be tested for the final demonstration.

Then, we focused the attention on the transparency characteristic of the optical backplane (see Chapter3). In order to allow a direct line-to-line connection for signals coming from an external network without any electro-optical (E/O) or opto-electrical (O/E) conversion, the so-called center - launching technique has been studied. 1.3 μm VCSEL-based transmission in legacy standard multimode fibre (MMF) by using the mode-field matched centre-launching technique has been experimentally demonstrated. A transmission bit rate of 12.5 Gbit/s has realized at 1.3 μm by direct modulation of a VCSEL suitable for high-speed applications. Performances without significant penalties, also compared with single mode fiber (SMF) propagation, are measured up to 10 km MMF coils, simply connected by fusion splicing without SMF patchcords. Since the backplane is placed in an environment affected by mechanical vibrations, detailed experimental analysis has been carried out in order to test the stability of the center launching technique considering the range of vibration frequencies reported in the ITU standard. Because no significant penalty appears, the center launching technique is very robust to environmental vibrations. No significant BER penalties are visible for vibration frequencies up to 1 kHz. The BER measurement has been performed first directly at the MMF output; then, a 30-cm SM fiber has been spliced at the MMF output in order to obtain a mode spatial filtering effect. No BER penalties due to modal noise are noticeable, i.e. the field propagating in the MM fiber is an high-purity fundamental mode. To confirm SMF-like propagation and to exclude multimode propagation in the MMF subjected to vibrations, also BER tests in case of a long MMF span in presence of a large amount of modal dispersion have been performed. It has been demonstrated that the vibrations do not affect the transmission performances. Therefore, the center-launching technique appears as a promising method to ensure full transparency to the transmitted signals for applications in board-to-board and data server inter-

connects.

The power consumption of information technology is now so large that it is starting to be environmentally significant. Power dissipation in information processing systems is a major limitation at many levels, including on complementary-metal-oxide semiconductor (CMOS) chip themselves. In the near future, where the objective is achieving 400Gb/s in the data center, the choice of the architecture and technology is fundamental to fulfill the requirements like low power consumption, low cost, low complexity and very high integration (see Chapter4). The attention has been focused on multilevel modulation format as a way to increase the transmission bandwidth in an optical backplane-based data center applications, maintaining the same number of optical interconnections. We have taken into account VCSEL-based and Silicon Photonics -based technology. A comparison between an On Off Keying (OOK) and 4-Pulse Amplitude Modulation (PAM) formats has been presented, in terms of performances and power consumption.
To evaluate the performances of a VCSEL-based link for short-range applications we worked in back-to-back condition. A multimode 850nm VCSEL has been exploited. If an OOK signal is transmitted it is not possible to achieve error free transmission (BER < 10^{-12}) at 60Gb/s and beyond, neither with pre-emphasis, due to VCSEL bandwidth limitation. Alternatively, 4-PAM modulation format permits to reach error free transmission up to 60Gb/s with 1dBm received power without pre-emphasis. With pre-emphasis is possible to reach 80Gb/s with about 4 dB power penalty with respect to 50Gb/s case (0dBm received power). The next step will be experimentally validating this very challenging result.
To find out the most performing technology to implement medium reach (>1km) links at 50Gb/s, further simulations have been carried out. The reach of VCSELs over multimode fiber is shrinking: 25Gb/s 850nm VCSELs are expected to reach only between 100 and 150 m. Hence, for km-reach distances as inter-chassis connectivity single mode fibers must be used. A single mode 1550nm source has been considered. The most recent single mode VCSEL has a maximum bandwidth of 15GHz, so it's not possible to reach error-free transmission with a 50Gb/s OOK directly modulated VCSEL. Using 4-PAM modulation signal 1-km propagating fiber is achieved with about 1.5dB power penalty with respect to the back-to-back configuration. Due to the high chirp (average linewidth enhancement factor > 3) of VCSELs, error-free transmission for 2km and beyond can't be achieved. For Silicon-Photonics a single-mode 1550 nm DFB externally

modulated by a Mach-Zehnder is used. In case of a 50Gb/s OOK modulation format, the transmission is limited by chromatic dispersion. Using 4-PAM is possible to reach error-free at 10km with just 2 dB power penalty with respect to the back-to-back case.
If a 1310nm source is employed, also with VCSEL combined with 4-PAM modulation format, error-free transmission is achieved with no visible penalties up to 10km. The performances are only limited by the attenuation of the SMF.
The proper accounting of power consumption and consideration of system reliability are critical when comparing transceivers. First, because often the reported typical-case power consumption generally report only TX and RX power, ignoring power consumed by common blocks shared by multiple lanes such as clocking circuitry or, in the case of integrated photonics, power consumed by the electronics needed for optical-electrical conversion. For the transmitter part it has been possible to used commercial-level data to make a comparison, unfortunately for the receiver side all information have not be available so we have used the experimental-level data.
In a VCSEL-based link the total energy dissipation is comparable in case of using OOK or 4-PAM modulation format (at 25Gb/s from $\sim$10 pJ/bit to $\sim$ 7.5 pJ/bit, respectively), and depending on the design, sometimes 4-PAM modulation format is more power efficiency than OOK at the same bit rate. The 4-PAM signal is generated by changing bias current levels, through directly modulated a VCSEL source. Using Silicon Photonics approach a segmented Mach-Zehnder is used to generate 4-PAM modulated signal. Thanks to this specific implementation, at the transmitter side, the dissipated energy for 4-PAM at 25Gb/s (22 pJ/bit) is a little bit less than OOK (24pJ/bit). At the receiver the power consumption is comparable with respect to the OOK case. The total energy dissipation of the link is about 28 pJ/bit for OOK case and 27pJ/bit for 4-PAM modulation format. Comparing the two technologies and excluding the ADC contribution, Silicon Photonics-based link consumes about 3 times more than VCSEL-based link. The main difference is due to the power consumption of the source and drivers.

In the next future, we expect significant evolution in terms of performance, power consumption and costs as soon as the optical backplane will be accepted by the industry and become widely used, accelerating the ability of the backplane to scale towards higher and higher capacity with low power consumption. The important choice is the technology used in the transmitter and receiver sides placed on the boards interconnected via op-

tical backplane. We demonstrated the capability for VCSEL-based link to achieve bit rate beyond 50Gb/s with help of 4-PAM modulation format and pre-emphasis achieving 80Gb/s. VCSEL-based and Silicon photonics based technology have been demonstrated to achieve error-free transmission at almost the same received power at 50Gb/s (-1dBm).
In this work, from a power consumption point of view, the VCSEL-based solution appears to be more convenient with respect to Silicon Photonics technology.
Many developments have been made for multimode short-wavelength VCSELs both in terms of dissipated power and bandwidth, but in order to achieve higher bit rate beyond 50Gb/s the use of multilevel modulation formats is mandatory for backplane-based applications, not only for low cost and low complexity solution but also for lower power consumptions. If the propagation distance is getting longer (for example intra-chassis or local area network) a single-mode VCSEL is needed but unfortunately, at present, long-wavelength VCSELs are not so mature to support very high bit rate (beyond 30Gb/s). The exploitation of advanced modulation formats becomes mandatory; considering the requirements of simplicity, scalability and bandwidth enhancement, the 4-PAM modulation seems the best trade-off for backplane applications.
For the second window, a 4-PAM VCSEL transmission at 1310 nm is the best choice considering power consumption and system performances. Unfortunately, the very high linewidth enhancement factor of VCSEL source limits the exploitation of this solution at 1550 nm, where dispersion is the main constraint.
Silicon Photonics combined with multi-level modulation format has been demonstrated to be more performing for medium reach applications and more scalable. A simple implementation of higher-order M-PAM (M>4) is possible with Silicon Photonics technology, decreasing the modulation dissipated energy per bit with respect to the OOK case. Obtaining the same scalability with VCSELs is, instead, very challenging, due to their intrinsic characteristics. Therefore Silicon Photonics is very attractive for integration. Since drivers and electronics part of receiver are silicon-based devices they are compatible with silicon photonics. More functionalities can be monolithically integrated with low cost process.

Based on my thesis results and considerations there is room to develop new future activities. Especially for datacom applications and between data-centers VCSEL-based technology in combination with PAM could be a very promising choice to increase bandwidth with low energy dissipation.

Next step may be the experimental evaluation of simulations for 1310 nm 25Gbaud/s VCSEL with 4-PAM modulation format. Some related results are not yet present in literature. Then, an interesting work should be to design a new real 4-PAM driver and receiver for VCSEL-based technology in order to minimize the consumption and using the newest CMOS technology, moving toward a real implementation of a 50Gb/s 4-PAM directly modulated 1310nm VCSEL-based system.

Publications

Journal Papers

A. Boletti, A. La Porta, B. J. Offrein, P. Boffi, P. Martelli, M. Ferrario and M. Martinelli, ”Comparison between VCSEL and Silicon Photonics-based optical link for datacom applications” submitted to *Optics Express*, February 2014

A. Boletti, D. Giacomuzzi, G. Parladori, P. Boffi, M. Ferrario and M. Martinelli, ”Performance Comparison between electrical copper-based and optical fiber-based backplanes” *Optics Express*, Vol. 21, Issue 16, pp. 19202-19208 (2013)

A. Boletti, P. Boffi, A. Gatto, P. Martelli, E. Centeno Nieves and M. Martinelli ”Robustness to mechanical perturbations of center-launching technique for transparent board-to-board and data server interconnects”, *Optics Express*, Vol. 21, Issue 10, pp. 12410-12418 (2013)

P. Boffi, A. Gatto, **A. Boletti**, P. Martelli and M. Martinelli, ”12.5 Gbit/s VCSEL-based transmission over legacy MMFs by centre-launching technique”, *Electronics Letters*, Vol. 48, Issue 20, p.1289-1290 (2012)

Patents

A. Boletti, M. Ferrario and M. Martinelli ”Schema di interconnessione per apparati di telecomunicazioni ed informatici” patent submitted to revision,

December 2013

Conferences

A. Boletti, A. La Porta, B. J. Offrein, P. Boffi, P. Martelli, M. Ferrario and M. Martinelli "Performance comparison of VCSEL and Silicon Photonics based links for high capacity data communications" submitted to *Convegno Italiano delle Technologie Fotoniche, Fotonica*, Napoli, 2014.

A. Boletti, A. La Porta, B. J. Offrein, P. Boffi, P. Martelli, M. Ferrario and M. Martinelli "Performance analysis of communication links based on VCSEL and Silicon Photonics technology for high-capacity data-intensive scenario" submitted to *19th European Conference on Network and Optical Communications, NOC*, Milano, 2014.

A. Boletti, P. Boffi, A. Gatto, P. Martelli, E. Centeno Nieves and M. Martinelli "Robustness to mechanical perturbations of centre-launching technique in multi-mode fibres for transparent optical interconnects" *Proc. of ICTON-International Conference on Transparent Optical Network*, Cartagena, 2013.

A. Boletti, D. Giacomuzzi, G. Parladori, P. Boffi and M. Martinelli, "Performance Comparison between Electrical and Optical Backplanes" *Proc. of Fotonica-Convegno Nazionale sulle Tecniche Fotoniche nelle telecomunicazioni*, Milano, 2013

A. Boletti, A. Gatto, P. Boffi, P. Martelli, E. Centeno Nieves and M. Martinelli "Mechanical Robustness of Datacom Interconnections by Center-Launching in multi-mode fiber" *Proc. of Fotonica-Convegno Nazionale sulle Tecniche Fotoniche nelle telecomunicazioni*, Milano, 2013

A. Boletti, A. Gatto, P. Boffi, P. Martelli, E. Centeno Nieves and M. Martinelli "Mechanical Robustness of MMF Datacom Interconnections using Center-Launching Technique", *Proc. of CLEO/Europe-EQEC, International Congress on Photonics in Europe*, Munich, 2013

A. Boletti, D. Giacomuzzi, G. Parladori, P. Boffi, M. Ferrario and M. Martinelli "Performance Comparison between Electrical and Optical Backplanes" *Proc. of CLEO/Europe-EQEC International Congress on Photonics in Europe*, Munich, 2013

Bibliography

[1] A. Benner, "Cost-effective optics: Enabling the exascale roadmap," in *17th IEEE Symposium on High Performance Interconnects, 2009. HOTI 2009*, 2009, pp. 133–137.

[2] J. B. Offrein, "Silicon photonics packaging requirements," in *IBM Silicon Photonics Workshop, Munich, Germany*, 2011, pp. 1–14. [Online]. Available: http://www.siliconphotonics.eu/munich_slides/2_IBM.pdf

[3] A. Mutig, *High Speed VCSELs for Optical Interconnects*. Springer, Jan. 2011.

[4] V. Ricchiuti, "Intra-rack optical interconnection links," in *2012 IEEE 16th Workshop on Signal and Power Integrity (SPI)*, 2012, pp. 137–140.

[5] E. Wu, "A framework for scaling future backplanes," *IEEE Communications Magazine*, vol. 50, no. 11, pp. 188–194, 2012.

[6] D. Kam, M. Ritter, T. Beukema, J. Bulzacchelli, P. Pepeljugoski, Y. Kwark, L. Shan, X. Gu, C. Baks, R. John, G. Hougham, C. Schuster, R. Rimolo-Donadio, and B. Wu, "Is 25 gb/s on-board signaling viable?" *IEEE Transactions on Advanced Packaging*, vol. 32, no. 2, pp. 328–344, 2009.

[7] V. Ricchiuti, F. de Paulis, and A. Orlandi, "Performance of signal link paths in presence of signal reference planes of EBG type," in

2010 IEEE 14th Workshop on Signal Propagation on Interconnects (SPI), 2010, pp. 97–100.

[8] M. Taubenblatt, "Optical interconnects for high-performance computing," *Journal of Lightwave Technology*, vol. 30, no. 4, pp. 448–457, 2012.

[9] A. Benner, M. Ignatowski, J. Kash, D. Kuchta, and M. Ritter, "Exploitation of optical interconnects in future server architectures," *IBM Journal of Research and Development*, vol. 49, no. 4.5, pp. 755–775, 2005.

[10] C. M. DeCusatis and C. J. S. DeCusatis, "Preface," in *Fiber Optic Essentials*. Burlington: Academic Press, 2006, pp. ix–xi. [Online]. Available: http://www.sciencedirect.com/science/article/pii/B978012208431750000X

[11] S. Gringeri, E. Basch, and T. Xia, "Technical considerations for supporting data rates beyond 100 gb/s," *IEEE Communications Magazine*, vol. 50, no. 2, pp. s21–s30, 2012.

[12] R. Michalzik, *VCSELs: fundamentals, technology and applications of vertical-cavity surface-emitting lasers*. Berlin; Heidelberg [u.a.]: Springer, 2013.

[13] A. Hangauer, J. Chen, and M. C. Amann, "Square-root law thermal response in VCSELs: experiment and theoretical model," in *Conference on Lasers and Electro-Optics/Quantum Electronics and Laser Science Conference and Photonic Applications Systems Technologies*, ser. OSA Technical Digest (CD). Optical Society of America, May 2008, p. JThA27. [Online]. Available: http://www.opticsinfobase.org/abstract.cfmURI=CLEO-2008-JThA27

[14] P. Westbergh, J. Gustavsson, B. Koegel, A. Haglund, and A. Larsson, "Impact of photon lifetime on high-speed VCSEL performance," *IEEE Journal of Selected Topics in Quantum Electronics*, vol. 17, no. 6, pp. 1603–1613, 2011.

[15] S. Palermo, *Design of High-Speed Optical Interconnect Transceivers*, 2007.

[16] M. Gobet, H. P. Bae, T. Sarmiento, and J. S. Harris, "GaInNAsSb/GaAs vertical cavity surface-emitting lasers (VCSELs): current challenges and techniques to realize multiple-wavelength laser

arrays at 1.55μm," vol. 6908, 2008, pp. 69 080N–69 080N–12. [Online]. Available: http://dx.doi.org/10.1117/12.762311

[17] A. Larsson, J. Gustavsson, A. Haglund, J. Bengtsson, B. Kogel, P. Westbergh, R. Safaisini, E. Haglund, K. Szczerba, M. Karlsson, and P. Andrekson, "High speed VCSELs for optical interconnects," in *2012 International Conference on Indium Phosphide and Related Materials (IPRM)*, 2012, pp. 269–272.

[18] P. Westbergh, R. Safaisini, E. Haglund, J. Gustavsson, A. Larsson, M. Geen, R. Lawrence, and A. Joel, "High-speed oxide confined 850-nm VCSELs operating error-free at 40 gb/s up to 85," *IEEE Photonics Technology Letters*, vol. 25, no. 8, pp. 768–771, 2013.

[19] P. Moser, J. A. Lott, P. Wolf, G. Larisch, N. N. Ledentsov, and D. Bimberg, "25 gb/s operation of oxide-confined 850-nm VCSELs with ultralow 56 fJ dissipated power per bit," in *Semiconductor Laser Conference (ISLC), 2012 23rd IEEE International*, 2012, pp. 157–158.

[20] P. Wolf, P. Moser, G. Larisch, H. Li, J. Lott, and D. Bimberg, "Energy efficient 40 gbit/s transmission with 850 nm VCSELs at 108 fJ/bit dissipated heat," *Electronics Letters*, vol. 49, no. 10, pp. –, 2013.

[21] R. Safaisini, K. Szczerba, E. Haglund, P. Westbergh, J. Gustavsson, A. Larsson, and P. A. Andrekson, "20 gbit/s error-free operation of 850 nm oxide-confined VCSELs beyond 1 km of multimode fibre," *Electronics Letters*, vol. 48, no. 19, pp. 1225–1227, 2012.

[22] P. Moser, P. Wolf, G. Larisch, H. Li, J. Lott, and D. Bimberg, "Energy efficient 850 nm vcsels for error-free 30 gb/s operation across 500 m of multimode optical fiber with 85 fj of dissipated energy per bit," in *2013 IEEE Optical Interconnects Conference*, 2013, pp. 13–14.

[23] E. Haglund, A. Haglund, P. Westbergh, J. S. Gustavsson, B. Koegel, and A. Larsson, "25 gbit/s transmission over 500 m multimode fibre using 850 nm VCSEL with integrated mode filter," *Electronics Letters*, vol. 48, no. 9, pp. 517–519, 2012.

[24] B. Lemoff, M. Ali, G. Panotopoulos, E. de Groot, G. Flower, G. Rankin, A. Schmit, K. Djordjev, M. Tan, A. Tandon, W. Gong, R. Tella, B. Law, L.-K. Chia, and D. Dolfi, "Demonstration of a compact low-power 250-gb/s parallel-WDM optical interconnect," *IEEE Photonics Technology Letters*, vol. 17, no. 1, pp. 220–222, 2005.

[25] K. Takaki, S. Imai, S. Kamiya, H. Shimizu, Y. Kawakita, K. Hiraiwa, T. Takagi, H. Shimizu, J. Yoshida, T. Ishikawa, N. Tsukiji, and A. Kasukawa, "1060nm VCSEL for inter-chip optical interconnection," vol. 7952, 2011, pp. 795 204–795 204–7. [Online]. Available: http://dx.doi.org/10.1117/12.873662

[26] A. Mutig and D. Bimberg, "Progress on high-speed 980nm VCSELs for short-reach optical interconnects," *Advances in Optical Technologies*, vol. 2011, Sep. 2011. [Online]. Available: http://www.hindawi.com/journals/aot/2011/290508/abs/

[27] S. Imai, K. Takaki, S. Kamiya, H. Shimizu, J. Yoshida, Y. Kawakita, T. Takagi, K. Hiraiwa, H. Shimizu, T. Suzuki, N. Iwai, T. Ishikawa, N. Tsukiji, and A. Kasukawa, "Recorded low power dissipation in highly reliable 1060-nm VCSELs for "green" optical interconnection," *IEEE Journal of Selected Topics in Quantum Electronics*, vol. 17, no. 6, pp. 1614–1620, 2011.

[28] P. Wolf, P. Moser, G. Larisch, W. Hofmann, and D. Bimberg, "High-speed and temperature-stable, oxide-confined 980-nm VCSELs for optical interconnects," *IEEE Journal of Selected Topics in Quantum Electronics*, vol. 19, no. 4, pp. 1 701 207–1 701 207, 2013.

[29] W. H. M. Mueller, "1.55μm high-speed VCSELs enabling error-free fiber-transmission up to 25 gbit/s," pp. 156 – 157, 2010.

[30] M. Muller, W. Hofmann, T. Grundl, M. Horn, P. Wolf, R. Nagel, E. Ronneberg, G. Bohm, D. Bimberg, and M.-C. Amann, "1550-nm high-speed short-cavity VCSELs," *IEEE Journal of Selected Topics in Quantum Electronics*, vol. 17, no. 5, pp. 1158–1166, 2011.

[31] W. Hofmann, M. Muller, P. Wolf, A. Mutig, T. Grundl, G. Bohm, D. Bimberg, and M.-C. Amann, "40 gbit/s modulation of 1550 nm VCSEL," *Electronics Letters*, vol. 47, no. 4, pp. 270–271, 2011.

[32] A. Gatto, A. Boletti, P. Boffi, C. Neumeyr, M. Ortsiefer, E. Ronneberg, and M. Martinelli, "1.3-μm VCSEL transmission performance up to 12.5 gb/s for metro access networks," *IEEE Photonics Technology Letters*, vol. 21, no. 12, pp. 778–780, 2009.

[33] A. Mereuta, G. Suruceanu, A. Caliman, V. Iacovlev, A. Sirbu, and E. Kapon, "10-gb/s and 10-km error-free transmission up to 100°C with 1.3μm wavelength wafer-fused VCSELs," *Optics Express*,

vol. 17, no. 15, pp. 12 981–12 986, Jul. 2009. [Online]. Available: http://www.opticsexpress.org/abstract.cfmURI=oe-17-15-12981

[34] N. S. Y. Onishi, "Long-wavelength GaInNAs vertical-cavity surface-emitting laser with buried tunnel junction," *Selected Topics in Quantum Electronics, IEEE Journal of*, no. 3, pp. 838 – 843, 2009.

[35] M. Mueller, C. Grasse, K. Saller, T. Grundl, G. Bohm, M. Ortsiefer, and M. C. Amann, "1.3 μm high-power short-cavity VCSELs for high-speed applications," in *2012 Conference on Lasers and Electro-Optics (CLEO)*, 2012, pp. 1–2.

[36] M. Muller, C. Grasse, and M. C. AMANN, "InP-based 1.3 μm and 1.55 μm short-cavity VCSELs suitable for telecom- and datacom-applications," in *2012 14th International Conference on Transparent Optical Networks (ICTON)*, 2012, pp. 1–4.

[37] M. Muller, P. Wolf, C. Grasse, M. P. I. Dias, M. Ortsiefer, G. Bohm, E. Wong, W. Hofmann, D. Bimberg, and M. C. Amann, "1.3 μm short-cavity VCSELs enabling error-free transmission at 25 gbit/s over 25 km fibre link," *Electronics Letters*, vol. 48, no. 23, pp. 1487–1489, 2012.

[38] P. Pepeljugoski, S. Member, S. E. Golowich, A. J. Ritger, P. Kolesar, and A. Risteski, "Modeling and simulation of next-generation multimode fiber links," *IEEE/OSA Journal of Lightwave Technology*, vol. 21, pp. 1242–1255, 2003.

[39] P. Pepeljugoski, M. Hackert, J. Abbott, S. Swanson, S. Golowich, A. Ritger, P. Kolesar, Y. Chen, and P. Pleunis, "Development of system specification for laser-optimized 50- μm multimode fiber for multigigabit short-wavelength LANs," *Journal of Lightwave Technology*, vol. 21, no. 5, pp. 1256–1275, 2003.

[40] D. M. Kuchta, "Progress in VCSEL-Based parallel links," in *VCSELs*, ser. Springer Series in Optical Sciences, R. Michalzik, Ed. Springer Berlin Heidelberg, Jan. 2013, no. 166, pp. 473–519. [Online]. Available: http://link.springer.com/chapter/10.1007/978-3-642-24986-0_16

[41] R. H. Johnson and D. M. Kuchta, "30 gb/s directly modulated 850 nm datacom VCSELs," in *Conference on Lasers and Electro-Optics/Quantum Electronics and Laser Science Conference and Photonic Applications Systems Technologies*, ser. OSA

Technical Digest (CD). Optical Society of America, May 2008, p. CPDB2. [Online]. Available: http://www.opticsinfobase.org/abstract.cfmURI=CLEO-2008-CPDB2

[42] M. Fields, J. Foley, R. Kaneshiro, L. McColloch, D. Meadowcroft, F. Miller, S. Nassar, M. Robinson, and H. Xu, "Transceivers and optical engines for computer and datacenter interconnects," in *Optical Fiber Communication (OFC), collocated National Fiber Optic Engineers Conference, 2010 Conference on (OFC/NFOEC)*, 2010, pp. 1–2.

[43] F. Doany, C. Schow, B. Lee, A. Rylyakov, C. Jahnes, Y. Kwark, C. Baks, D. Kuchta, and J. Kash, "Dense 24 TX + 24 RX fiber-coupled optical module based on a holey CMOS transceiver IC," in *Electronic Components and Technology Conference (ECTC), 2010 Proceedings 60th*, 2010, pp. 247–255.

[44] F. Doany, B. Lee, C. Schow, C. Tsang, C. Baks, Y. Kwark, R. John, J. Knickerbocker, and J. Kash, "Terabit/s-class 24-channel bidirectional optical transceiver module based on TSV si carrier for board-level interconnects," in *Electronic Components and Technology Conference (ECTC), 2010 Proceedings 60th*, 2010, pp. 58–65.

[45] D. Jubin, R. Dangel, N. Meier, F. Horst, T. Lamprecht, J. Weiss, R. Beyeler, B. J. Offrein, M. Halter, R. Stieger, and F. Betschon, "Polymer waveguide-based multilayer optical connector," vol. 7607, 2010, pp. 76 070K–76 070K–9. [Online]. Available: http://dx.doi.org/10.1117/12.841904

[46] R. Dangel, C. Berger, R. Beyeler, L. Dellmann, M. Gmur, R. Hamelin, F. Horst, T. Lamprecht, T. Morf, S. Oggioni, M. Spreafico, and B. Offrein, "Polymer-waveguide-based board-level optical interconnect technology for datacom applications," *IEEE Transactions on Advanced Packaging*, vol. 31, no. 4, pp. 759–767, 2008.

[47] F. Doany, C. Schow, C. Baks, D. Kuchta, P. Pepeljugoski, L. Schares, R. Budd, F. Libsch, R. Dangel, F. Horst, B. Offrein, and J. Kash, "160 gb/s bidirectional polymer-waveguide board-level optical interconnects using CMOS-Based transceivers," *IEEE Transactions on Advanced Packaging*, vol. 32, no. 2, pp. 345–359, 2009.

[48] F. Doany, C. Schow, B. Lee, R. Budd, C. Baks, R. Dangel, R. John, F. Libsch, J. Kash, B. Chan, H. Lin, C. Carver, J. Huang, J. Berry,

and D. Bajkowski, "Terabit/sec-class board-level optical interconnects through polymer waveguides using 24-channel bidirectional transceiver modules," in *Electronic Components and Technology Conference (ECTC), 2011 IEEE 61st*, 2011, pp. 790–797.

[49] R. A. Soref, "Silicon-based optoelectronics," *Proceedings of the IEEE*, vol. 81, no. 12, pp. 1687–1706, 1993.

[50] R. Soref, "The past, present, and future of silicon photonics," *IEEE Journal of Selected Topics in Quantum Electronics*, vol. 12, no. 6, pp. 1678–1687, 2006.

[51] D. Guckenberger, S. Abdalla, C. Bradbury, J. Clymore, P. de Dobbelaere, D. Foltz, S. Gloeckner, M. Harrison, S. Jackson, D. Kucharski, Y. Liang, C. Lo, M. Mack, G. Masini, A. Mekis, A. Narasimha, M. Peterson, T. Pinguet, J. Redman, S. Sahni, B. Welch, K. Yokoyama, and S. Yu, "Advantages of CMOS photonics for future transceiver applications," in *2010 36th European Conference and Exhibition on Optical Communication (ECOC)*, 2010, pp. 1–6.

[52] S. Assefa, W. M. Green, A. Rylyakov, C. Schow, F. Horst, and Y. Vlasov, "CMOS integrated nanophotonics: Enabling technology for exascale computing systems," in *Optical Fiber Communication Conference/National Fiber Optic Engineers Conference 2011*, ser. OSA Technical Digest (CD). Optical Society of America, Mar. 2011, p. OMM6. [Online]. Available: http://www.opticsinfobase.org/abstract.cfmURI=OFC-2011-OMM6

[53] S. Assefa, F. Xia, and Y. A. Vlasov, "Reinventing germanium avalanche photodetector for nanophotonic on-chip optical interconnects," *Nature*, vol. 464, no. 7285, pp. 80–84, Mar. 2010. [Online]. Available: http://www.nature.com/nature/journal/v464/n7285/full/nature08813.html

[54] F. Horst, "Silicon integrated waveguide devices for filtering and wavelength demultiplexing," in *Optical Fiber Communication (OFC), collocated National Fiber Optic Engineers Conference, 2010 Conference on (OFC/NFOEC)*, 2010, pp. 1–3.

[55] J. Van Campenhout, W. M. Green, S. Assefa, and Y. A. Vlasov, "Low-power, 2x2 silicon electro-optic switch with 110-nm bandwidth for broadband reconfigurable optical networks," *Optics Express*, vol. 17, no. 26, p. 24020, Dec. 2009. [Online]. Available: http://www.opticsinfobase.org/oe/fulltext.cfmURI=oe-17-26-24020

[56] B. Lee, W. M. J. Green, J. Van Campenhout, C. Schow, A. Rylyakov, S. Assefa, M. Yang, J. Rosenberg, J. Kash, and Y. Vlasov, "Comparison of ring resonator and mach-zehnder photonic switches integrated with digital CMOS drivers," in *IEEE Photonics Society, 2010 23rd Annual Meeting of the*, 2010, pp. 327–328.

[57] H. Thacker, I. Shubin, Y. Luo, J. Costa, J. Lexau, X. Zheng, G. Li, J. Yao, J. Li, D. Patil, F. Liu, R. Ho, D. Feng, M. Asghari, T. Pinguet, K. Raj, J. Mitchell, A. Krishnamoorthy, and J. Cunningham, "Hybrid integration of silicon nanophotonics with 40nm-CMOS VLSI drivers and receivers," in *Electronic Components and Technology Conference (ECTC), 2011 IEEE 61st*, 2011, pp. 829–835.

[58] S. Kipp, "The limits of switch bandwidth," in *Optical Fiber Communication Conference/National Fiber Optic Engineers Conference 2011*, ser. OSA Technical Digest (CD). Optical Society of America, Mar. 2011, p. OMV1. [Online]. Available: http://www.opticsinfobase.org/abstract.cfmURI=OFC-2011-OMV1

[59] N. Fehratovic and S. Aleksic, "Power consumption and scalability of optically switched interconnects for high-capacity network elements," in *Optical Fiber Communication Conference and Exposition (OFC/NFOEC), 2011 and the National Fiber Optic Engineers Conference*, 2011, pp. 1–3.

[60] D. Kuchta, A. V. Rylyakov, C. L. Schow, J. E. Proesel, C. Baks, C. Kocot, L. Graham, R. Johnson, G. Landry, E. Shaw, A. MacInnes, and J. Tatum, "A 55Gb/s directly modulated 850nm VCSEL-based optical link," in *2012 IEEE Photonics Conference (IPC)*, 2012, pp. 1–2.

[61] P. Boffi, A. Gatto, A. Boletti, P. Martelli, and M. Martinelli, "12.5 gbit/s VCSEL-based transmission over legacy MMFs by centre-launching technique," *Electronics Letters*, vol. 48, no. 20, pp. 1289–1290, 2012.

[62] Pcb analysis with hyperlynx. [Online]. Available: http://www.mentor.com/pcb/hyperlynx/

[63] Altera stratix v. [Online]. Available: http://www.altera.com/devices/fpga/stratix-fpgas/stratix-v/stxv-index.jsp

[64] P. Westbergh, R. Safaisini, E. Haglund, B. Koegel, J. S. Gustavsson, A. Larsson, M. Geen, R. Lawrence, and A. Joel, "High-speed 850 nm

VCSELs with 28 GHz modulation bandwidth operating error-free up to 44 gbit/s," *Electronics Letters*, vol. 48, no. 18, pp. 1145–1147, 2012.

[65] W. Hofmann and D. Bimberg, "VCSEL-Based light sources-scalability challenges for VCSEL-Based multi-100- gb/s systems," *IEEE Photonics Journal*, vol. 4, no. 5, pp. 1831–1843, 2012.

[66] N. Ledentsov, J. A. Lott, P. Wolf, P. Moser, J. R. Kropp, and D. Bimberg, "High speed VCSELs for energy-efficient data transmission," in *Semiconductor Laser Conference (ISLC), 2012 23rd IEEE International*, 2012, pp. 151–152.

[67] P. Moser, J. A. Lott, P. Wolf, G. Larisch, H. Li, N. Ledentsov, and D. Bimberg, "56 fJ dissipated energy per bit of oxide-confined 850 nm VCSELs operating at 25 gbit/s," *Electronics Letters*, vol. 48, no. 20, pp. 1292–1294, 2012.

[68] S. Blokhin, J. Lott, A. Mutig, G. Fiol, N. Ledentsov, M. Maximov, A. Nadtochiy, V. Shchukin, and D. Bimberg, "Oxide-confined 850 nm VCSELs operating at bit rates up to 40 gbit/s," *Electronics Letters*, vol. 45, no. 10, pp. 501–503, 2009.

[69] A. M. Rashed and D. R. Selviah, "Modelling of polymer taper waveguide for optical backplane," 2004. [Online]. Available: http://discovery.ucl.ac.uk/2692/

[70] J. B. Iv, N. Bamiedakis, A. Wonfor, R. V. Penty, I. H. White, J. V. D. Jr, K. Hueston, T. V. Clapp, and M. Glick, "A terabit capacity passive polymer optical backplane based on a novel meshed waveguide architecture," *Applied Physics A*, vol. 95, no. 4, pp. 983–988, Jun. 2009. [Online]. Available: http://link.springer.com/article/10.1007/s00339-009-5108-3

[71] N. Bamiedakis, A. Hashim, R. Penty, and I. White, "Polymer waveguide-based backplanes for board-level optical interconnects," in *2012 14th International Conference on Transparent Optical Networks (ICTON)*, 2012, pp. 1–6.

[72] A. Freilikhman and S. Arnon, "Unguided optical bus for next-generation computers: Simulation of the motherboard," in *2010 IEEE 26th Convention of Electrical and Electronics Engineers in Israel (IEEEI)*, 2010, pp. 000 906–000 910.

[73] B. Zhu, T. Taunay, M. Yan, M. Fishteyn, G. Oulundsen, and D. Vaidya, "70-gb/s multicore multimode fiber transmissions for optical data links," *IEEE Photonics Technology Letters*, vol. 22, no. 22, pp. 1647–1649, 2010.

[74] T. Hayashi, T. Nagashima, O. Shimakawa, T. Sasaki, and E. Sasaoka, "Crosstalk variation of multi-core fibre due to fibre bend," in *2010 36th European Conference and Exhibition on Optical Communication (ECOC)*, 2010, pp. 1–3.

[75] D. Molin, F. Achten, W. van Meer, A. Medawar, G. Kuyt, M. Boon, and P. Sillard, "Multimode fiber bending sensitivity for multi-gigabit ethernet application," in *58th International Wire & Cable Symposium (IWCS^{a})*, ser. OSA Technical Digest (CD). International Wire and Cable Symposium by Omnipress, 2009, p. 442. [Online]. Available: http://iwcs.omnibooksonline.com/

[76] W. C. Hurley and T. L. Cooke, "Bend-insensitive multimode fibers enable advanced cable performance," in *58th International Wire & Cable Symposium (IWCS^{a})*, ser. OSA Technical Digest (CD). International Wire and Cable Symposium by Omnipress, 2009, p. 458. [Online]. Available: http://iwcs.omnibooksonline.com/

[77] D. Molin, M. Bigot-Astruc, K. de Jongh, and P. Sillard, "Trench-assisted bend-resistant OM4 multi-mode fibers," in *2010 36th European Conference and Exhibition on Optical Communication (ECOC)*, 2010, pp. 1–3.

[78] D. Molin, G. Kuyt, M. Bigot-Astruc, and P. Sillard, "Recent advances in MMF technology for data networks," in *Optical Fiber Communication Conference/National Fiber Optic Engineers Conference 2011*, ser. OSA Technical Digest (CD). Optical Society of America, Mar. 2011, p. OWJ6. [Online]. Available: http://www.opticsinfobase.org/abstract.cfmURI=OFC-2011-OWJ6

[79] T. Irujo and J. Kamino. Multimode or single-mode fiber? [Online]. Available: www.ofsoptics.com/resources

[80] M. F. Hanna, "Mpo/mtp connectors targeted for high-density parallel optics," *Lightwave*, vol. 25, no. 2, p. 13, 2008. [Online]. Available: http://www.lightwaveonline.com/articles/print/volume-25/issue-2/technology/tech-trends/mpomtp-connectors-targeted-for-high-density-parallel-optics-54884412.html

[81] N. Shimoji, J. Yamakawa, and M. Shiino, "Development of the mini-mpo connector," *Furukawa Review*, no. 18, 1999.

[82] K. Suematsu, M. Shinoda, T. Shigenaga, J. Yamakawa, M. Tsukamoto, Y. Ono, and T. Ando, "Super low-loss, super high-density multi-fiber optical connectors," *Furukawa Review*, no. 23, 2003.

[83] M. Iwase, M. Shiino, T. Yagi, M. Tanaka, K. Yujob *et al.*, "Optical components for high-density optical inter-connect system: Optounity," *Furukawa Review*, no. 32, 2007.

[84] N. Nishimura, K. Suematsu, M. Shinoda, and M. Shiino, "High-density multi-fiber connectors for optical interconnection," *Furukawa Review*, no. 34, 2008.

[85] A. Nishimura, S. Numata, H. Nemoto, and T. Toyoda, "Development of super low-loss mt-type connector ferrule," in *59th International Wire & Cable Symposium (IWCS^{a})*, ser. OSA Technical Digest (CD). International Wire and Cable Symposium by Omnipress, Nov. 2010, pp. 18–21. [Online]. Available: http://iwcs.omnibooksonline.com/

[86] M. Iwaya, K. Suematsu, H. Inaba, R. Sugizaki, K. Fuse, T. Nishimoto, and K. Kamoto, "Development of optical wiring technology for optical interconnects," *Furukawa Review*, no. 41, 2012.

[87] V. Basile, I. Fassi, and G. Guadagno, "Sistema di assemblaggio a fibre ottiche," Italy Patent, Submitted March, 2013.

[88] Micropod[a] and minipod[a] 120g transmitters/receiver. [Online]. Available: http://www.avagotech.com/pages/minipod_micropod

[89] XLINX. Field programmable gate array (fpga). [Online]. Available: http://www.xilinx.com/training/fpga/fpga-field-programmable-gate-array.htm

[90] A. W. Snyder and W. R. Young, "Modes of optical waveguides," *Journal of the Optical Society of America*, vol. 68, no. 3, pp. 297–309, Mar. 1978. [Online]. Available: http://www.opticsinfobase.org/abstract.cfmURI=josa-68-3-297

[91] E. Snitzer, "Cylindrical dielectric waveguide modes," *Journal of the Optical Society of America*, vol. 51, no. 5, pp. 491–498, May 1961. [Online]. Available: http://www.opticsinfobase.org/abstract.cfmURI=josa-51-5-491

[92] D. Gloge, "Weakly guiding fibers," *Applied Optics*, vol. 10, no. 10, pp. 2252–2258, Oct. 1971. [Online]. Available: http://ao.osa.org/abstract.cfmURI=ao-10-10-2252

[93] P. M. Morse and H. Feshbach, *Methods of Theoretical Physics, Part I*, reprint ed. McGraw-Hill Science/Engineering/Math, Jun. 1953.

[94] R. Adler, "Waves on inhomogeneous cylindrical structures," *Proceedings of the IRE*, vol. 40, no. 3, pp. 339–348, 1952. [Online]. Available: 10.1109/JRPROC.1952.273796

[95] A. Snyder and J. Love, *Optical Waveguide Theory*, 1st ed. Springer, Nov. 1983.

[96] A. W. Snyder, "Asymptotic expressions for eigenfunctions and eigenvalues of a dielectric or optical waveguide," *IEEE Transactions on Microwave Theory and Techniques*, vol. 17, no. 12, pp. 1130–1138, 1969.

[97] N. S. Kapany and J. J. J. J. Burke, *Optical waveguides*, ser. Quantum electronics–principles and applications. New York,: Academic Press, 1972, includes bibliographies.

[98] D. Marcuse, *Light Transmission Optics*. Krieger Pub Co, May 1989.

[99] E. Snitzer and H. Osterberg, "Observed dielectric waveguide modes in the visible spectrum*," *Journal of the Optical Society of America*, vol. 51, no. 5, pp. 499–505, May 1961. [Online]. Available: http://www.opticsinfobase.org/abstract.cfmURI=josa-51-5-499

[100] G. Charlet, E. Corbel, J. Lazaro, A. Klekamp, R. Dischler, P. Tran, W. Idler, H. Mardoyan, A. Konczykowska, F. Jorge, and S. Bigo, "WDM transmission at 6-tbit/s capacity over transatlantic distance, using 42.7-gb/s differential phase-shift keying without pulse carver," *Journal of Lightwave Technology*, vol. 23, no. 1, pp. 104–107, 2005.

[101] P. Boffi, M. Ferrario, L. Marazzi, P. Martelli, P. Parolari, A. Righetti, R. Siano, and M. Martinelli, "Stable 100-gb/s POLMUX-DQPSK transmission with automatic polarization stabilization," *IEEE Photonics Technology Letters*, vol. 21, no. 11, pp. 745–747, 2009.

[102] P. Pepeljugoski, D. Kuchta, and A. Risteski, "Modal noise BER calculations in 10-gb/s multimode fiber LAN links," *IEEE Photonics Technology Letters*, vol. 17, no. 12, pp. 2586–2588, 2005.

[103] D. H. Sim, Y. Takushima, and Y. C. Chung, "High-speed multimode fiber transmission by using mode-field matched center-launching-technique," *Journal of Lightwave Technology*, vol. 27, no. 8, pp. 1018–1026, Apr. 2009. [Online]. Available: http://jlt.osa.org/abstract.cfmURI=jlt-27-8-1018

[104] H. S. Chung, S. H. Chang, and K. Kim, "6 x 86 gb/s WDM transmission over 2 km multimode fiber using center launching technique and multi-level modulation," *Optics Express*, vol. 17, no. 10, pp. 8098–8102, May 2009. [Online]. Available: http://www.opticsexpress.org/abstract.cfmURI=oe-17-10-8098

[105] Z. Haas and M. Santoro, "A mode-filtering scheme for improvement of the bandwidth-distance product in multimode fiber systems," *Journal of Lightwave Technology*, vol. 11, no. 7, pp. 1125–1131, 1993.

[106] M. Webster, L. Raddatz, I. White, and D. G. Cunningham, "A statistical analysis of conditioned launch for gigabit ethernet links using multimode fiber," *Journal of Lightwave Technology*, vol. 17, no. 9, pp. 1532–1541, 1999.

[107] L. Raddatz, I. White, D. G. Cunningham, and M. Nowell, "An experimental and theoretical study of the offset launch technique for the enhancement of the bandwidth of multimode fiber links," *Journal of Lightwave Technology*, vol. 16, no. 3, pp. 324–331, 1998.

[108] European standards: Etsi en 300 019-2-2 v2.2.1 (2012-01); etsi en 300 019-2-3 v2.2.2 (2003-04); etsi en 300 019-2-4 v2.2.2 (2003-04). [Online]. Available: http://www.etsi.org/standards

[109] D. H. Sim, Y. Takushima, and Y. Chung, "Robustness evaluation of MMF transmission link using mode-field matched center-launching technique," in *Conference on Optical Fiber communication/National Fiber Optic Engineers Conference, 2008. OFC/NFOEC 2008*, 2008, pp. 1–3.

[110] A. Gatto, A. Boletti, P. Boffi, and M. Martinelli, "Adjustable-chirp VCSEL-to-VCSEL injection locking for 10-gb/s transmission at 1.55μm," *Optics Express*, vol. 17, no. 24, pp. 21 748–21 753, 2009.

[111] J. N. Blake, B. Y. Kim, and H. J. Shaw, "Fiber-optic modal coupler using periodic microbending," *Optics Letters*, vol. 11,

no. 3, pp. 177–179, Mar. 1986. [Online]. Available: http://ol.osa.org/abstract.cfmURI=ol-11-3-177

[112] A. Li, A. Al Amin, X. Chen, and W. Shieh, "Reception of mode and polarization multiplexed 107-gb/s CO-OFDM signal over a two-mode fiber," in *Optical Fiber Communication Conference and Exposition (OFC/NFOEC), 2011 and the National Fiber Optic Engineers Conference*, 2011, pp. 1–3.

[113] Ieee p802.3ba 40gb/s and 100gb/s ethernet task force. [Online]. Available: http://www.ieee802.org/3/ba/

[114] d. Brown. Nrz *vs.* pam-n for 400gbe in the data center. [Online]. Available: http://www.ethernetsummit.com/English/Conference/Proceedings_Chrono.html

[115] H. Zhu and B. Mukherjee, "Online connection provisioning in metro optical WDM networks using reconfigurable OADMs," *Journal of Lightwave Technology*, vol. 23, no. 10, p. 2893, Oct. 2005. [Online]. Available: http://jlt.osa.org/abstract.cfmURI=jlt-23-10-2893

[116] A. Gatto, M. Tacca, P. Martelli, P. Boffi, and M. Martinelli, "Free-space orbital angular momentum division multiplexing with bessel beams," *Journal of Optics*, vol. 13, no. 6, p. 064018, Jun. 2011. [Online]. Available: http://iopscience.iop.org/2040-8986/13/6/064018

[117] Analog receiver performance comparison of pam-4 and pam-2. [Online]. Available: http://www.ieee802.org/3/bj

[118] A comparison of 25 gbps nrz & pam-4 modulation used in legacy & premium backplane channels. [Online]. Available: www.te.com/content/.../designcon-2012-whitepaper-chadmorgan.pdf

[119] J. Lee, M.-S. Chen, and H.-D. Wang, "Design and comparison of three 20-gb/s backplane transceivers for duobinary, PAM4, and NRZ data," *IEEE Journal of Solid-State Circuits*, vol. 43, no. 9, pp. 2120–2133, 2008.

[120] B. Min and S. Palermo, "A 20Gb/s triple-mode (PAM-2, PAM-4, and duobinary) transmitter," in *2011 IEEE 54th International Midwest Symposium on Circuits and Systems (MWSCAS)*, 2011, pp. 1–4.

[121] W. I. Eugen Lach, "Modulation formats for 100G and beyond," *Optical Fiber Technology - OPT FIBER TECHNOL*, vol. 17, no. 5, pp. 377–386, 2011.

[122] G. P. Agrawal, *Lightwave technology: telecommunication systems*. Hoboken, N.J.: Wiley-Interscience, 2005.

[123] K. Szczerba, B. Olsson, P. Westbergh, A. Rhodin, J. S. Gustavsson, A. Haglund, M. Karlsson, A. Larsson, and P. Andrekson, "37 gbps transmission over 200 m of MMF using single cycle subcarrier modulation and a VCSEL with 20 GHz modulation bandwidth," in *2010 36th European Conference and Exhibition on Optical Communication (ECOC)*, 2010, pp. 1–3.

[124] T. Pham, R. Rodes, J. Estaran, J. Jensen, and I. Monroy, "Half-cycle modulation for VCSEL based 6-gbaud 4-QAM transmission over 1 km multimode fibre link," *Electronics Letters*, vol. 48, no. 17, pp. 1074–1076, 2012.

[125] T.-T. Pham, R. Rodes, J. B. Jensen, C. J. Chang-Hasnain, and I. T. Monroy, "Sub-cycle QAM modulation for VCSEL-based optical fiber links," *Optics Express*, vol. 21, no. 2, p. 1830, Jan. 2013. [Online]. Available: http://www.opticsinfobase.org/oe/fulltext.cfmURI=oe-21-2-1830

[126] S. C. J. Lee, F. Breyer, S. Randel, D. Cardenas, H. P. A. Van den Boom, and A. M. J. Koonen, "Discrete multitone modulation for high-speed data transmission over multimode fibers using 850-nm VCSEL," in *Conference on Optical Fiber Communication - incudes post deadline papers, 2009. OFC 2009*, 2009, pp. 1–3.

[127] Y. Benlachtar, P. M. Watts, R. Bouziane, P. Milder, D. Rangaraj, A. Cartolano, R. Koutsoyannis, J. C. Hoe, M. Puschel, M. Glick, and R. I. Killey, "Generation of optical OFDM signals using 21.4 GS/s real time digital signal processing," *Optics Express*, vol. 17, no. 20, pp. 17 658–17 668, Sep. 2009. [Online]. Available: http://www.opticsexpress.org/abstract.cfmURI=oe-17-20-17658

[128] J. Ingham, R. Penty, I. White, and D. Cunningham, "40 gb/s carrierless amplitude and phase modulation for low-cost optical datacommunication links," in *Optical Fiber Communication Conference and Exposition (OFC/NFOEC), 2011 and the National Fiber Optic Engineers Conference*, 2011, pp. 1–3.

[129] R. Rodes, M. Wieckowski, T. T. Pham, J. B. Jensen, J. Turkiewicz, J. Siuzdak, and I. T. Monroy, "Carrierless amplitude phase modulation of VCSEL with 4 bit/s/Hz spectral efficiency for use in WDM-PON," *Optics Express*, vol. 19, no. 27, pp. 26 551–26 556, Dec. 2011. [Online]. Available: http://www.opticsexpress.org/abstract.cfmURI=oe-19-27-26551

[130] M. Othman, X. Zhang, L. Deng, M. Wieckowski, J. Jensen, and I. Monroy, "Experimental investigations of 3-d-/4-d-CAP modulation with directly modulated VCSELs," *IEEE Photonics Technology Letters*, vol. 24, no. 22, pp. 2009–2012, 2012.

[131] D. Watanabe, A. Ono, and T. Okayasu, "CMOS optical 4-PAM VCSEL driver with modal-dispersion equalizer for 10Gb/s 500m MMF transmission," in *Solid-State Circuits Conference - Digest of Technical Papers, 2009. ISSCC 2009. IEEE International*, 2009, pp. 106–107,107a.

[132] T. Toifl, C. Menolfi, M. Ruegg, R. Reutemann, P. Buchmann, M. Kossel, T. Morf, J. Weiss, and M. Schmatz, "A 22-gb/s PAM-4 receiver in 90-nm CMOS SOI technology," *IEEE Journal of Solid-State Circuits*, vol. 41, no. 4, pp. 954–965, 2006.

[133] K. Szczerba, P. Westbergh, J. Karout, J. Gustavsson, O. Haglund, M. Karlsson, P. Andrekson, E. Agrell, and A. Larsson, "30 gbps 4-PAM transmission over 200 m of MMF using an 850 nm VCSEL," *Optics Express*, vol. 19, no. 26, pp. B203–B208, Dec. 2011. [Online]. Available: http://www.opticsexpress.org/abstract.cfmURI=oe-19-26-B203

[134] K. Szczerba, P. Westbergh, J. Karout, J. Gustavsson, A. Haglund, M. Karlsson, P. Andrekson, E. Agrell, and A. Larsson, "4-PAM for high-speed short-range optical communications," *IEEE/OSA Journal of Optical Communications and Networking*, vol. 4, no. 11, pp. 885–894, 2012.

[135] Y. Tsunoda, M. Sugawara, H. Oku, S. Ide, and K. Tanaka, "25-gb/s transmitter for optical interconnection with 10-gb/s VCSEL using dual peak-tunable pre-emphasis," in *Optical Fiber Communication Conference and Exposition (OFC/NFOEC), 2011 and the National Fiber Optic Engineers Conference*, 2011, pp. 1–3.

[136] I.-C. Lu, J.-W. Shi, H.-Y. Chen, C.-C. Wei, S.-F. Tsai, D.-Z. Hsu, Z.-R. Wei, J.-M. Wun, and J. Chen, "Ultra low power VCSEL for 35-gbps 500-m OM4 MMF transmissions employing FFE/DFE equalization for optical interconnects," in *Optical Fiber Communication Conference and Exposition and the National Fiber Optic Engineers Conference (OFC/NFOEC), 2013*, 2013, pp. 1–3.

[137] S. Nakagawa, D. Kuchta, C. Schow, R. John, L. Coldren, and Y.-C. Chang, "1.5mW/Gbps low power optical interconnect transmitter exploiting high-efficiency VCSEL and CMOS driver," in *Conference on Optical Fiber communication/National Fiber Optic Engineers Conference, 2008. OFC/NFOEC 2008*, 2008, pp. 1–3.

[138] P. Wolf, P. Moser, G. Larisch, M. Kroh, A. Mutig, W. Unrau, W. Hofmann, and D. Bimberg, "High-performance 980 nm VCSELs for 12.5 gbit/s data transmission at 155°c and 49 gbit/s at -14°," *Electronics Letters*, vol. 48, no. 7, pp. 389–390, 2012.

[139] T. Anan, N. Suzuki, K. Yashiki, K. Fukatsu, H. Hatakeyama, T. Akagawa, K. Tokutome, and M. Tsuji, "High-speed 1.1μm range ingaas vcsels," in *Conference on Optical Fiber communication/National Fiber Optic Engineers Conference, 2008. OFC/NFOEC 2008*, 2008, pp. 1–3.

[140] D. Kuchta, C. Schow, A. Rylyakov, J. Proesel, F. Doany, C. Baks, B. Hamel-Bissell, C. Kocot, L. Graham, R. Johnson, G. Landry, E. Shaw, A. MacInnes, and J. Tatum, "A 56.1Gb/s NRZ modulated 850nm VCSEL-based optical link," in *Optical Fiber Communication Conference and Exposition and the National Fiber Optic Engineers Conference (OFC/NFOEC), 2013*, 2013, pp. 1–3.

[141] J. E. Proesel, B. G. Lee, A. V. Rylyakov, C. W. Baks, and C. L. Schow, "Ultra-low-power 10 to 28.5gb/s CMOS-Driven VCSEL-Based optical links," *Journal of Optical Communications and Networking*, vol. 4, no. 11, pp. B114–B123, Nov. 2012. [Online]. Available: http://jocn.osa.org/abstract.cfmURI=jocn-4-11-B114

[142] J. Proesel, B. G. Lee, C. W. Baks, and C. Schow, "35-gb/s VCSEL-Based optical link using 32-nm SOI CMOS circuits," in *Optical Fiber Communication Conference/National Fiber Optic Engineers Conference 2013*, ser. OSA Technical Digest (online). Optical Society of America, Mar. 2013, p. OM2H.2. [Online]. Available: http://www.opticsinfobase.org/abstract.cfmURI=OFC-2013-OM2H.2

[143] C. Schow, F. Doany, A. Rylyakov, B. Lee, C. V. Jahnes, Y. Kwark, C. Baks, D. Kuchta, and J. Kash, "A 24-channel, 300 gb/s, 8.2 pJ/bit, full-duplex fiber-coupled optical transceiver module based on a single "holey" CMOS IC," *Journal of Lightwave Technology*, vol. 29, no. 4, pp. 542–553, 2011.

[144] F. E. Doany, B. Lee, A. Rylyakov, D. M. Kuchta, C. Baks, C. Jahnes, F. Libsch, and C. Schow, "Terabit/sec VCSEL-Based parallel optical module based on holey CMOS transceiver IC," in *Optical Fiber Communication Conference*, ser. OSA Technical Digest. Optical Society of America, Mar. 2012, p. PDP5D.9. [Online]. Available: http://www.opticsinfobase.org/abstract.cfmURI=OFC-2012-PDP5D.9

[145] J. Cheng, "Topics in VCSEL-based high-speed WDM optical interconnects," in *2008 IEEE Avionics, Fiber-Optics and Photonics Technology Conference*, 2008, pp. 65–66.

[146] W. Hofmann, E. Wong, M. Ortsiefer, M. Gorblich, G. Bohm, and M. C. AMANN, "One and two-dimensional long-wavelength VCSEL arrays for WDM applications and optical interconnects," in *Semiconductor Laser Conference, 2008. ISLC 2008. IEEE 21st International*, 2008, pp. 165–166.

[147] C. Sciancalepore, B. Ben Bakir, S. Menezo, X. Letartre, D. Bordel, and P. Viktorovitch, "CMOS-Compatible photonic crystal VCSEL arrays for wavelength division multiplexing," in *CLEO: 2013*, ser. OSA Technical Digest (online). Optical Society of America, Jun. 2013, p. CF2F.3. [Online]. Available: http://www.opticsinfobase.org/abstract.cfmURI=CLEO_SI-2013-CF2F.3

[148] N. Quadir, P. Ossieur, and P. Townsend, "A 56Gb/s PAM-4 VCSEL driver circuit," in *Signals and Systems Conference (ISSC 2012), IET Irish*, 2012, pp. 1–5.

[149] K. Szczerba, P. Westbergh, M. Karlsson, P. Andrekson, and A. Larsson, "60 gbits error-free 4-pam operation with 850 nm vcsel," *Electronics Letters*, vol. 49, no. 15, pp. 953–955, 2013.

[150] R. Rodes, M. Mueller, B. Li, J. Estaran, J. Jensen, T. Gruendl, M. Ortsiefer, C. Neumeyr, J. Rosskopf, K. Larsen, M. Amann, and I. Monroy, "High-speed 1550 nm VCSEL data transmission link employing 25 GBd 4-PAM modulation and hard decision forward er-

ror correction," *Journal of Lightwave Technology*, vol. 31, no. 4, pp. 689–695, 2013.

[151] F. Karinou, R. Rodes, K. Prince, I. Roudas, and I. T. Monroy, "IM/DD vs. 4-PAM using a 1550-nm VCSEL over short-range SMF/MMF links for optical interconnects," in *Optical Fiber Communication Conference/National Fiber Optic Engineers Conference 2013*, ser. OSA Technical Digest (online). Optical Society of America, Mar. 2013, p. OW4A.2. [Online]. Available: http://www.opticsinfobase.org/abstract.cfmURI=OFC-2013-OW4A.2

[152] J. L. Wei, J. Ingham, D. Cunningham, R. Penty, and I. White, "Performance and power dissipation comparisons between 28 gb/s NRZ, PAM, CAP and optical OFDM systems for data communication applications," *Journal of Lightwave Technology*, vol. 30, no. 20, pp. 3273–3280, 2012.

[153] F. Karinou, L. Deng, R. R. Lopez, K. Prince, J. B. Jensen, and I. T. Monroy, "Performance comparison of 850-nm and 1550-nm VCSELs exploiting OOK, OFDM, and 4-PAM over SMF/MMF links for low-cost optical interconnects," *Optical Fiber Technology*, vol. 19, no. 3, pp. 206–212, Jun. 2013. [Online]. Available: http://www.sciencedirect.com/science/article/pii/S1068520013000059

[154] X. Zheng, D. Patil, J. Lexau, F. Liu, G. Li, H. Thacker, Y. Luo, I. Shubin, J. Li, J. Yao, P. Dong, D. Feng, M. Asghari, T. Pinguet, A. Mekis, P. Amberg, M. Dayringer, J. Gainsley, H. F. Moghadam, E. Alon, K. Raj, R. Ho, J. E. Cunningham, and A. V. Krishnamoorthy, "Ultra-efficient 10Gb/s hybrid integrated silicon photonic transmitter and receiver," *Optics Express*, vol. 19, no. 6, pp. 5172–5186, Mar. 2011. [Online]. Available: http://www.opticsexpress.org/abstract.cfmURI=oe-19-6-5172

[155] L. Vivien, J. Osmond, J.-M. Fedeli, D. Marris-Morini, P. Crozat, J.-F. Damlencourt, E. Cassan, Y. Lecunff, and S. Laval, "42 GHz p.i.n germanium photodetector integrated in a silicon-on-insulator waveguide," *Optics Express*, vol. 17, no. 8, pp. 6252–6257, Apr. 2009. [Online]. Available: http://www.opticsexpress.org/abstract.cfmURI=oe-17-8-6252

[156] J. Buckwalter, X. Zheng, G. Li, K. Raj, and A. Krishnamoorthy, "A monolithic 25-gb/s transceiver with photonic ring modulators and ge

detectors in a 130-nm CMOS SOI process," *IEEE Journal of Solid-State Circuits*, vol. 47, no. 6, pp. 1309–1322, 2012.

[157] Y. Vlasov, "Silicon CMOS-integrated nano-photonics for computer and data communications beyond 100G," *IEEE Communications Magazine*, vol. 50, no. 2, pp. s67–s72, 2012.

[158] X. Zheng, F. Liu, J. Lexau, D. Patil, G. Li, Y. Luo, H. Thacker, I. Shubin, J. Yao, K. Raj, R. Ho, J. Cunningham, and A. Krishnamoorthy, "Ultralow power 80 gb/s arrayed CMOS silicon photonic transceivers for WDM optical links," *Journal of Lightwave Technology*, vol. 30, no. 4, pp. 641–650, 2012.

[159] S. Assefa, S. Shank, W. Green, M. Khater, E. Kiewra, C. Reinholm, S. Kamlapurkar, A. Rylyakov, C. Schow, F. Horst, H. Pan, T. Topuria, P. Rice, D. Gill, J. Rosenberg, T. Barwicz, M. Yang, J. Proesel, J. Hofrichter, B. Offrein, X. Gu, W. Haensch, J. Ellis-Monaghan, and Y. Vlasov, "A 90nm CMOS integrated nano-photonics technology for 25Gbps WDM optical communications applications," in *Electron Devices Meeting (IEDM), 2012 IEEE International*, 2012, pp. 33.8.1–33.8.3.

[160] Cmos nanophotonics for exascale. [Online]. Available: http://researcher.ibm.com/researcher/

[161] P. Dong, L. Chen, C. Xie, L. L. Buhl, and Y.-K. Chen, "50-gb/s silicon quadrature phase-shift keying modulator," *Optics Express*, vol. 20, no. 19, pp. 21 181–21 186, Sep. 2012. [Online]. Available: http://www.opticsexpress.org/abstract.cfmURI=oe-20-19-21181

[162] L. Xu, J. Chan, A. Biberman, H. Lira, M. Lipson, and K. Bergman, "DPSK transmission through silicon microring switch for photonic interconnection networks," *IEEE Photonics Technology Letters*, vol. 23, no. 16, pp. 1103–1105, 2011.

[163] M. Kroh, L. Zimmermann, H.-G. Bach, K. Voigt, A. Beling, M. Nielsen, R. Ludwig, J. Bruns, and G. Unterboarsch, "Integrated receivers on silicon-on-insulator for advanced modulation formats," *IET Optoelectronics*, vol. 5, no. 5, pp. 211–217, 2011.

[164] Investigation of 100gbe based on pam-4 and pam-8. [Online]. Available: www.ieee802.org/3/bm/public/sep12/ghiasi_01a_0912_optx.pd

[165] Investigation of pam-4/6/8 signaling and fec for 100 gb/s serial transmission. [Online]. Available: www.ieee802.org/3/bm/public/nov12/ghiasi_01a_1112_optx.pdf

[166] High speed nrz and pam optical modulation using cmos photonics. [Online]. Available: www.ieee802.org/3/.../public/.../dama_01_0312_NG100GOPTX.pdf

[167] X. Wu, B. Dama, P. Gothoskar, P. Metz, K. Shastri, S. Sunder, J. Van der Spiegel, Y. Wang, M. Webster, and W. Wilson, "A 20Gb/s NRZ/PAM-4 1V transmitter in 40nm CMOS driving a si-photonic modulator in 0.13 μm CMOS," in *Solid-State Circuits Conference Digest of Technical Papers (ISSCC), 2013 IEEE International*, 2013, pp. 128–129.

[168] S. Walklin and J. Conradi, "Multilevel signaling for increasing the reach of 10 gb/s lightwave systems," *Journal of Lightwave Technology*, vol. 17, no. 11, pp. 2235–2248, 1999.

[169] E. Agrell, J. Lassing, E. Strom, and T. Ottosson, "On the optimality of the binary reflected gray code," *IEEE Transactions on Information Theory*, vol. 50, no. 12, pp. 3170–3182, 2004.

[170] K. Shastri and B. Dama, "Optical modulator utilizing multi-level signaling," U.S. Patent US20 080 095 486 A1, Apr., 2008, U.S. Classification 385/3, 398/188; International Classification G02F1/035; Cooperative Classification G02F1/0123, G02F1/2255; European Classification G02F1/01D2, G02F1/225H.

[171] Optsim product overview. [Online]. Available: http://optics.synopsys.com/rsoft/rsoft-system-network-optsim.html

[172] T. D. Wickens, *Elementary signal detection theory*. Oxford; New York: Oxford University Press, 2002.

[173] C. Jeruchim, "Techniques for estimating the bit error rate in the simulation of digital communication systems," *IEEE Journal on Selected Areas in Communications*, vol. 2, no. 1, pp. 153–170, 1984.

[174] Y. Tsunoda, M. Sugawara, H. Oku, S. Ide, and K. Tanaka, "Twenty-five gigabit per second transmitter using pre-emphasis," *SPIE Newsroom*, May 2012. [Online]. Available: http://spie.org/x87089.xml

[175] P. Westbergh, M. Karlsson, A. Larsson, P. Andrekson, and K. Szczerba, "60 gbits error-free 4-PAM operation with 850 nm VCSEL," *Electronics Letters*, vol. 49, no. 15, pp. 953–955, Jul. 2013. [Online]. Available: http://digital-library.theiet.org/content/journals/10.1049/el.2013.1755

[176] M. Moller, "High-speed electronic circuits for 100 gb/s transport networks," in *Optical Fiber Communication (OFC), collocated National Fiber Optic Engineers Conference, 2010 Conference on (OFC/NFOEC)*, 2010, pp. 1–3.

[177] C. Menolfi, J. Hertle, T. Toifl, T. Morf, D. Gardellini, M. Braendli, P. Buchmann, and M. Kossel, "A 28Gb/s source-series terminated TX in 32nm CMOS SOI," in *Solid-State Circuits Conference Digest of Technical Papers (ISSCC), 2012 IEEE International*, 2012, pp. 334–336.

[178] J. Proesel, C. Schow, and A. Rylyakov, "25Gb/s 3.6pJ/b and 15Gb/s 1.37pJ/b VCSEL-based optical links in 90nm CMOS," in *Solid-State Circuits Conference Digest of Technical Papers (ISSCC), 2012 IEEE International*, 2012, pp. 418–420.

[179] C. Menolfi, T. Toifl, R. Reutemann, M. Ruegg, P. Buchmann, M. Kossel, T. Morf, and M. Schmatz, "A 25Gb/s PAM4 transmitter in 90nm CMOS SOI," in *Solid-State Circuits Conference, 2005. Digest of Technical Papers. ISSCC. 2005 IEEE International*, 2005, pp. 72–73 Vol. 1.

[180] S. Assefa, H. Pan, S. Shank, W. Green, A. Rylyakov, C. Schow, M. Khater, S. Kamlapurkar, E. Kiewra, T. Topuria, P. Rice, C. W. Baks, and Y. Vlasov, "Monolithically integrated silicon nanophotonics receiver in 90nm CMOS technology node," in *Optical Fiber Communication Conference/National Fiber Optic Engineers Conference 2013*, ser. OSA Technical Digest (online). Optical Society of America, Mar. 2013, p. OM2H.4. [Online]. Available: http://www.opticsinfobase.org/abstract.cfmURI=OFC-2013-OM2H.4

[181] I. Young, E. Mohammed, J. Liao, A. Kern, S. Palermo, B. Block, M. Reshotko, and P. Chang, "Optical I/O technology for tera-scale computing," in *Solid-State Circuits Conference - Digest of Technical Papers, 2009. ISSCC 2009. IEEE International*, 2009, pp. 468–469,469a.

List of Figures

List of Tables